Assessment of a storm surge barrier

A probabilistic fragility-based framework for the assessment of complex hydraulic structures

by

D.G. Fiolet

Delft University of Technology and Witteveen+Bos

to obtain the degree of Master of Science
at the Delft University of Technology

Student number:	4036743	
Date:	08-01-2019	
Thesis committee:	Prof. dr. ir. S.N.Jonkman	TU Delft, committee chair
	Ir. W.F. Molenaar	TU Delft, supervisor
	M. Muttray, PhD	TU Delft
	Ir. J. Lansink	Witteveen+Bos

TU Delft Witteveen+Bos

Preface

Safety against flood risk is an essential part of life in the Netherlands, as the countries has dealt with flooding for centuries. In the last century, more complex and unique structures have been build in the Netherlands to ensure that the risk of a catastrophic flood is kept at a minimum. The thesis in front of you looks at the safety assessment of one of these complex flood defence structures, the methodologies that are currently applied and introduces a new assessment framework. This thesis was written as part of the graduation requirement of the Master of Science degree of Civil Engineering, at Delft University of Technology in 2018. The research was performed in cooperation with Witteveen+Bos.

I would like to thank everybody that contributed to this work, both by offering insight and feedback on the work, as well as on a more personal level. First of all, I would like to thank the members of my graduation committee; Prof. dr. ir. S.N. Jonkman for his ability to offer an astonishing amount of feedback within only several days, Ir. W.F. Molenaar for his enthusiasm and his patience with me during the discussions we had, and M. Muttray, Phd. for the valuable feedback which he offered, particularly on the structuring of the thesis. I would like to issue special thanks to Ir. J. Lansink, for his guidance during the past year, both on the technical content of this report, as well as on the subject of personal growth and development.

I would like to thank all my colleagues at Witteveen+Bos, which are too many to all name here individually, for the professional, yet very welcoming atmosphere and their input and ideas on this work. I would like to thank Anton van der Meer, for his seemingly endless amount of energy when explaining and discussing all types of subjects. I would also like to thank Krijn Saman, for his help and explanations regarding the workings of the Eastern Scheldt barrier, as well as the probabilistic tools currently used by the barrier administration.

Finally, I would like to thank my parents, brothers, Suzan and all the friends I encountered during my studies. Your support has been invaluable.

D.G. (Daniel) Fiolet
December, 2018

Cover image: Roompot section of the Eastern Scheldt barrier, source: Van den Dool, 2012

Summary

Flood risk assessment in the Netherlands is performed with the rules and guidelines of the so called 'Wettelijk BeoordelingsInstrumentarium 2017'. Within this WBI2017, semi-probabilistic assessment tools are described, which can be used in the assessment of the dikes and structures that make up the Dutch primary flood defenses. These tools are often based on approximations and calibrations, making them less well equipped when more complex and/or unique structures are to be assessed. Even though the WBI2017 offers (mostly) semi-probabilistic assessment tools, flood risk assessment has moved into a risk-based direction over the last years. As a result, the semi-probabilistic tools applied in the past are, currently or in the near-future, being replaced with probabilistic tools wherever possible. Since the applicability of the standard tools available in the WBI2017 is limited, a custom assessment needs to be developed for complex structures. One of these complex structures is the Eastern Scheldt barrier, a 8km long storm surge barrier situated in the south-western Netherlands. Aside from the need to assess probabilistically, the main problem that has been identified are the limited ways in which statistical dependency can be taken into account when assessing the different elements within the barrier. This can result in assessments which are unnecessarily conservative, which may lead engineers to incorrectly label the barrier as unsafe. This report looks at the Eastern Scheldt barrier and attempts to offer a custom and probabilistic assessment.

A new assessment framework is introduced in which structures are assessed on the basis of fragility. This concept of fragility discretizes a loading parameter and calculates the conditional failure probability per loading realization. The failure probability of a structure is then acquired by integration along the original probability density of the considered loading parameter. Due to this 2-step method, additional assumptions regarding statistical dependency are possible, which is shown to reduce conservatism. Additionally, due to the probabilistic nature of the fragility-based assessment, the conservative nature of the semi-probabilistic assessment tools currently used can be avoided. This new fragility-based assessment methodology is applied to assess the Eastern Scheldt barrier. Several failure mechanisms are studied to research how this fragility based methodology differs from currently applied assessment tools, and whether it can offer any gains.

The failure mechanism 'height' is assessed for the lock of the Eastern Scheldt barrier. Two mechanisms, overtopping and overflow, and two elements, protection on the coupure and bottom protection behind the lock, are combined into a single assessment. As such it is shown that dependency in loading over these different mechanisms and elements can be taken into account, leading to a less conservative assessment. Additionally, by drawing the multi-dimensional fragility surfaces, insight into the processes that govern failure is shown to be increased. The failure probability of the lock due to the failure mechanism 'height' has been computed to be 7.14E-6 per year. This failure probability is mostly caused by high water levels endangering the doors of the lock.

The failure mechanism 'failure due to failure to close' is assessed, which requires a custom assessment for the Eastern Scheldt barrier. In this custom assessment the risk of one of the gates failing to close when requested is assessed. Additionally, the transfer probability of failure of the bottom protection is computed. This transfer probability describes the probability that the barrier fails, after the bottom protection has failed. These transfer probabilities are assessed by computing the scour that occurs after failure of the bottom protection, as well as the probability of this scour directly endangering the barrier.

The bottom protection is shown to be vulnerable to the high flow velocities which can occur behind a gate that is open when a water level difference is present over the barrier. Most notable, by assessing the bottom protection as a large amount of elements within a series system, the most vulnerable locations have been identified. By assessing the barrier conditionally, the transfer probabilities could be described conditionally as well. A conditional approach to transfer probabilities is then used to describe the scour that occurs after the bottom protection has failed, given the flow conditions under which it has failed. These flow conditions, under which the bottom protection fails, determine whether the scour holes which occur after this failure of the bottom protection can endanger the barrier.

This has allowed a custom assessment of all elements of the bottom protection behind the barrier. With this custom assessment, the failure of the bottom protection behind the barrier at certain location could be shown to not endanger the barrier on the short term, greatly increasing insight into failure of this complex system. The failure probability has been computed for two flow scenarios; an optimistic and a conservative scenario. In the optimistic scenario the failure probability of the barrier due to the failure mechanism 'failure due to failure to close' is computed to be 2.78E-11 per closure request. This failure probability is mostly caused by failure of the bottom protection close to the barrier. In the conservative scenario the failure probability has been computed to be 2.78E-4 per closure request. This higher failure probability is caused by failure of the bottom protection at a distance of 50m from the barrier, for deeper parts of the Eastern Scheldt. At these locations an increase in the failure probability of the bottom protection occurs, while scour at these locations can directly endanger the barrier.

Contents

1 Introduction

The safety of flood defences in the Netherlands is governed within Dutch law, in article 2.12 of the so called Waterwet (literally translated; the 'water law'). In this section of Dutch law it is stated that a full assessment of the hydraulic state of all primary flood defences in the country is to be completed every 12 years. These assessments are then to be reported to the governing minister of Infrastructure and Water Management (Dutch: ministerie van Infrastructuur en Waterstaat). Each of these 12 year cycle assessment rounds (Dutch: toetsronden), new rules and guideline regarding the assessment of flood safety are introduced, based on the legally allowed risk [35] (individual, economical or societal [36]) as well as on the state of hydraulic knowledge and expertise at the time [52]. The current assessment round of the primary flood defences, which ends in 2023, is done with the guideline of the so called Wettelijk Beoordelingsinstrumentarium 2017 (WBI2017). This WBI2017 is not set in stone however. When, during the 12 year cycle, new knowledge or insights are gained which significantly changes the situation, the WBI2017 is adjusted accordingly. An example can be the discovery of a new failure mechanism [52]. Currently the WBI2017 is going through such a change [20]. This change regards the switch between semi-probabilistic- and probabilistic reliability methods. At the time of this report (2018), several failure mechanisms have already been implemented in a probabilistic manner within the WBI2017 guidelines and software, while other failure mechanisms have not [54]. The target for the coming years is to, wherever possible, introduce probabilistic methods [20]. Semi-probabilistic reliability methods are often based on approximations, which cause conservatism [32][34] and by switching to probabilistic reliability methods, this conservatism can be reduced. For this reason, flood defences which have already been assessed semi-probabilistic during the current assessment round, will always pass the probabilistic assessment as well [20] (making this change in the middle of the assessment round possible). The addition of the new probabilistic assessment tools can thus be seen as an additional check on flood defences that failed the semi-probabilistic assessment. As such, the probabilistic methods can lead to economic gains, as strengthening or replacement of flood defences can potentially be postponed [23].

This change in reliability methods within the WBI2017 forms the background of this report.

Within this changing background, this report will look at the assessment of the Eastern Scheldt storm surge barrier. This will start with an description of the barrier in Chapter 2. This description will be followed with an introduction to Dutch flood risk assessment in Chapter 3. This chapter looks at the recent changes introduced by the WBI2017, to see where the assessment of the Eastern Scheldt barrier fits within Dutch flood risk assessment and why potential problems arise. Chapter 4 then introduces a new methodology which can be applied in flood risk assessment, in the form of fragility-based assessment. These first chapters form the first part of the report, which culminates with an overview of the problems and the research questions investigated in this report in Chapter 5. The second part of this report will assess and apply the fragility-based methodology. This will start with two analyses, in Chapter 6 and Chapter 7. In these chapters the problems of currently applied assessment tools will be explored, and compared to the fragility-based assessment. Subsequently, in Chapter 8 and Chapter 9, a fragility-based assessment will be applied to assess the barrier in two cases; the height of the Roompotsluis and failure due to a door failing to close when requested. Conclusions will then be drawn in Chapter 10, which will also feature several recommendations on the methodology as well as on subjects of further research.

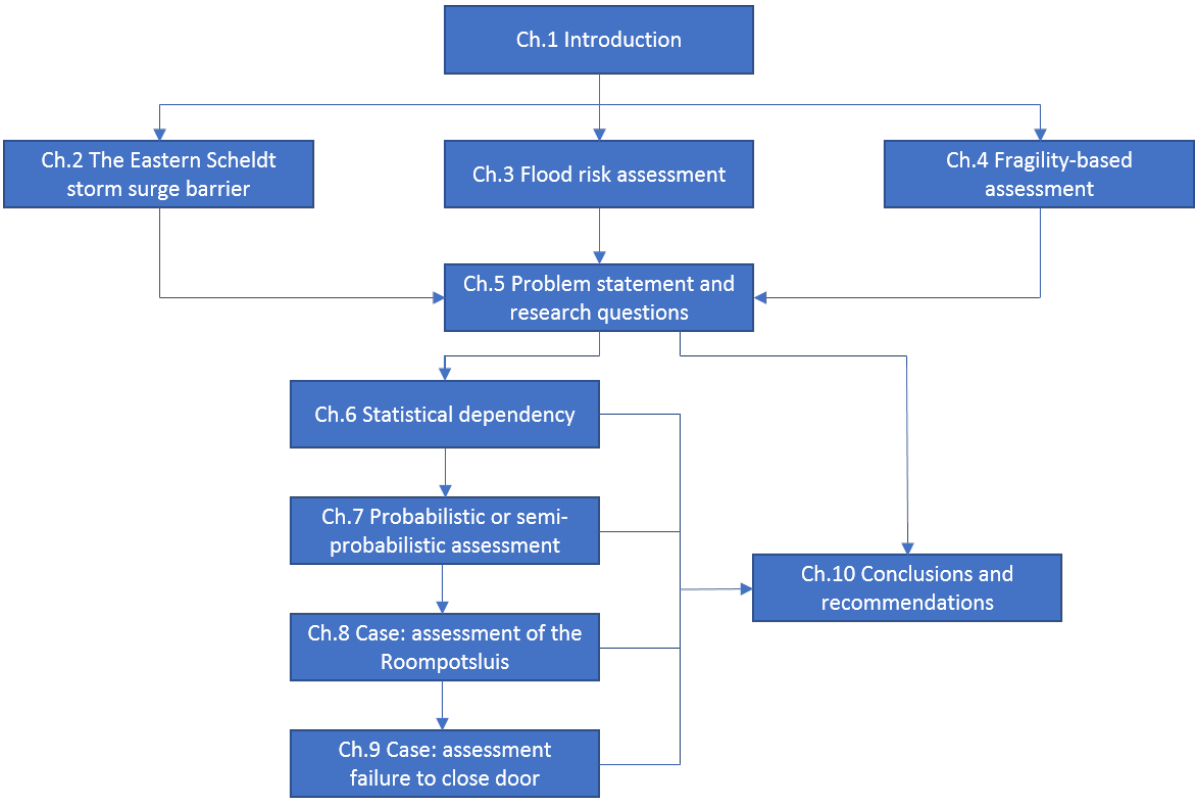

Figure 1.1: Overview report

2

The Eastern Scheldt storm surge barrier

This chapter will give an overview of the Eastern Scheldt barrier, as well as some terminology on storm surge barriers in general. The goal of this chapter is to show some aspects of the barrier, as well as the general complexity of the barrier.

The Eastern Scheldt barrier is situated in the Eastern Scheldt estuary and is a unique construction, both in scale and in function. Completed in 1986, it is one of the largest storm surge barriers in the world, having the largest cumulative span of any storm surge barrier at 2600m [42]. The barrier is the largest construction in the so called Delta-works, a grand-scale flood protection project initiated after the disastrous flooding in the Dutch province of Zeeland in 1953 [1]. Originally designed to fully close the Eastern Scheldt estuary, concerns regarding the environment led to a design change into a partially movable storm surge barrier [78]. Under normal conditions, the barrier would be open, which causes the basin to remain under the influence of the North Sea tide. During heavy storms (with a predicted water level of NAP+3.00m[12]), the barrier would be closed off, protecting the coast of Zeeland [83].

As a storm surge barrier, the Eastern Scheldt barrier protects an estuary, and features three types of elements; gated sections, dam sections and a lock. An overview of this general layout of a storm surge barrier, as well as the typical elements within a storm surge barrier can be seen in Figure 2.1 and Figure 2.2.

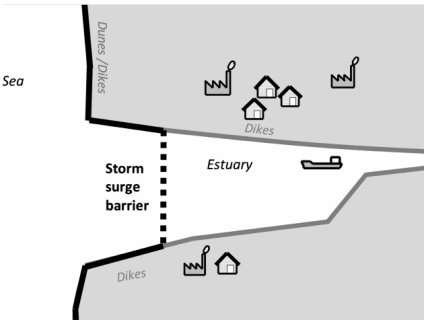

Figure 2.1: General layout of a storm surge barrier [42]

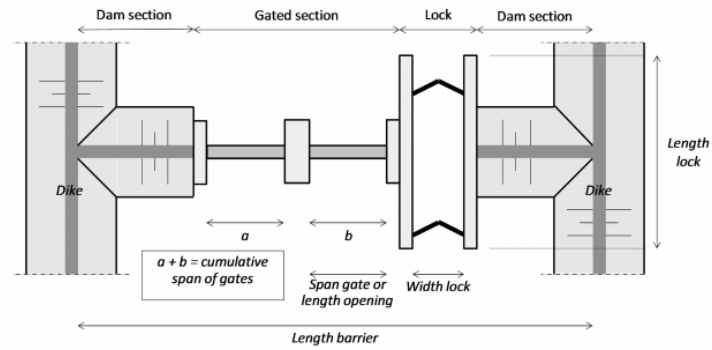

Figure 2.2: General elements within a storm surge barrier [42]

The gated sections of a storm surge barrier define this type of barrier. These are the parts of the barrier which can be closed off during heavy storms. The permanently closed parts of the barrier are called the dam sections. These can be dams, put these can also be (artificial) islands, which is the case for the Eastern Scheldt barrier. Most storm surge barriers also feature one or more locks, to allow for shipping [42].

When looking at Figure 2.2, it can already be seen that the complexity of the barrier can lead to complexity in the flood safety assessment. Different types of elements might require different assessments, while statistically dependent on each other through certain variables. As a result, scale models are often applied during the design phase [52].

As stated, the Eastern Scheldt barrier is one of the largest storm surge barriers in the world [42]. An overview of the barrier location as well as various parts of the barrier can be seen in Figure 2.3.

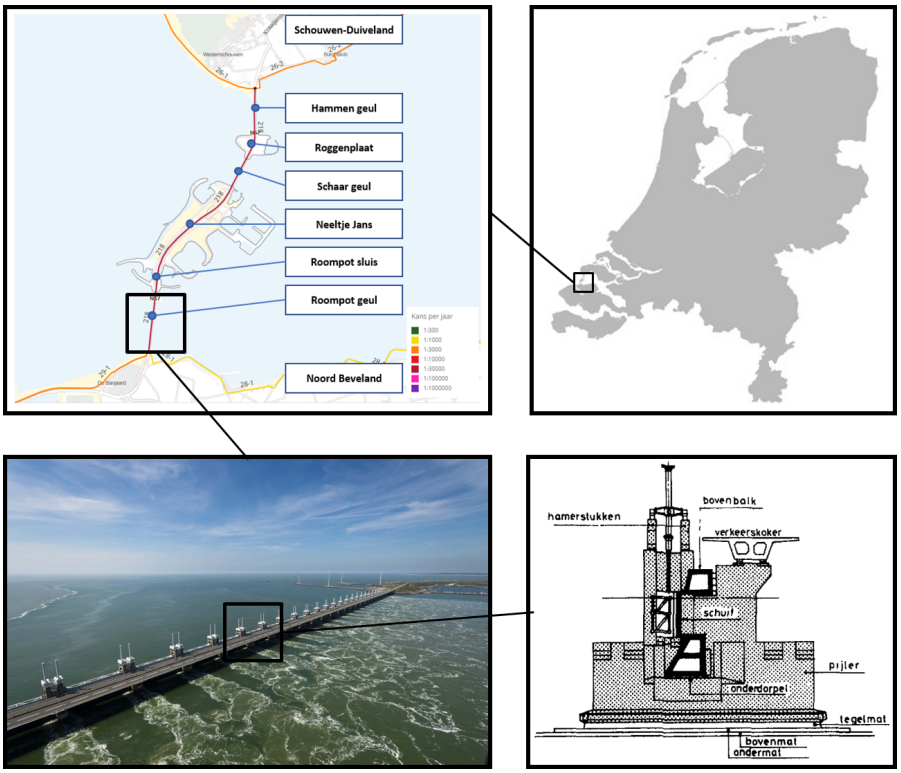

Figure 2.3: Top right: the location of the Eastern Scheldt barrier in the Netherlands [41]. Top left: An overview of the various parts making up the barrier (original source: [30], edit Fiolet, 2018). Bottom left: the gates of the Roompot barrier in open position [90]. Bottom right: Sketch of a pier [84]

The barrier can be seen to consist of two islands, which make up the dammed sections of the barrier. These islands, Roggenplaat and Neeltje Jans, were build as the first parts of the original design; a full close-off of the Eastern Scheldt estuary [83]. They are connected to each other and the Zeeland islands of Schouwen-Duiveland (to the north) and Noord-Beveland (to the south) by large, gated sections that cross the tidal inflow gullies. These barriers are referred to as the Hammen-, Schaar- and Roompot barriers, after the gullies they cross. On the island of Neeltje Jans a lock is situated called the Roompotsluis[1]. These elements will be discussed in some more detail in the next subsections.

2.1. The gated sections

When a water level on the North Sea of 3.00m+NAP is forecast, the barrier gates (which are open under normal conditions) will be shut, and the entire barrier will form a closed flood defence line. Over the entire barrier there are a total of 62 gates, with a flow carrying width of approximately 40 meters per gate when opened [83]. One of these gates can be seen in Figure 2.4, with different parts numbered. The flow gaps through the barrier are separated by piers (1), which are built on large caissons filled with sand (15) and connected to each other by two beams. The lower beam is called the sill beam (8). The sill beam closes the lower part of the gate (7). If the gate would be lowered directly onto the bed/bottom protection, the gap would never be able to be closed off perfectly, and high flow velocities through small gaps would quickly erode the granular material. The upper beam (6) closes the upper part of the gate. The piers also carry the traffic load, with the road supported by a large girder (10), which rests on top of the piers.

[1] It should be noted that there are various other parts making up the barrier which have not been included in this categorization. The gated sections of the barrier connect with the mainland and the islands with (quite permeable [23]) rubble dams for example. These rubble dams themselves connect to the mainland/islands with dam heads, also in itself a distinctly different type of flood defence. Additionally, there are various coupures in the dikes along the island, each of which could be seen as its own element within the barrier. These have not been included in this report, but all add complexity when assessing the barrier as a whole.

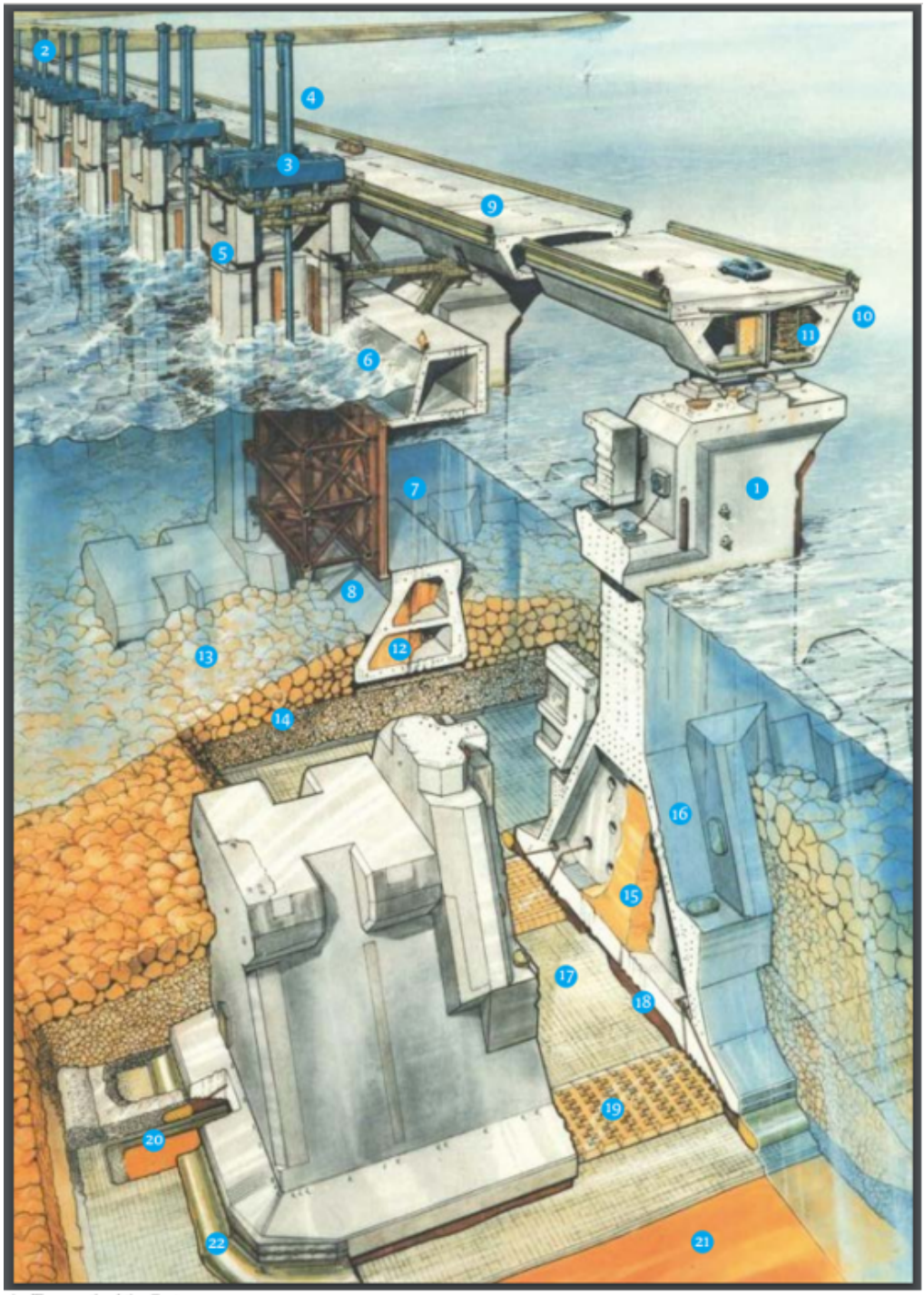

A. The mouth of the Eastern Scheldt
B. Piers in the construction dock
C. The storm surge barrier in detail
1 pier
2 quarry stone dam for land abutment construction
3 beam supporting operating equipment
4 hydraulic cylinders
5 capping unit
6 upper beam
7 gate
8 sill beam
9 road
10 road box girder and machinery for gate operation
11 power supply duct
12 sand filling of sill beam
13 top layer of sill
14 core of sill
15 sand filling of pier base slab
16 sill beam stops/bearings
17 upper mattress
18 grout filling
19 block mattress
20 bottom mattress
21 compacted sand under the bed of the Eastern Scheldt
22 gravel bag

Figure 2.4: Overview of the elements within the movable section of the barrier [49]

Between the piers, a sill has been constructed. This sill is made of various types of rock layers and bottom protections, which can be seen in Figure 2.5. It can be seen that the rocks forming the top layer, especially when near the barrier, have large dimensions, as the flow velocities over these stones can get very large. Especially when a gate would fail to close, for whatever reason (failure to close, breakdown of the gate), it was foreseen that the high water level difference over the barrier could cause extreme flow velocities through the gate [84]. This 'extreme situation' was during the design already marked as a potential danger [84]. On both sides of the gates a long bottom protection is present to keep potential scour far from the barrier [13].

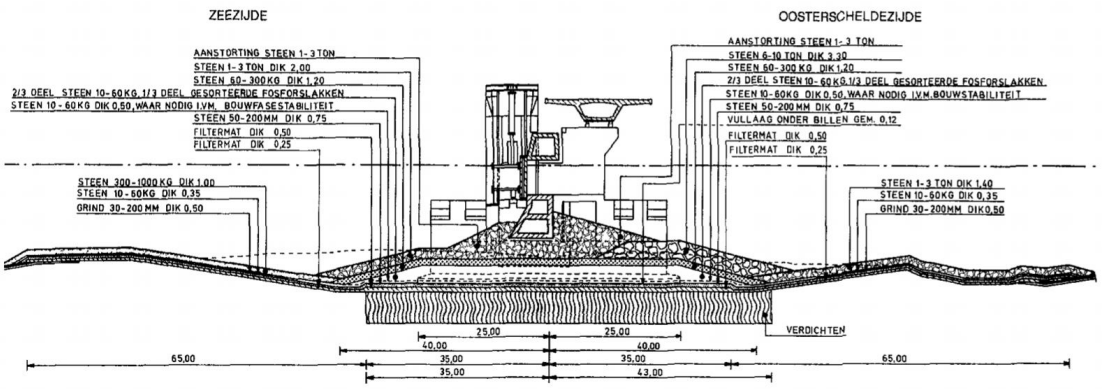

Figure 2.5: An overview of the many different rock classes making up the different layers of the sill [83]

2.2. The dammed sections

The islands of Roggenplaat and Neeltje Jans form the dammed section of the barrier. Originally, these islands where the beginning of a full, permanent closure of the estuary, but due to environmental concerns the design was altered. Nonetheless, these already constructed parts of the barrier were preserved and integrated in the new barrier design. Along the islands, a dike forms the primary water defence. These primary dikes have a crest height of 12.00m+NAP and are covered in grass and asphalt revetments [84]. The two islands can be seen in Figure 2.6 along with the location of the lock on Neeltje Jans. The dike crosses both islands approximately along a North-South axis. A secondary dike is present on western side of the Roggenplaat island, but this dike is not part of the primary flood defence and neglected in most safety assessments [23].

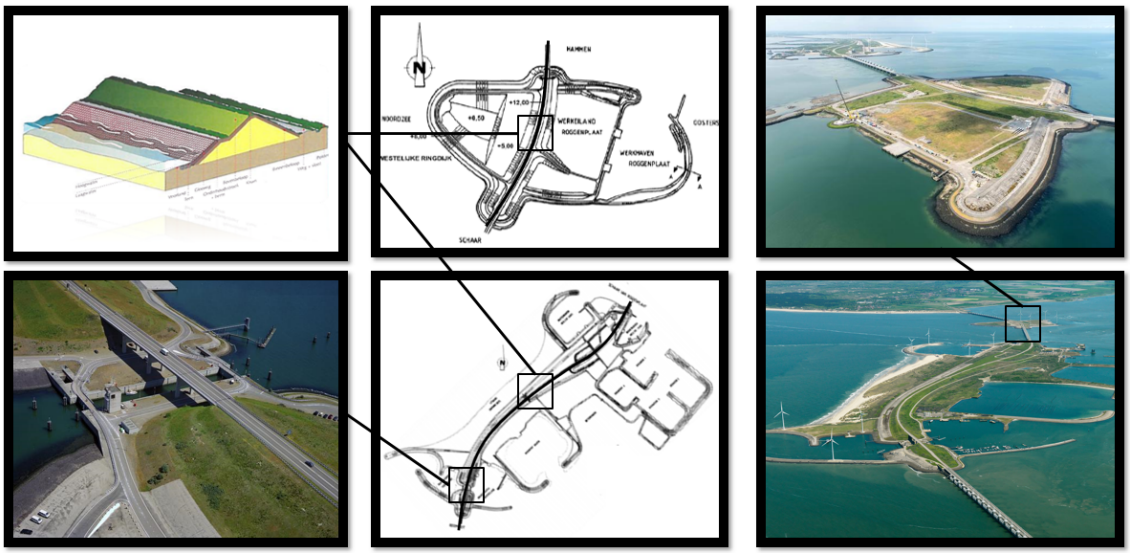

Figure 2.6: The islands of Roggenplaat (upper middle [85] and upper right) and Neeltje Jans (lower middle [85] and lower right), not to scale. The primary dike (example upper left) crosses both islands as indicated and the location of the lock (lower right) can be seen to be on the south end of Neeltje Jans

As the islands were already constructed before the design of the barrier was altered from a permanent closing into a storm surge barrier, the dikes on the island follow the original design for the most part. Nonetheless, there is no real 'integral' design for the dike on the islands [85]. Instead, the original design of the dike is locally fitted and adjusted, taking more functional design criteria into account (such as the design of the road and landscaping [85]). The only real hydraulic design criterion applied is the so called Delta criterium, which sets the maximum allowed overtopping. Although locally the original design is altered, the original design dimensions still give a good indication of the final design and can be seen in Figure 2.7.

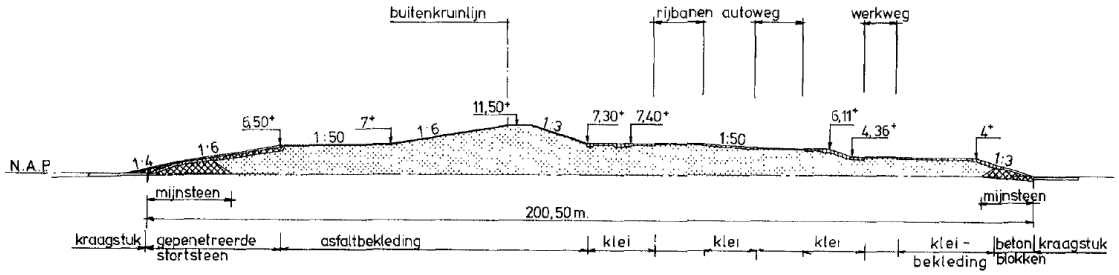

Figure 2.7: The original design of the Eastern Scheldt dam (Dutch). The most notable difference with the final design is the relocation of the road from the inner berm to the crest, raising the crest to a height of 12.00m+NAP [85]

2.3. The Roompot lock

The Roompotsluis is a lock situated on the southern end of the island Neeltje Jans, as can be seen in Figure 2.6. It forms a connection between the Eastern Scheldt and the North Sea for shipping. The lock has an entrance depth of -5.70m+NAP and a footprint of 100 x 16 m2 [85]. The lock has a foundation on steel and on both ends of the lock piping screens have been built into the ground. The top has a retaining height of 5.80m+NAP. This relatively low height (the original design water level is 5.50m+NAP) means that the lock is potentially vulnerable against overtopping [85][45]. The lock is situated in a coupure in the primary dike, which has a similar height of 5.80m+NAP [68]. The width of this coupure is approximately 100m. As the vulnerability of the lock and the coupure to overtopping was predicted in the original design, the coupure itself has been covered in protective revetment [84]. An image of the Roompotsluis can be seen in Figure 2.8.

Figure 2.8: An aerial photo of the Roompotsluis, [50]

2.4. Bottom protection repairs

The Eastern Scheldt barrier was constructed as part of the Delta works. These works were designed on the basis of the advises offered by the so called Delta commission. The Delta commission allowed for a probability of 1E-7 per year of parts of Zeeland to flood. This probability of Zeeland flooding meant that the Eastern Scheldt barrier was to be designed to withstand a storm with an expected exceedance frequency of 2.5E-4 per year [83]. Additionally, the barrier was designed to have an expected lifespan of 200 years. During design, the bottom protection was given a failure probability of 4E-6 per year.

This bottom protection has been reinforced several times however, due to concerns regarding the state of the bottom protection. The asphalt layer, which in the original design protected the bottom over a distance 110-270m out of the axis of the barrier. In the 90s this asphalt layer was reinforced with dumped stones, after damage to the asphalt was discovered [13]. The block mattresses, located at the end of the bottom protection, were reinforced with a filter layer of phosphor slags and a top layer of dumped stones and basalt [13].

When assessing a permit to allow the construction of a tidal power station in 2012, damage was found to the end of the bottom protection [38]. At the edge of the bottom protection large scour holes were discovered. These scour holes were predicted in the original design, but nonetheless the holes raised concerns. Most notable, the dikes of the Eastern Scheldt, on the banks of Noord-Beveland, were deemed vulnerable to instability as a result of these scour holes, as these dikes were not taken into account in the original design [38]. Additionally, the holes could lead to erosion below the block mattresses, which could lead to the edges of the different layers of bottom protection not overlapping correctly anymore.

The different concerns regarding the bottom protection behind the barrier has led to a lot of repair dumps, where additional stones were dumped on vulnerable areas and steep scour hole slopes. In Figure 2.9, an overview of the repair dumps until 2011 can be seen.

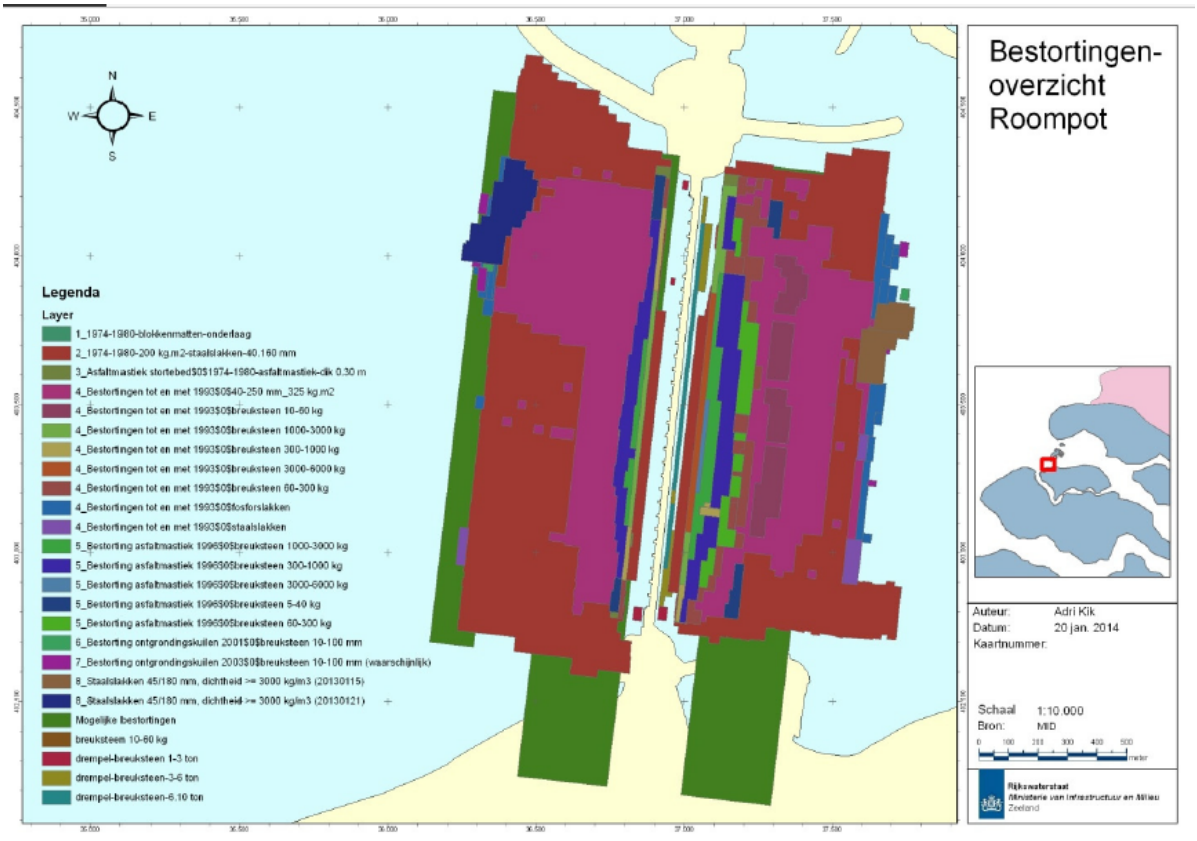

Figure 2.9: Overview repair dumps until 2011 [13]

3

Flood risk assessment

This chapter will give a short overview of flood risk assessment in the Netherlands, in order to get insight into the current available tools. By looking into the tools available, it can be seen where an assessment of the Eastern Scheldt barrier would fit, within the current assessment framework. Within the newly introduced Wettelijk BeoordelingsInstrumentarium 2017 (WBI2017), flood defences are to be assessed on the basis of risk, which has led to several changes in Dutch flood risk assessment; the change from an assessment per dike ring to an assessment per dike section, and the change from a exceedance probability to a failure probability. These two changes will first be discussed as they give insight into the underlying ideas of the WBI2017, as well as into the unsuitability of previously applied assessments. Subsequently, an overview will be given of the assessment tools available in the WBI2017.

3.1. Changes in flood risk assessment

Before 2017, flood risk was assessed per dike ring, meaning that a certain dike ring has a demanded safety that is uniform over the entire ring. The demanded safety was dependent on the inhabitants and infrastructure located in inside the ring, with the different dike rings visible in Figure 3.2. Studies showed however, that the location of a dike failure can greatly influence the resulting damages, as seen in Figure 3.1, which led to a reevaluation of this system [66]. A large flood safety study, called 'Veiligheid Nederland in Kaart' [35] (VNK2), calculated the probabilities and effects of a dike failure for all dike sections in the Netherlands and mapped the individual, economic and societal risks [36].

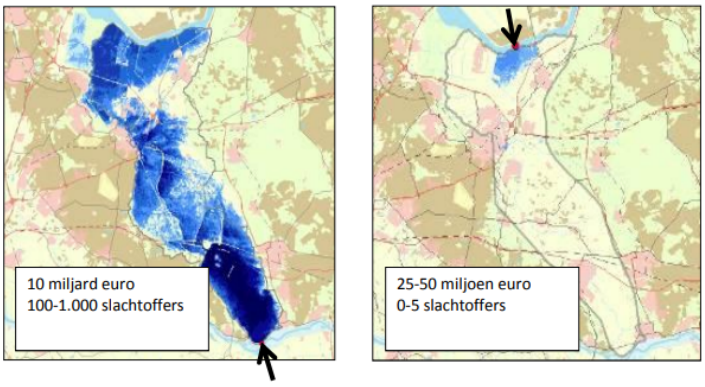

Figure 3.1: The different results of a dike failure within the same dike ring (Gelderse Vallei) [66] (Dutch)

Based on the risks calculated in these VNK2 studies, new safety norms were introduced per dike section. These new safety norms would have to guarantee that each inhabitant of the Netherlands would have a certain standard of protection, which was set to be a probability of being killed by flooding of less than 10^{-5} per year [66]. Additionally, more protection was given to locations with large groups of people living together,

potentially large economic damages and/or vital and vulnerable infrastructure [66]. This resulted in the dike norms applied in the WBI2017 [52], which can be seen in Figure 3.2. In this new system, dike sections were introduced, which allowed for different norms to be selected for different stretches of dike, which would previously be part of the same (uniform) dike ring.

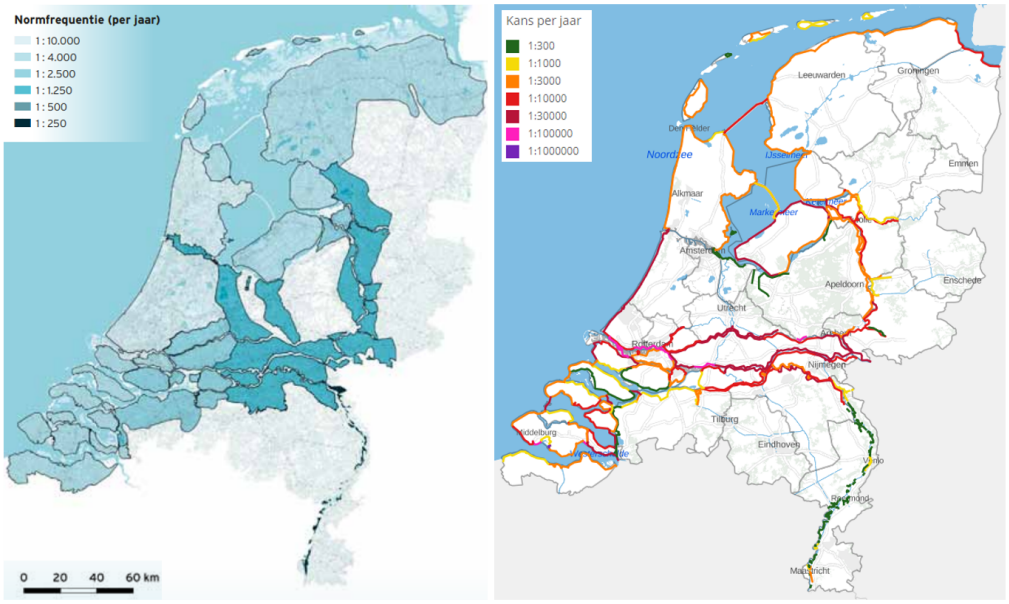

Figure 3.2: The dike rings and norm frequency (left) [35] and the new norms per dike section (right) [30]

As can be seen in Figure 3.2, the design and safety assessment of flood defences were previously based on a so called norm frequency. This means that a flood defence would be designed to withstand hydraulic conditions with a return frequency equal to norm which was given to the dike ring [66]. If a dike ring had a norm frequency of 1:4000 for example, all dikes in the ring would be designed and assessed for a design storm with a return period of 4000 years. With the new risk-based norms introduced in the WBI2017, based on the VNK2 studies, flood defences now needs to be assessed based on failure probability. This failure probability is the probability that the flood defence loses its water retaining capabilities leading to deadly victims and/or substantial economic damages [12]. As failure of certain forward barriers, such as the Eastern Scheldt barrier, does not immediately imply a flooding with deadly victims and/or substantial economic damages, the norms for these barriers are defined as the probability that the flood defence loses its water retaining capabilities leading to an substantial increase in the hydraulic load on the dikes behind the barrier [12]. As these new norms introduce a maximum allowed failure probability per flood defence, assessment of this flood defence requires the computation of a failure probability. As such, flood risk assessment needed to move towards more probabilistic assessment tools. These probabilistic assessment tools were applied through different assessment types, which will be explained further in Section 3.2.

3.2. Assessment types

The assessment methods described in the WBI2017 follow a prescribed procedure per failure mechanism [52]. Within this procedure, different assessment types are presented; simple, detailed and custom assessment[1].

Simple assessment

With the so called simple assessment (Dutch: eenvoudige toets), the applicability of a certain failure mechanism on a certain section of defence can be assessed. This simple assessment only checks whether the failure mode is applicable or negligible (or impossible), with the application of rules of thumb. Sometimes these rules are quantitative, but more often they are qualitative. If the occurrence of a the failure mechanism can

[1] Not all of these assessment types are described for every failure mechanism. Certain failure mechanisms, such as 'erosion of the crest and inner slope for grass revetments', cannot be ruled out with a simple assessment [55]. This means that at least a detailed assessment is always required. For other failure mechanisms, such as 'overpressure for asphalt revetment', no detailed assessment is offered [55]. This means that either the mechanism is ruled out with the simple assessment, or a complex custom assessment is necessary.

not be ruled out with the simple assessment, the detailed assessment is prescribed [52]. As the simple assessment is a very rough assessment, it introduces a very large amount of conservatism. An example of the application of the simple assessment would be the conclusion that the failure mechanism piping can be neglected when assessing a sand dike on a sand subsoil, regardless of the hydraulic loading on a structure [55]. An other example would be that no erosion will occur on an outer dike slope when the wave height is below 0.25m [55].

Detailed assessment
When a failure mechanism can not be deemed negligible through the application of the simple assessment, the detailed assessment (Dutch: gedetaileerde toets) is applied. In the detailed assessment a quantitative assessment is performed, with prescribed formulae [55]. For certain failure mechanisms a probabilistic assessment is offered, while for others a semi-probabilistic assessment is offered. As the name implies, the detailed assessment is more complex than the simple assessment, but it also offers reduced conservatism. An example of the application of the detailed assessment would be the calculation of the critical water level difference for which piping doesn't occur and comparing this to the occurring water level difference [55].

Custom assessment
When a failure mechanism fails the detailed assessment as custom assessment (Dutch: toets op maat) can be applied. Due to the nature of the custom assessment, there are very few guidelines described for it in the WBI2017. Rather the WBI2017 offers suggestions for custom assessments. These can either be a new assessment tool or approach, or the further reduction of conservatism through more detailed analysis. An example of a custom assessment can be an analysis of the residual strength of the dike after the occurrence of a failure mechanisms. An other example can be a probabilistic assessment, when the detailed assessment only prescribes a semi-probabilistic assessment [55].

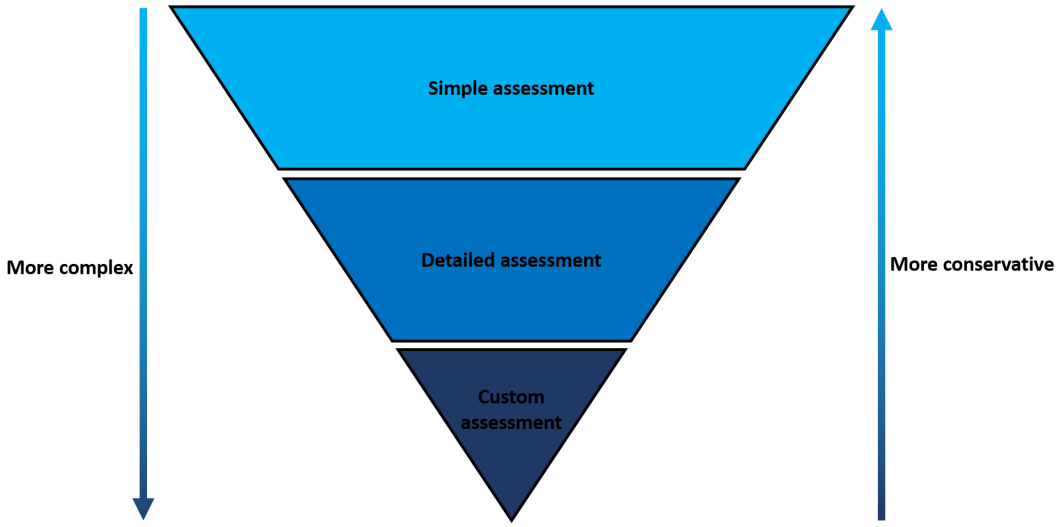

Figure 3.3: With more complex assessments, conservatism can be reduced

It is important to notice that the increase in complexity from simple to detailed to custom assessment offers an increase in accuracy. As an increase in accuracy means a reduction of the required conservatism, the custom assessment should always lead to a lower failure probability than the detailed assessment, while a detailed assessment will never fail a flood defence that was deemed safe with the simple assessment. As such, when a flood defence passes an assessment, a more complex assessment is not required. This can be seen in Figure 3.3. As a result of the changes in norm, one of the goals of the WBI2017 has been to introduce probabilistic assessment methods for as many failure probabilities as possible. After all, only when a probabilistic assessment is performed, the output is a failure probability. Nonetheless, these required probabilistic assessments as not yet fully developed (for all mechanisms). For mechanisms where the detailed assessment currently describes a semi-probabilistic assessment, the detailed assessment can either be replaced with a probabilistic assessment, or the probabilistic assessment can offer a custom assessment[2].

[2]Or be an additional custom assessment; as the custom assessment is not prescribed, various options can exist as custom assessment of a failure mechanism at the same time.

4

Probabilistics and fragility

As stated in Chapter 3, different assessment types exist within the WBI2017, in which a distinction is made between probabilistic and semi-probabilistic assessments. This chapter will give an overview on the concepts applied in probabilistic assessments, and extend these concepts into a fragility-based assessment tool. A short overview on some applications of the concept of fragility in flood risk can be found in Appendix F.

4.1. Strength and load

The concepts of strength and load are essential when performing a safety assessment. Whenever a construction or device is assessed, a comparison is drawn between the two concepts. These assessments usually take the form of a limit state function, also sometimes referred to as a Z-function. In this type of function the strength is compared to the load and whenever the load exceeds the strength, the function considers the construction as failed.

In most literature the strength of a construction is indicated by the term R for resistance. This strength term can be indicative of many different forms of strength. Examples include:

- The weight-carrying capacity of a column before buckling start to occur
- The discharge over a sill before its bottom protection downstream is damaged
- The amount of times one can bend a paperclip before it snaps due to fatigue

The loading term is usually denoted with the term S for solicitation. This term can indicate the loading that 'endangers' the construction by potentially exceeding R. For the examples listed above, examples of S could be:

- The weight a column carries
- The discharge over a sill
- The amount of times a paperclip is bend

Interestingly, for certain variables it is not always immediately clear whether they are a strength term or loading term. Some variables increase both the strength and load at the same time. Larger particle sizes of grains on a shore line might increase the strength against erosion, while the increased steepness of the shore it implies increases the reflection of waves, thus increasing the wave height and loading. However the underlying models or formulas for R and S are chosen, the transition between the real world and the modeled/theoretical world always brings uncertainties and/or inaccuracies. These can be caused by the simplification brought by the model, but also by the uncertainty in data. Consider the following fictional example:

When a stone is tested in laboratory conditions to determine the critical flow before it moves, the critical flow velocity can be found. The first stone might be found to have a critical flow velocity of 4.012 m/s. For the second stone this might be 4.276 m/s and for the third stone 3.429 m/s. These differences are mostly

caused by differences between the stones: the sizes slightly vary as does the density for example. These are examples of spread/uncertainty in strength, R. The loading, S, might also not be constant however: there might be a varying amount of turbulence, which makes the local flow velocity around a stone different for similar (average) flow velocities in the flume in which the stones are tested. Both the strength (R) and the load (S) thus have a certain amount of uncertainty. If a model is set up to predict the critical flow velocity of a stone, this model is often based in empiricism (Shields, Izbash, etc.) and relies on fitted coefficients. This brings model uncertainty, which also represents a form of variability [1]. These different types of uncertainty can be expressed in the form of a so called probability density function (PDF). The PDF of a stochastic variable shows the distribution of the likely values that a variable can take, with the surface below the PDF equal to the probability of occurrence. When the PDF's of both R and S are plotted, the probability of R<S can be seen in the area under R or S where R<S. This area has been shaded red in Figure 4.1.

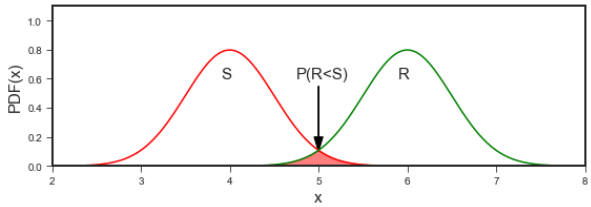

Figure 4.1: Variability in R and S expressed as PDF's

4.2. Fragility curves

When only the uncertainty in strength is considered at first, a certain distribution of the values of R can be found. This can be a normal distribution for the critical flow velocities of the stones considered earlier for example. The probability density function (PDF) of a normal distribution with mean (μ) 4.0 and standard deviation (σ) 1.0 can be seen in Figure 4.2. Often one is interested not in the probability of values for R however, but in the probability of (non-)exceedence of these values for R. Instead of the probability density, the cumulative density offers this insight. The cumulative density function (CDF) for the distribution with $\mu = 4.0$ and $\sigma = 1.0$ can be seen in Figure 4.2. As the surface below a PDF indicates a probability, the CDF is the integral of the PDF.

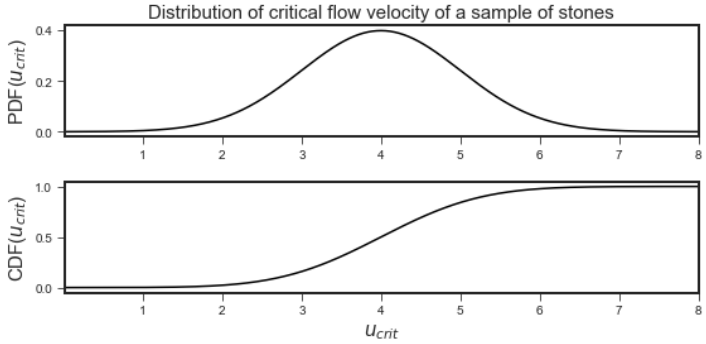

Figure 4.2: PDF (above) and CDF (below) of critical flow velocity (example distribution not based on physics!)

The CDF of the strength is an indication of the uncertainties in strength. This means that all strength uncertainties, such as in the example of the stones, the different stones sizes, densities, the manner in which they are laid down, etc, are within this graph. For each given value along the x-axis of this CDF, the CDF gives the probability that R is smaller than this value. As such, the CDF gives the conditional failure probability along the values displayed on the x-axis; the probability of failure, if S were equal to that value. This set of conditional probabilities is called a fragility curve. If a fragility curve of the entire distribution of R is constructed,

[1] Model uncertainty also occurs in purely theoretical models that are not based on empiricism. The empiricism is mentioned here as an example as it makes it conceptually easier to understand model uncertainty. Since all models are simplifications of reality, by definition, all models introduce model uncertainty.

it is equal to the CDF of R. More often however, only a part of R is considered, such as a single loading parameter. As the fragility curve only contains data from the 'strength part' of the assessment, it cannot in itself be used for the safety assessment. After all, the loading is not yet considered: in the fragility curve only discretized values of the loading are presented (on the x-axis), without any description on the likelihood of these values occurring. Each load on the x-axis is thus assumed as a deterministic scenario; if this load where to occur, this conditional failure probability would follow.

In other words: for each of these deterministic loading scenarios a conditional failure probability is plotted in the fragility curve: the probability that the strength, R, is lower than the load, S, considered on the x-axis. When the system as a whole (strength and load) needs to be assessed, the probability of occurrence for these loading scenarios is introduced. This probability of occurrence can be in the form of a PDF of the loading variables considered. This can be seen in Figure 4.3.

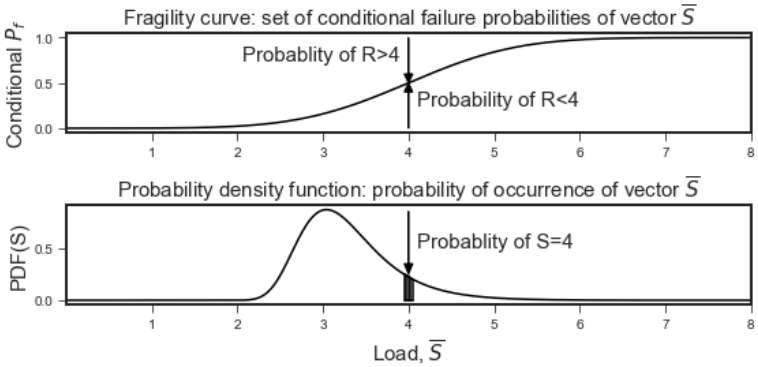

Figure 4.3: Fragility curve and PDF(Load)

The probability of occurrence of the loading scenario is determined by the surface below the loading PDF[18]. This means that the probability of a single, exact, value is always 0, as the width of this surface is 0. This makes sense, as in our analog 'real' world, values that aren't integers don't take exact values. A probability from a PDF can thus only be given for an interval. In Figure 4.3, the interval [3.95,4.05] is shaded for example. As the probability space below the entirety of the PDF has to add up to 1.0 (as the loading variable has to always have a value in the real world), this means that integration of the fragility curve over the entire loading PDF (meaning all possible loading scenarios are considered) leads to the failure probability of the system for all possible scenarios.

This is known as the law of total probability, where the failure probability in each scenario is multiplied by their respective probability of occurrence and then summed. The law of total probability can be seen in Equation 4.1. As the amount of scenarios considered becomes larger, this summation approaches the integral of the fragility curve multiplied by the PDF of the load.

$$P(F) = \underbrace{\sum_{i=1}^{n} P(F|S_i)P(S_i)}_{\text{Law of total probability}} = \int_{-\infty}^{\infty} \underbrace{P(R<S|S)}_{\text{Fragility curve}} \underbrace{f(S)}_{\text{PDF(S)}} dS \tag{4.1}$$

As stated above, traditionally, R and S are assessed in a so called limit state function or Z-function. This limit state function usually takes a form comparable to Equation 4.2, where the system fails when $Z < 0$. R and S can be expressed as functions of a set of stochastic variables, X_1, X_2,...X_n.

$$Z = R - S \quad \text{, where} \quad R = f(X_1, X_2, ..., X_n) \quad \text{and} \quad S = f(X_1, X_2, ..., X_n) \tag{4.2}$$

When a fragility curve has to be constructed, S is taken to be a deterministic vector or set; $\overline{S}$. This means that for each value of S_i out of $\overline{S}$ considered, a 'simplified' limit state function[2], Z_i, can be determined, see

[2] Simplified indicates that the loading variables that were previously a full distribution are now replaced by a deterministic value, S_i. As such, the amount of variables in the limit state function (now called Z_i instead of Z) is reduced, which can mean that it requires significantly less computational effort to solve.

Equation 4.3. The loading is thus now considered as a set of known deterministic values (to be plotted on an axis), but R is still the function of a set of underlying stochastic variables. Hence, the fragility curve only contains uncertainty from the strength part of the assessment.

$$\text{for} \quad S_i = \underbrace{s_1, s_2, ..., s_n}_{\text{Set of loading scenarios, } \overline{S}} \quad : \quad Z_i = R - S_i \quad \text{and} \quad \underbrace{P(F|S_i)}_{\text{Conditional } P_{f,i}} = P(\underbrace{f(X_1, ..., X_n)}_{\text{Distribution}} < \underbrace{S_i}_{\text{Deterministic}}) \tag{4.3}$$

In order to solve for the failure probability (Equation 4.1) in a fragility based method, two steps are required:

First an iteration of probabilistic reliability methods has to be applied, in order to solve Equation 4.3 for all elements in set $\overline{S}$. This iteration computes a set of conditional failure probabilities, i.e. the fragility curve. This means that for the computation of each point on the fragility curve (Conditional $P_{f,i}$), a full probabilistic assessment of the limit state function, Z_i, is required. This probabilistic assessment can be done through a level II (e.g. FORM) or a level III (e.g. Monte Carlo) calculation[3]. Several probabilistic reliability methods are discussed in Section 4.3. The construction of a fragility curve (the first step in the assessment) can be seen in Figure 4.4.

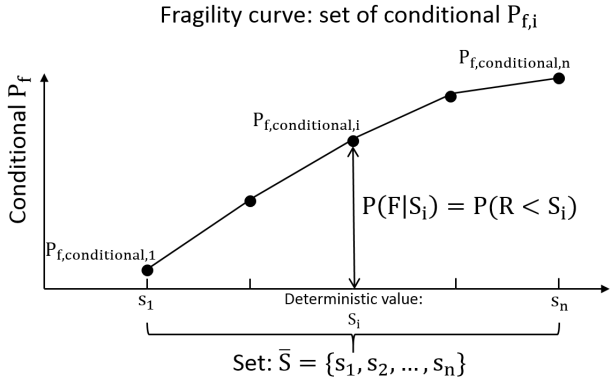

Figure 4.4: Fragility curve construction

These multiple probabilistic assessments mean that computational effort required for a fragility based method is significantly longer than for a traditional probabilistic assessment of the limit state function. After all, this traditional probabilistic assessment needs to be done a multitude of times[4]. It also means that, as the resolution rises/the number of points is made larger, the computational effort required increases rapidly. This becomes of greater concern when the amount of loading parameters is increased, and the fragility curve is extended into a 2-dimensional (or multi-dimensional) fragility surface. Here the main disadvantage of a fragility curve based methodology is found, requiring increased computational effort.

The second step of the assessment is the integration of the fragility curve (the set of conditional failure probabilities computed with Equation 4.3) over the loading conditions. This step thus solves Equation 4.1, by summing the conditional probabilities through the law of total probability.

4.3. Probabilistic reliability methods

When considering a limit state function, either in the form of a traditional function like in Equation 4.2 or in the form of a fragility based function like in Equation 4.3 (which iterates slightly varying, simplified limit state functions), the failure probabilities described by these functions can be computed with several reliability methods. These methods can be grouped into 4 levels (of increasing complexity/computational effort) [37]:

Level I methods are semi-probabilistic, meaning that the full distributions of the variables are no longer applied. Instead, in a semi-probabilistic approach, a safety factor is applied over the mean of distribution. This

[3] In literature other types of probabilistic assessments can be found as well [64]. In the past fragility curves have been constructed using expert judgment as the probabilistic assessment. In the electronics industry fragility curves have been constructed with empirical plot fitting. These types of fragility curves will not be considered in this report, unless indicated otherwise.

[4] The computation time per probabilistic assessment may be shorter, but the overall assessment takes significantly longer.

safety factor stands for a safe enough value for a distribution. The WBI2017 is based on a semi-probabilistic approach [20] (although it is calibrated by a fully probabilistic approach [34]).

Level II methods are based on approximating the distributions of variables with normal distributions. These variables are then modelled by a mean and a standard deviation. This means that the joint distribution of the variables is simplified. The computational effort required is reduced as well by linearizing the limit state function. This is usually done through a First Order Reliability Method (FORM) or a Second Order Reliability Method (SORM, which models the limit state quadratic instead of linearly). The FORM analysis will be explained in Subsection 4.3.1.

Level III methods are numerical models, where the full, original distributions of variables are applied. Numerical integration is used to calculate failure probabilities, which is an exact method. The Monte Carlo simulation is a well known example of a level III reliability method. Level III methods are not always applicable, as the computational effort grows with growing numbers of variables. Monte Carlo simulations will be explained in Subsection 4.3.2.

Level IV methods are risk based analyses, where the consequences/costs of failure are taken into account. Risk is used as the measure of reliability, where normally probability is the main measurement. Level IV methods are not considered in this report.

4.3.1. FORM analysis

The FORM analysis is known as a fast, level II, probabilistic method, which is the main reason of its usage [20]. Two simplifications make this fast analysis possible. Firstly, the variables underlying the limit state are assumed to be distributed normally. This leads to limit state that is normally distributed as well [37]. Secondly, the limit state function is assumed to be linear. When the limit state is linear, the statistical moments of the limit state can be computed[37]. These simplifications mean that the reliability index and thus failure probability can be computed by calculating the probability that the limit state is negative. If the limit state function is not linear (the second assumption), which will often be the case, a linearization is done. This linearization can be done through a taylor expansion for example. This linearization is applied in the so called design point, see Figure 4.6. The design point is defined as the most probable combination of variables for which failure (Z=0) will occur. An illustration of the design point can be seen in Figure 4.5 and Figure 4.6.

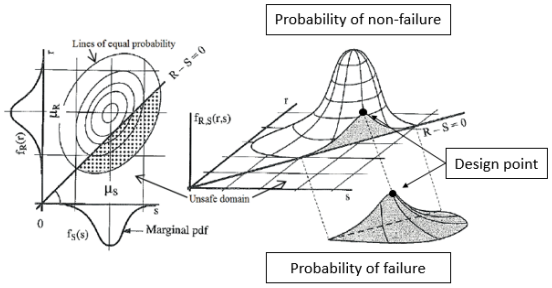

Figure 4.5: Design point in probability space [37]

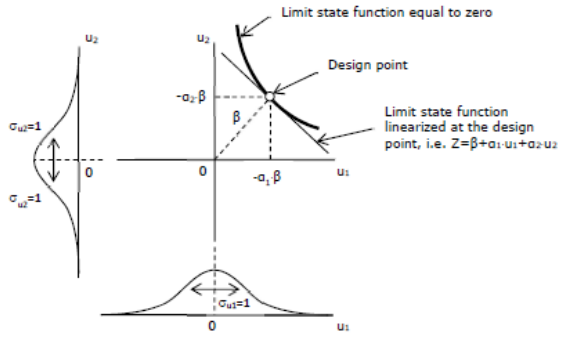

Figure 4.6: Reliability index and importance factors in standard space [20]

When the design point is calculated (in standard space), the reliability index is the shortest distance between the limit state and the origin. This can be seen in Figure 4.6. The projection of the design point to the marginals gives the importance factors, this can also be seen in Figure 4.6. The importance factors give an indication of the amount of influence that each variable has. For certain limit state functions a FORM analysis can experience convergence problems. This is mainly due to strongly non linear limit state functions or to the existence of local maxima/minima [88]. These can lead to large errors in the outcome of FORM analysis. For this reason the FORM analysis is not applied in this report. Instead, a numerical Monte Carlo simulation is applied.

4.3.2. Monte Carlo simulation

A numerical Monte Carlo simulation, which is a level III method and thus exact, takes many samples from all variables and tries many combinations for which the value of the limit state function is calculated. The failure probability is then calculated by dividing the amount of failed limit states by the total amount of limit states calculated. Due to the high number of samples and limit states considered the Monte Carlo simulation is computationally expensive [64], but it can be applied in all situations (unlike the FORM analysis). An example of the output of a Monte Carlo simulation can be seen in Figure 4.7.

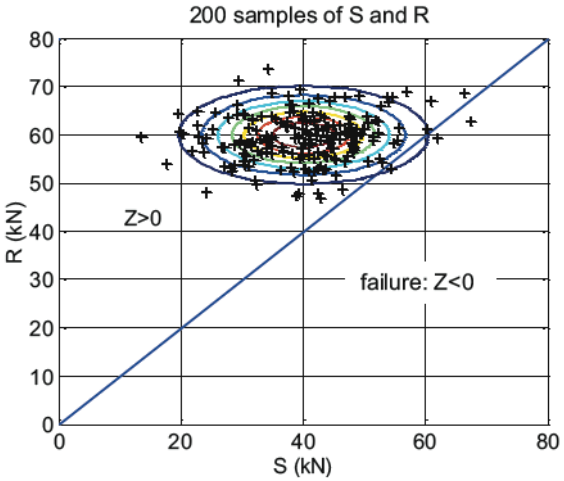

Figure 4.7: Monte Carlo simulation, with the line showing the limit state Z=0. The failure probability is 3/200 in this example [37]

Several techniques exist to increase the efficiency of this sampling process, such as Latin Hypercube Sampling (LHS), which reduces the amount of randomness in the sampling to get a more evenly spread sample output [15]. Additionally several intelligent Monte Carlo techniques exist to increase the efficiency of the simulation. In this report subset sampling will be applied.

4.3.3. Subset sampling

When a small or very small failure probability needs to be computed with a Monte Carlo simulation, computational costs can quickly grow large. After all, to accurately compute such a probability (P_f) at least $1/P_f$ samples would be needed (on average). For a failure probability in the order of 1E-4 for example, at least 1E4 samples are required (more if a higher accuracy is required). Several intelligent Monte Carlo techniques have been developed to reduce this computational effort, such as importance sampling (which shifts the sampling towards the limit state), directional sampling (which samples in specified directions to locate the distance to the limit state in that direction) and stratified sampling (which divides the samples into exclusive and exhaustive groups).

As an alternative to compute such small probabilities, Au and Beck (2001) [5] developed subset sampling. Subset sampling attempts to decompose a small probability failure event into a sequence of conditional events, that have a higher probability of occurrence. These larger probabilities can be computed against lower computational costs.

Consider a sequence of conditional events, each a subset of the next, so that:

$$F_1 \supset F_2 \supset ... \supset F_M = F \tag{4.4}$$

Where m is the number of intermediate conditional failure probabilities that are defined. Failure is then defined as the failure of all sub-events:

$$F_k = F_1 \cap F_2 \cap ... \cap F_m, \quad \text{for} \quad k = 1, ..., m \tag{4.5}$$

Since the final (and 'real') failure state, M, is defined as $F_M = \{u : Z(u) \leq 0\}$; the probability that limit state function Z(u) is smaller than zero, the intermediate failure states, i, can be defined as $F_i = \{u : Z(u) \leq C_i\}$,

where $C_1 > C_2 > ... > C_M = 0$; the probability that limit state function Z(u) is smaller than a given value, C_i. The value for C_i is made smaller as the final failure state, where $C_i = C_M = 0$, is approached. By choosing the values for C_i, and thus the intermediate failure states, a certain (targeted) failure probability per intermediate state $P(F_i|F_{i-1}) = p_0$ can be reached. Au and Beck (2001) [5] suggested a value of 0.1 for p_0, which is followed in this report.

The failure probability can then be calculated as a sequence of conditional probabilities, when the law of total probability is applied:

$$P(F) = \underbrace{P(F_m|F_{m-1})P(F_{m-1})}_{\text{Law of total probability}} = \underbrace{P(F_1)}_{\substack{\text{First probability} \\ \text{estimate}}} * \underbrace{\prod_{i=2}^{m} P(F_i|F_{i-1})}_{\substack{\text{Sequence of conditional probabilities} \\ \text{generated with Markov Chains}}} \tag{4.6}$$

An illustration of this first probability estimate and sequence of subsequent conditional probabilities can be seen in Figure 4.8.

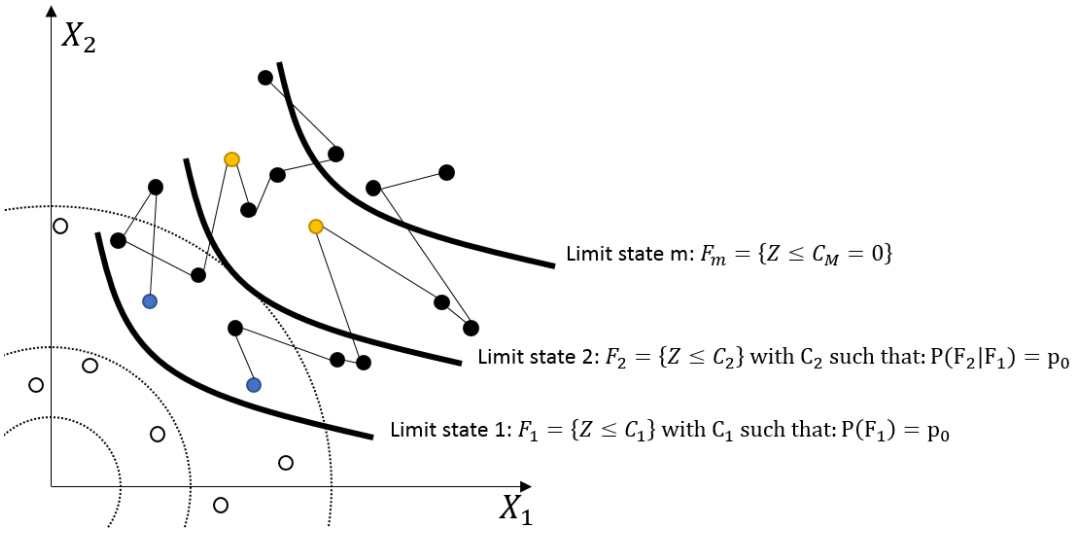

Figure 4.8: Subset sample generation using Markov chains to generate sequence of conditional samples, with example p_0=0.25

A subset simulation thus works by first performing a Monte Carlo sampling simulation. This can be seen in Figure 4.8 as the 6 white dots and 2 blue dots as drawn samples. Considering these first samples, a limit state F_1 is drawn, by choosing C_1 such that $P(F_1) = p_0$. This is done by setting C_1 equal to the p_0-percentile of the samples (so that a fraction of the samples with size p_0 will fail, per definition). The shape of the limit state is determined by the limit state function Z under consideration. These failed samples (indicated as the two blue dots) are starting points (seeds) for a Markov chain. A Markov chain is, simply put, a sequence of events without memory, meaning that each new step is dependent only on the position of the current point. A Markov chain can be used to build a random walk as sampling procedure. This is called Markov Chain Monte Carlo sampling, or sometimes a Metropolis-Hastings algorithm [6]. The samples drawn from this all exist in the failure domain of limit state 1: they are conditional on F_1 and thus can not cross into the space $Z > C_1$. From the new set of drawn samples (the first 4x2 dots drawn from the blue dots), a new failure state is drawn, such that $P(F_2|F_1) = p_0$. The samples that failed this limit state (indicated as the 2 yellow dots) indicate conditional failure $F_2|F_1$. A new Markov Chain Monte Carlo sampling simulation is started, within the conditional failure space F_2, applying the failed samples from $F_{i-1} = F_1$ as seeds. This sequence is repeated until limit state M is reached: $F_m|F_{m-1}$. This final limit state is reached when the p_0-percentile becomes negative, as this indicates $C_i < 0$, which implies that the original limit state function, $Z \leq 0$, has been reached.

This report will mostly apply subset sampling algorithms to solve limit state functions, due to the efficiency in solving for low failure probabilities. For additional information regarding subset sampling this report refers to [4], [5] and [6].

4.4. Transfer probabilities

The transfer probability[5] describes the probability of failure of a system given the failure of a subsystem. In past safety studies regarding the Eastern Scheldt barrier, these transfer probabilities have been identified as a knowledge gap when assessing the barrier for flood safety [13]. The transfer probabilities between the failure of/damage to the bottom protection and failure of the barrier are the probability of failure of the barrier given failure of the bottom protection, which is thus a conditional probability:

$$P_{\text{f,barrier}} = P_{\text{f,bottom protection}} * \underbrace{P_{\text{f,barrier}|f,\text{bottom protection}}}_{\text{Transfer probability},P_{\text{transfer}}} \tag{4.7}$$

In past safety studies, the transfer probability was a deterministic value, independent of the failure probability of the bottom protection (set to 1[13], which is conservative). This independence is not physically sound however, as failure due to a failing bottom protection is caused by the formation and instability of a scour hole, and the stability of this hole is determined by its size and geometry [61]. These are dependent on the flow characteristics, as is the failure probability of the bottom protection [61]. In other words, the transfer probability should be determined by the conditions under which the bottom protection fails. If the failure probability of the bottom protection is a function of distributions R and S, then the transfer probability is a function of a different distribution R and a specific s_i out of the distribution S. In a traditional probability assessment this is problematic, however a fragility based method (which assesses failure probabilities at all scenarios s_i out of the set/distribution of S) is well suited for this purpose. For each loading scenario, the conditional failure probability of the bottom protection is calculated, as well as the conditional consequence; the transfer probability. The transfer probabilities (now conditional on the load) can then be assessed accurately:

$$\text{for} \quad S_i = s_1, s_2, ..., s_n: \quad P_{\text{f,barrier}|S_i} = \underbrace{P_{\text{f,bottom protection}|S_i}}_{\text{Conditional failure probability}} * \underbrace{P_{\text{transfer}|S_i}}_{\text{Conditional consequence}} \tag{4.8}$$

4.5. Comparison between fragility based and traditional methods

As aforementioned, probabilistic assessment tools exist and these are well capable in assessing a limit state function and resulting failure probabilities. A fragility based methodology basically consists of a multitude of these assessments, for every deterministic loading scenario. Computational effort is thus increased for a fragility based method, which can be a problem depending on the reliability method applied. Depending on the assessment, this increase in computational effort might be justified, as fragility based methods can offer some advantages over traditional methods.

When insight into failure mechanisms and behaviour of a limit state function is important, a fragility curve based method can offer this increased insight. If fragility curves are constructed for different parts of structures, the behaviour of a structure under varying circumstances can be mapped for example, which might allow for a risk based maintenance routine. If parts of a structure require maintenance, which would increase the load on different parts of the structure, the computational effort increase of a fragility curve based method might be justified to show the effect of this load reassignment [12]. These types of insight increasing effects are explored in Chapter 8. Additionally, the statistical dependency within systems can be controlled in various ways due to the separate assessment of strength (R) and load (S). When more complex structures, such as the Eastern Scheldt barrier are to be assessed, this control of dependency might be necessary to take various failure mechanisms into account for example. Due to the separate assessment of R and S the dependency within R and within S can does not have to be equal. This effect is in Chapter 6. Finally, the consequences of failure can be made conditional when this is required. This is mainly of use for indirect failure mechanisms, such as failure of a bottom protection in this report. These conditional consequences of failure can allow for a better assessment of transfer probabilities, explored in Chapter 9.

[5]The transfer probability is a conditional probability, as can be seen in Equation 4.7 and traditionally is often referred to as the conditional probability. In this report a case will be presented to make this transfer probability conditional on the loading scenario under which it occurs, S_i. To avoid confusion, the term transfer probability will be applied in this report. As such, the term conditional transfer probability can be used to indicate a transfer probability conditional on a loading scenario, as seen in Equation 4.8. The term "conditional$_{\text{on loading scenario } S_i}$, conditional$_{\text{on failure bottom protection}}$ probability" is considered by the author as being too confusing.

5

Problem description and research questions

In the first part of this report, 3 subjects have been explored. First, the Eastern Scheldt barrier was introduced, as a complex flood defence in Chapter 2. Secondly, the recent changes in Dutch flood risk assessment were described in Chapter 3. In this chapter it was also explained how flood risk assessments can be categorized into different types, of varying complexity. Thirdly, a new assessment type was introduced, with fragility-based assessment. This chapter will give an overview of the main findings in these previous chapters and pose the research questions of this report.

5.1. Problem description: custom assessment Eastern Scheldt barrier

In Chapter 2, it can be seen that the Eastern Scheldt barrier is composed of different types of flood defences, with dikes covering the islands, a lock situated in a coupure, and gated sections of barrier of different sizes. These different types of elements make the barrier unique, as well as very complex and as such a custom assessment of the barrier is always required when assessing for safety [23]. As previous assessments can no longer be applied, due to the changes in Dutch flood risk assessment described in Chapter 3, a new custom assessment will need to be developed for the current assessment round [23]. While unique and complex in form and scale, the function of the Eastern Scheldt barrier is unusual as a flood defence as well. The barrier is functions as a so called forward barrier [53] (Dutch: voorliggende kering). Forward barriers are barriers that do not directly defend the hinterland, but instead reduce the load on the flood defences behind it. Other examples of this type of barrier include the Afsluitdijk and the Maeslantkering [53]. Forward barriers are rather unique and therefore described as a special category of barrier [53] as the approximations applied in the semi-probabilistic assessment methods of the WBI2017 are less applicable and thus a custom assessment (again, but for different reasons) is required [23].

Considering the background described at in Chapter 1 and Chapter 3, of a changing WBI2017, combined with this already existing need for a new custom assessment for the Eastern Scheldt barrier (due to the complexity of the barrier and the subsequent unsuitability of the WBI2017 methods), Rijkswaterstaat has voiced the necessity for a new assessment method for the Eastern Scheldt barrier and was interested in knowing what the best assessment strategy for the barrier would be. This question was posed to Witteveen+Bos in a first scope study [12]. A secondary objective within this report was to study whether the assessment could offer increased insight into the processes governing the complex system of the barrier. The reason for this was twofold. Firstly, as the years since the construction of the barrier have gone on, less builders and engineers that were involved during the design and construction of the barrier were still involved. To keep knowledge and insight into the barrier available (especially when considering the need for risk-based management and maintenance), a non-black box model was therefore preferred [12]. Secondly, an assessment strategy applicable to the Eastern Scheldt barrier could serve as a blueprint for the assessment of other forward barriers in the Netherlands, such as the aforementioned Afsluitdijk and Maeslantkering. The development of a new assessment strategy could thus contribute to the insight into the assessment of forward barriers (which are

all difficult to assess with current WBI2017 methods) [12]. The study by Witteveen+Bos, 2017 concluded that an assessment based on the concept of fragility could offer the type of assessment that Rijkswaterstaat was interested in. The main disadvantage of a fragility based assessment, it was concluded, would lie in the unfamiliarity of the hydraulic engineering community with this reliability method and the fact that no methods or software applying the methodology currently exist. Considering this, the first step forward advised by the study was to start with a proof of concept of a fragility-based assessment.

5.2. Research questions

The requirement for a fragility-based assessment of the Eastern Scheldt barrier forms the *direct basis* for this report and, together with the aforementioned *background*, forms the research questions. This report will assess whether the methods offer advantages over current assessment tools and attempt a custom, probabilistic assessment of the Eastern Scheldt barrier. As such, the main research question and sub-questions of this report will be posed:

How can a fragility-based reliability method be developed and applied in a custom and probabilistic safety assessment of the Eastern Scheldt storm surge barrier and other complex flood defences?

- How can a fragility-based reliability method be applied to offer an assessment?
- How can statistical dependency be taken into account in a fragility-based assessment?
- Can a fragility-based custom assessment be shown to be less conservative than a detailed assessment?
- How can a fragility-based reliability method be applied to offer a custom assessment of a unique flood defence, such as the Eastern Scheldt barrier?
- Can a fragility-based assessment offer increased insight into the processes that influence the failure probability?

Within these questions, there are two distinct components; the development of a new fragility-based assessment method and the assessment of the Eastern Scheldt barrier. These two components are conflicting however, as the development of a new methodology involves depth, while the assessment of the barrier involves 'completeness'/assessment of a lot of failure mechanisms. As this report is written as a master graduation thesis, in which only a limited amount of time and resources are available, the scope of a full assessment of all failure mechanisms was deemed to large. Therefore, a decision was made to focus on the development of this new methodology, while assessing a limited number of failure mechanisms. Past safety studies [67][13][45] have been consulted to identify these failure mechanisms. A summary of these studies can be found in Appendix C. The safety studies done in the past all point to the assessment of the bottom protection as well as the height of the lock as the most relevant failure mechanisms for the Eastern Scheldt barrier.

This report will focus on these two mechanisms, while developing an assessment tool that is probabilistic (as requested by the background of a changing WBI2017 [52]) and offers insight (as requested by Rijkswaterstaat [12]). Additionally, this assessment tool should offer increased applicability to unique (forward) barriers, as this is limited for the current available semi-probabilistic tools [12]. This report follows a straight-forward to complex build-up structure. This means that first simplified examples will be examined, after which gradual complexity is introduced. As such, this report will start with analyses to identify possible advantages of fragility-based assessment. In Chapter 6, the effects of statistical dependency will be explored, while in Chapter 7, the differences between semi-probabilistic and probabilistic assessments will be gauged. In Chapter 8 and Chapter 9 the fragility-based assessment will be applied to the Eastern Scheldt barrier.

6

Dependency in a fragility-based assessment

In order to assess a fragility-based assessment the differences with currently applied methodology needs to be researched. A first scope study by Witteveen+Bos in 2017, which looked at several methods of assessing the Eastern Scheldt barrier, theorized that the dependency within this complex system could be assessed more accurately with a fragility-based method [12]. The study concluded that a proof of concept was needed to show this. This chapter will look at what dependency is, explore how dependency is currently handled in flood risk and assess whether a fragility-based assessment can offer advantages.

6.1. Dependency

When multiple events are part of an assessment, say events A and B, several combinations of these events can occur. Sometimes the probability of both events occurring at the same time is relevant. An example of this is a lamp hanging from the ceiling with two cables, A and B, as seen in Figure 6.1.

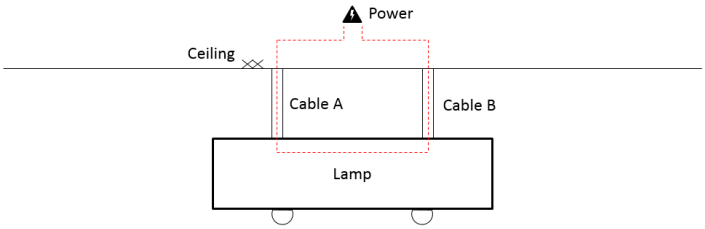

Figure 6.1: Example of a lamp hanging from cables A and B

If the probability that the lamp falls down is to be calculated, both the cables need to fail. To calculate the probability of several events occurring simultaneously, traditional statistics teaches that their probabilities of occurrence need to be multiplied. The probability that the lamp falls down can thus be calculated with Equation 6.1[37]. This type of system, where all subsystems need to fail for full system failure, is called a parallel system.

$$P_f(A \text{ and } B) \equiv P_f(A \cap B) = P_f(A) * P_f(B) \tag{6.1}$$

When a single cable breaks the lamp doesn't work anymore however, as the electric circuit runs through the cables and is interrupted when a cable fails. Failure of a single cable could thus be considered as failure of the system, instead of failure of all cables. To calculate the probability of either of several events occurring, traditional statistics teaches that their probabilities of occurrence need to be summed. The probability that the lamp stops working can thus be calculated with Equation 6.2[37]. This type of system, where 1 subsystem needs to fail for full system failure, is called a series system.

$$P_f(A \text{ or } B) \equiv P_f(A \cup B) = P_f(A) + P_f(B) \tag{6.2}$$

Equation 6.1 and Equation 6.2 only holds if events A and B are independent however. In the example of the lamp, this might not be the case: the cables are perhaps made of the same (flawed) material, the lamp can move and thus put strain on both cables, etc. One large factor of dependence can come from load redistribution after failure. When cable A breaks, cable B will take over the weight previously supported by A. Failure of cable A then increases the failure probability of B. Generally speaking (this holds for the lamp, but also for most failure events [37]):

$$P_f(A \text{ given } P_f(B)) \equiv P_f(A|B) \neq P_f(A) \tag{6.3}$$

The failure of A given the failure of B is not equal to the failure of A: the events are (sometimes only minutely) dependent. Dependency between events is challenging to determine quantitatively however. For this reason, there is a tendency in statistics to assume independence between events [37].

6.2. Series and parallel systems

As was shown in the example with the hanging lamp, two types of systems can be distinguished: parallel and series systems. When looking at the failure probabilities of systems, Venn diagrams are often used to visualize the (often considered abstract) concepts of overlap and union[81]. A Venn diagram of two events can be seen in Figure 6.2.

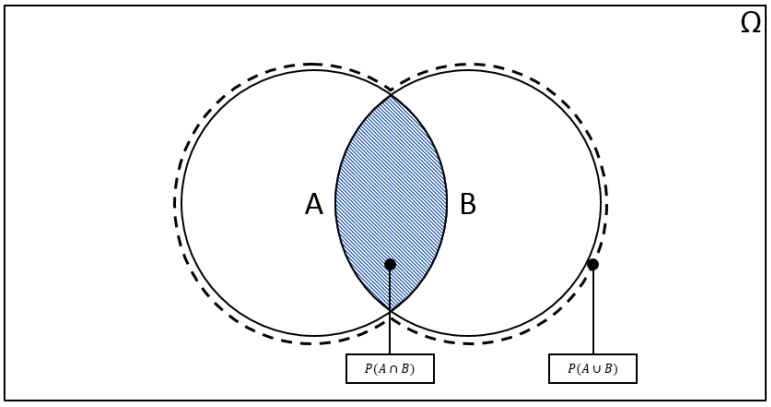

Figure 6.2: Example of Venn diagram used to visualize concepts of overlap and union

The entire space within the square in Figure 6.2 is the entirety of probability space. Per definition it has a size of 1, and is usually denoted by Ω. Venn diagrams can now be drawn inside Ω to indicate probabilities, with the surface of the diagram equal to the probability. In Figure 6.2 the probabilities of two events have been drawn, A and B. The different combinations of probabilities can be described with the terms; overlap and union.

Overlap
The probability of both events occurring has been shaded: $P(A \cap B)$. It is the area within Ω, that is also within A and within B. As such this area is called the overlap of A and B. It is used to calculate within parallel systems. In fault tree analysis the overlap is modelled as an AND-gate, as it describes the probability that A and B occur [37].

Union
The probability of either event occurring has been circled with the dotted line: $P(A \cup B)$. It is the area within Ω, that is either in A or B (or both). As such this area is called the union of A and B. It is used to calculate within series systems. In fault tree analysis the union is modelled as an OR-gate, as it describes the probability that A or B occurs [37]. When calculating the union of a system, it is important not to count the overlap , $P(A \cap B)$, twice. After all, $P(A \cap B)$ is equal to $P(B \cap A)$ and $P(A \cup B)$ only contains this area of the Venn diagrams once.

With Venn diagrams, the amount of dependence can be visualize easily with the amount over overlap that is present between the diagrams. Additionally they can give an indication of the amount of dependence between the events. This will be shown for both series and parallel systems.

6.2.1. Series systems

Series systems describe systems where failure of a single element implies failure of the system. In the example of the lamp a series system can be seen in the electric circuit, which fails when either one of the cables fails. The Venn diagram of a three element series system has been drawn in Figure 6.3, for both a fully dependent system and a fully independent system.

When the elements in a series system are considered dependent, failure of one implies failure of all. This means that the Venn diagrams of the elements within the system fully overlap, as seen in Figure 6.3. The union is then equal to the largest of the failure probabilities of the elements. As such, for elements with equal failure probabilities, an increase in the amount of elements does not lead to an increase in the failure probability of the system. The assumption of full dependence in a series system is optimistic. This can be seen in Figure 6.3, where reducing the dependence of a fully dependent system moves the Venn diagrams further apart and thus increases their union and failure probability.

When the elements in a series system are considered independent, the failure probability of the system can be calculated by calculating the union. This can be done by adding the surfaces of the Venn diagrams. The overlap of the diagrams is subtracted, to avoid double counting events[1]. The assumption of independence in a series system is conservative. This can be seen in Figure 6.3, where adding dependence to a fully independent system moves the Venn diagrams closer together and thus decreases their union and failure probability.

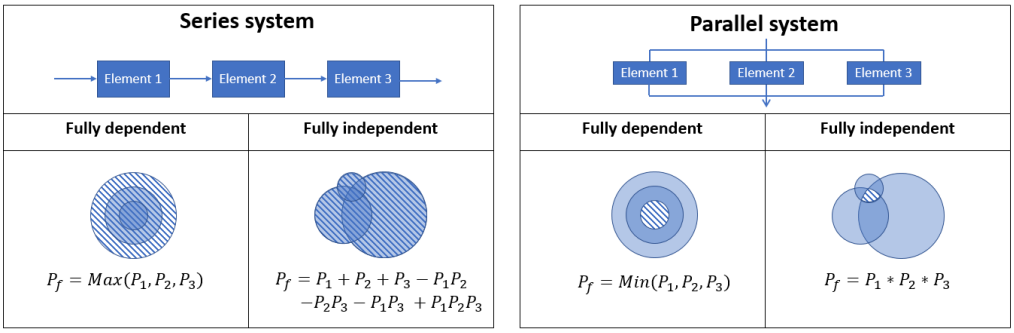

Figure 6.3: The effects of dependence in a series system and a parallel system

6.2.2. Parallel systems

Parallel systems describe systems where every element needs to fail before the system fails. In the example of the lamp the two cables carrying the lamp form a parallel system. If one of the cables fails, the other still caries the lamp. Only when both fail does the lamp fall down. The Venn-diagram of a three element parallel system has been drawn in Figure 6.3, for both a fully dependent and a fully independent system.

When the elements in a parallel system are considered dependent, failure of one implies failure of all. This means that the Venn diagrams fully overlap, as seen in Figure 6.3. The overlap is then equal to the smallest of the failure probabilities of the elements. As such, for elements with equal failure probabilities, an increase in the amount of elements does not lead to a decrease in the failure probability of the system. The assumption of dependence in a parallel system is conservative. This can be seen in Figure 6.3, where reducing the dependence of a fully dependent system moves the Venn diagrams further apart and thus decreases their overlap and failure probability.

When the elements in in a parallel system are considered fully independent, failure probability of the system can be calculated by calculating the overlap. This overlap can be calculated by multiplying the probabilities

[1] When a three element union is calculated, like in Figure 6.3, subtracting P_1P_2, P_2P_3 and P_1P_3 leaves the middle part, $P_1P_2P_3$ uncounted for. After all, $P_1P_2P_3$ was added three times (it is part of P_1, P_2 and P_3, but also subtracted 3 times (it is also part of P_1P_2, P_2P_3 and P_1P_3). As such, to correctly calculate the union of P_1, P_2 and P_3, $P_1P_2P_3$ needs to be added again.

of the elements. The assumption of independence in a parallel system is optimistic. This can be seen in Figure 6.3, where adding dependence to a fully independent system moves the Venn diagrams closer together and thus increases their overlap and failure probability.

6.3. Dependency in flood risk assessment

When flood risk is to be assessed, two main forms of dependency need to be taken into account; dependency between (sub)failure mechanisms and dependency between cross-sections. This sections looks at the assumptions done in these assessments with regards to the dependency and the choice of system (parallel or series). These choices can will then be shown to be conservative.

6.3.1. Dependency between failure mechanisms

Different failure mechanisms can occur for a single dike cross-section. Therefore, when a cross-section is assessed, several different failure mechanisms are to be assessed as a series system: occurrence of a single failure mechanism implies failure of the cross-section. To keep the different mechanisms into account properly, a so called failure probability budget is applied[32]. A failure probability budget allocates failure space from the total allowed failure probability to the different failure probabilities per failure mechanism. For example when a dike section has a maximum allowed failure probability of 1:1000 per year, and piping has a failure probability budget of 24%, the maximum allowed failure probability for piping is $1/1000 * 0.24 = 2.4\text{E}-4$ per year. In the WBI2017, the different failure mechanisms are assumed to be exclusive [32], so that the summation of all components of the failure probability budget will never exceed the total allowed failure probability[34]. For a series system this is a conservative assumption, as seen in Figure 6.3. After all, when events are exclusive, their Venn diagrams are completely separated with no overlap, as seen in Figure 6.4

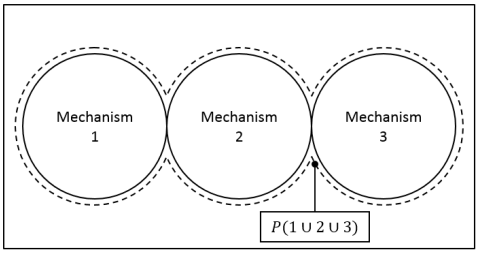

Figure 6.4: Venn diagram of the union of 3 exclusive failure mechanisms

A standardized failure probability budget is described by the WBI2017, however changes to the budget are allowed if necessary. This can be due to local circumstances for example. The standardized budget is based on expert judgment[34] and can be seen in Table 6.1. A failure probability budget is conservative, per definition [32]. Although the standard failure probability budget can be changed, failure space that becomes available in a certain failure mechanism, cannot be used by another failure mechanism.

Type of defence	Failure mechanism	Sandy coast	Dikes
Dike	Overflow and overtopping	0%	24%
	Bursting and piping	0%	24%
	Macro-stability inner slope	0%	4%
	Revetment	0%	10%
Structure	Failure to close	0%	4%
	Piping	0%	2%
	Structural failure	0%	2%
Dune	Dune erosion	70%	0%
Other		30%	30%
Total		100%	100%

Table 6.1: Standard failure probability budget [32]

Certain failure mechanisms are parallel systems in itself however. This means that they consist of several sub-mechanisms, that all need to occur before the failure mechanism occurs. An example of this is piping, which consists of the sub-mechanisms lift-up, heave and internal erosion. These sub-mechanisms are considered fully dependent when assessing for piping [55]. This is a conservative assumption for a parallel system, as seen in Figure 6.3.

6.3.2. Dependency between cross-sections

The dependency between cross-sections is important as there are infinite cross-sections that can be considered in any dike-section (even though the section has finite length). Fully independent cross-sections would lead to a failure probability of 1.0 for all dike sections, everywhere. After all, a series system with infinite, independent sub-systems will always fail if $P_{f,sub} \neq 0$. The length effect factor is introduced, as an indicator for the amount of independent, normative cross-sections that need to be considered in a dike section. The length effect factor is determined by the fraction of the dike section that is sensitive to the mechanism, a factor that indicates the sensitivity of the mechanism to length effects, and the length of the dike section. The length effect factor will always be larger than 1, as there is always minimally a single normative cross-section per dike-section.

To give an explanation of what the length effect factor represents, consider the dike section seen in Figure 6.5, where 3 cross-sections have been drawn in the dike-section.

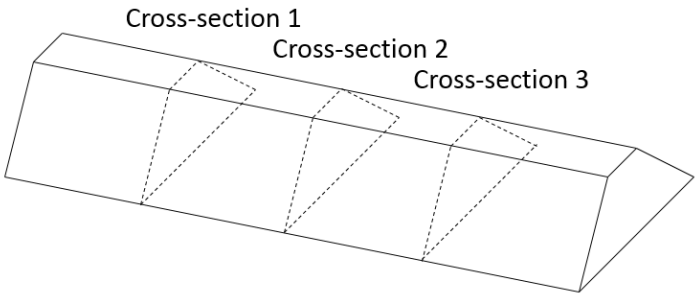

Figure 6.5: Example dike-section with 3 cross-sections drawn

If 3 cross-sections are considered, the Venn diagrams of the failure probability per cross-section can be drawn as seen in Figure 6.6. The different cross-sections have varying failure probabilities, but there is overlap. This is caused by the dependency between the cross-sections, for example due to the same soil that makes up the dike. There are also small differences between the cross-sections, as variations in space exist. Perhaps the crest height of the dike varies slightly along the length, or the wave load on a certain cross-section is somewhat higher due to the bathymetry. Since the different cross-sections are a series system, the combined failure probability is calculated with the union, which can be seen in Figure 6.6.

When more cross-sections are considered, the same effect can be noticed. Every cross-section added, adds a slightly varying failure probability to the system. At a certain amount of cross-sections however, adding a cross-section does not add to the failure probability anymore: the new Venn diagram is already fully covered by the Venn diagrams of the other cross-sections. The length effect factor, N, is the multiplication factor that should be applied on a single Venn-diagram (failure probability) of the normative cross-section to transform it to the Venn-diagram (failure probability) of the dike-section. This can be seen in Figure 6.6.

6.4. Dependency in a fragility based assessment

It was shown in the previous sections that dependency is not taken into account in WBI2017 methodology. Both when considering failure mechanisms and when considering cross-sections, full independence is assumed. When considering parallel sub-mechanisms, like the sub-mechanisms for piping, full dependence is assumed. All of these assumptions are conservative. If it is assumed that dependence cannot be taken into account quantitatively, only the options of fully independent and fully dependent remain available. Applying

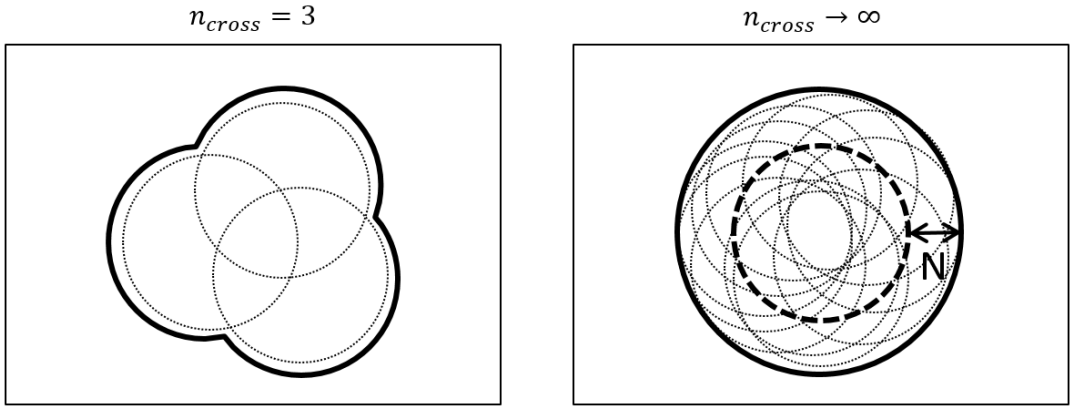

Figure 6.6: Visual representation of the length effect factor N, with the union of 3 cross-sections (left) and the union of infinite cross-sections (right)

fragility allows for a third options however. When assessing by calculating fragility, conditional failure probabilities are assessed instead of (actual) failure probabilities. This allows for the dependency to be set for the conditional failure probabilities. This means that the dependency in strength can be made different from the dependency in loading. Physically, this makes sense as often very different strength parameters are loaded by very similar loading parameters. This will be shown for both a series system and a parallel system.

6.4.1. Dependency in a series system when applying fragility

Consider a bottom protection made of stones in a flow trough, protecting a sand layer which is vulnerable to scour, as can be seen in Figure 6.7. All stones in the protection are from completely independent origins, meaning different quarries, stone type, rock class, etc. The stones are thus independent in strength. While they are independent in strength, they experience the same loading. If no turbulence and mixing layers are considered, the flow velocity along the trough is the same for every stone. As such the stones can be considered fully dependent in loading.

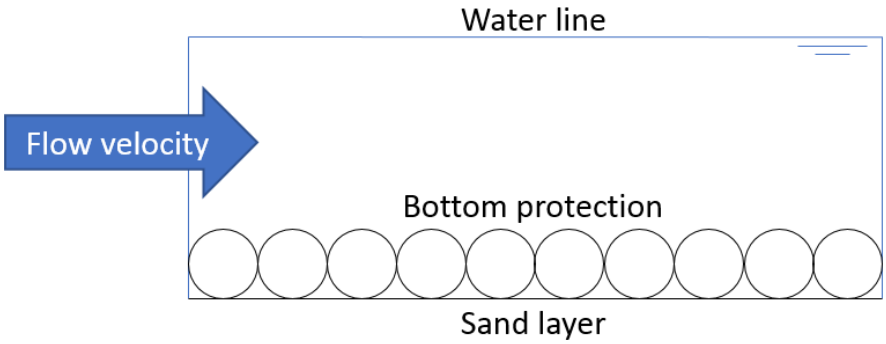

Figure 6.7: Stones protecting a sand layer from scour

Failure of a single stone exposes the sand layer, which leads to scour. The stones thus function as a series system. The critical flow velocity of a single stone (R) can be described with a fragility curve, which can be seen in Figure 6.8. The flow velocity, u, which forms the loading on the stones, can be described with a PDF as can be seen in Figure 6.8. This PDF is described with a log-normal distribution with a mean and coefficient of variance of 0.5. The failure probability of a single stone can then be obtained by evaluating the following integral:

$$P_{\mathrm{f}} = \int_{-\infty}^{\infty} P_{\mathrm{f,conditional,1}} \mathrm{PDF}(u) \mathrm{d}u = 5.2\mathrm{E}-3 \quad \text{per year} \tag{6.4}$$

If a 10-element series system of stones is to be assessed, as can be seen in Figure 6.7, fully dependent stones

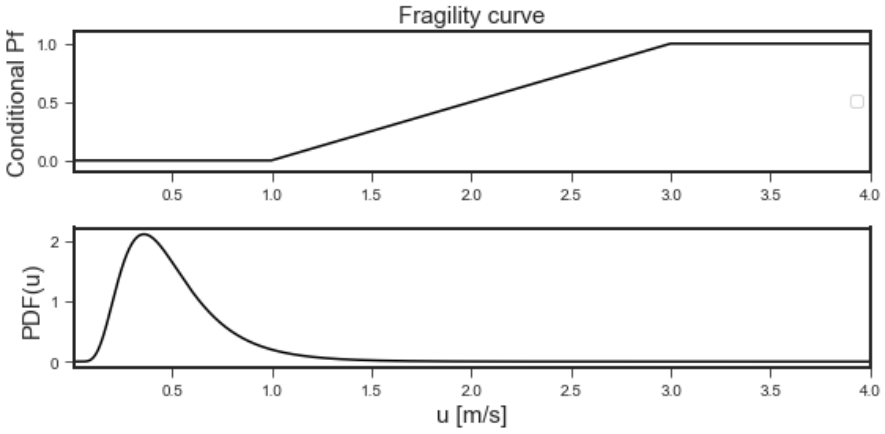

Figure 6.8: Fragility curve and probability density function of the load for the stability of a single stone (example, not based on physics)

and fully independent stones can be considered. The formulae for computing the union of a series system can be seen in Figure 6.3, and leads to Equation 6.5 and Equation 6.6.

$$P_{f,\text{fully dependent}} = \text{Max}(P_i) = 5.2\text{E}-3 \quad \text{per year} \tag{6.5}$$

$$P_{f,\text{fully independent}} = \text{Union}_{10}(P_i) = 5.1\text{E}-2 \quad \text{per year} \tag{6.6}$$

When the failure probabilities of the stones are considered fully dependent, the failure probability of the system is governed by the largest failure probability of the elements. Since every stone has the same failure probability of 5.2E−3 per year, the addition of stones does not influence the failure probability of the system.

When the failure probabilities of the stones are considered fully independent, the failure probability of the system is governed by the union of the failure probabilities of the elements. The failure probability of the system grows with growing number of stones considered, as the probability that one of the stones considered is especially weak grows.

When applying a fragility curve based method a 'middle ground' can be applied, where the elements are considered fully independent in strength and fully dependent in load. This can be done by taking the union of the conditional failure probabilities instead of the actual failure probabilities. By first taking the union of the conditional failure probabilities, only the strength parameters are considered. Integration over the loading parameters then implies the exact same (thus dependent) loading conditions for all elements. As such a state of independent strength and dependent loading can be described. Since the union of conditional failure probabilities is also a conditional failure probability (but now of a system instead of an element), a fragility curve of the union can be constructed, which can be seen in Figure 6.9.

The failure probability of the fragility curve can be obtained by integration of the integral:

$$P_\text{f} = \int_{-\infty}^{\infty} P_{\text{f,conditional,10}} \text{PDF}(u) \text{d}u = 2.4\text{E}-2 \quad \text{per year} \tag{6.7}$$

By applying full independence on the strength and full dependence on the loading, the conservatism has been reduced, but not so far as to be considered too optimistic under the assumption of full independence in strength. This assumption may not hold however, as maybe the stones do have dependence in strength. Perhaps the stones are all from the same rock class or all from the same quarry. Lets assume that instead of independence between every stone, independence can be assumed between every other stone. The stones are thus assessed in dependent groups of 2 stones. As the groups are considered dependent within the group, the failure probability of a group of 2 stones is also 5.2E−3 per year. The calculation of the fully dependent, the fully independent and the fragility based failure probabilities is thus the same as when assessing a 5-element set:

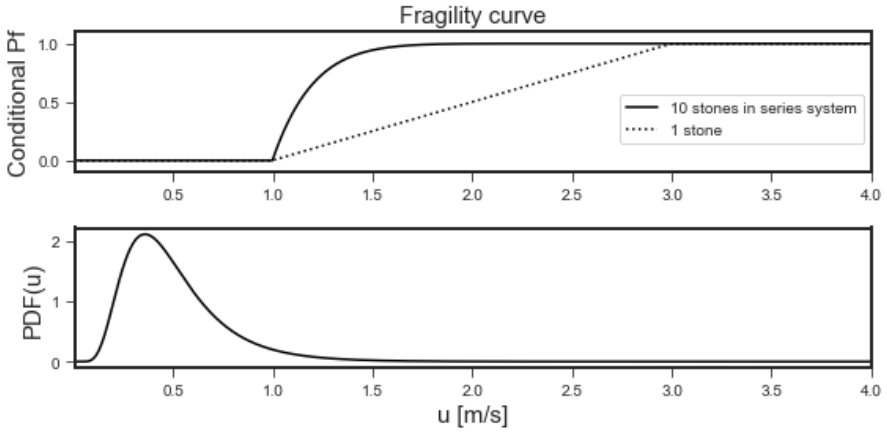

Figure 6.9: Fragility curve with the union of the conditional failure of 10 stones

$$P_{f,\text{fully dependent}} = \text{Max}(P_i) = 5.2\text{E}-3 \quad \text{per year} \tag{6.8}$$

$$P_{f,\text{fully independent}} = \text{Union}_5(P_i) = 2.6\text{E}-2 \quad \text{per year} \tag{6.9}$$

The fragility curves of a 1 stone, 5 stone and 10 stone system can be seen in Figure 6.10. Through integration the failure probability of the 5-element system can be obtained:

$$P_\text{f} = \int_{-\infty}^{\infty} P_{\text{f,conditional,5}} \text{PDF}(u) \text{d}u = 1.7\text{E}-2 \quad \text{per year} \tag{6.10}$$

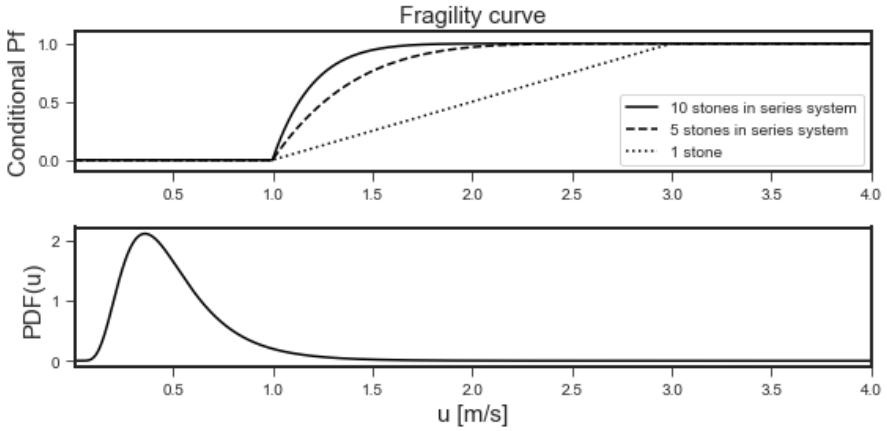

Figure 6.10: Fragility curve with the union of the conditional failure of 5 stones and 10 stones

The failure probabilities of the stones can be calculated for increasing numbers of stones, which can be seen in Table 6.2.

It can be seen that when the number of elements increases enough, the set as a whole starts to act more deterministic. When the flow velocity exceeds 1.0 m/s, the probability of 1 element out of 1000 failing (and thus the system as it is a series system) becomes almost certain. This means that the failure probability becomes equal to the probability that the flow velocity exceeds 1.0m/s, which can be calculated from the PDF without the fragility curve. The probability of exceedance of 1.0m/s is 4.4E-2 per year, which can also be seen to be the failure probability of a 1000-element system, with independent strength and dependent loading.

Amount of elements	Independent strength, independent loading	Dependent strength, dependent loading	Independent strength, dependent loading
1	$5.2 * 10^{-3}$ year^{-1}	$5.2 * 10^{-3}$ year^{-1}	$5.2 * 10^{-3}$ year^{-1}
2	$1.0 * 10^{-2}$ year^{-1}	$5.2 * 10^{-3}$ year^{-1}	$9.2 * 10^{-3}$ year^{-1}
5	$2.6 * 10^{-2}$ year^{-1}	$5.2 * 10^{-3}$ year^{-1}	$1.7 * 10^{-2}$ year^{-1}
10	$5.1 * 10^{-2}$ year^{-1}	$5.2 * 10^{-3}$ year^{-1}	$2.4 * 10^{-2}$ year^{-1}
100	0.41 year^{-1}	$5.2 * 10^{-3}$ year^{-1}	$4.1 * 10^{-2}$ year^{-1}
1000	0.99 year^{-1}	$5.2 * 10^{-3}$ year^{-1}	$4.4 * 10^{-2}$ year^{-1}

Table 6.2: Failure probability with increasing number of elements

6.4.2. Dependency in a parallel system when applying fragility

Instead of a bottom protection made from stones, a bottom protection made from stacked mats is considered, as seen in Figure 6.11. The sandy layer is now only exposed after all layers of the bottom protection fail; a parallel system. It is assumed that a layer failing instantly removes the entire layer (without residual strength).

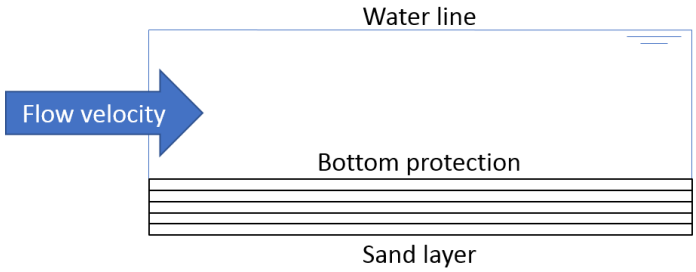

Figure 6.11: Mats protecting a sand layer from scour

The mats are assumed to have the same behaviour as the stones considered in Subsection 6.4.1. This means that the same fragility curve and PDF can be applied as seen in Figure 6.8 and the failure probability of a single element (which is now a single mat instead of a single stone) is equal to 5.2E-3 per year. When increasing number of elements in a parallel system, a behaviour that can be considered the opposite of a series system can be seen in the fragility curves (showing the overlap of the conditional failure probabilities). In Table 6.3 the failure probabilities of a parallel system under increasing number of elements can be seen.

When the mats and loading are considered fully independent, the failure probabilities of the system tend to zero [2]. When the mats and loading are considered fully dependent, the failure probability of the system is not affected by the amount of elements, this was also found for the series system. When applying independence in strength and dependence in loading, a middle ground can be found.

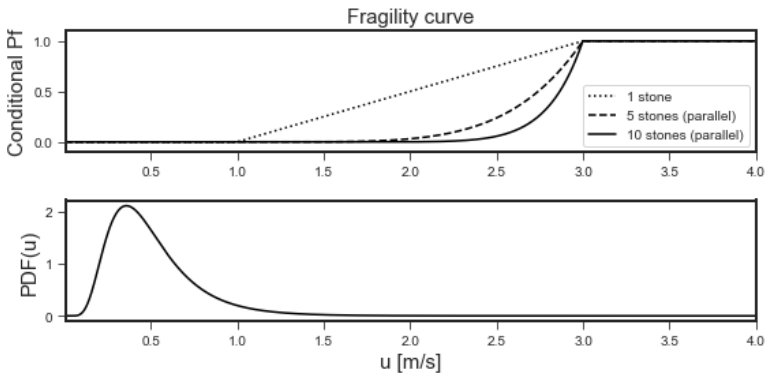

Figure 6.12: Combined fragility curve for increasing number of stones

[2] A failure probability of 0 is found for 1000 elements. This is caused by the amount of decimals being to large for most calculators. It is technically incorrect however, as there is still a (almost infinitely) small probability of failure.

Amount of elements	Independent strength, independent loading	Dependent strength, dependent loading	Independent strength, dependent loading
1	$5.2 * 10^{-3}$ year^{-1}	$5.2 * 10^{-3}$ year^{-1}	$5.2 * 10^{-3}$ year^{-1}
2	$2.7 * 10^{-5}$ year^{-1}	$5.2 * 10^{-3}$ year^{-1}	$1.3 * 10^{-3}$ year^{-1}
5	$3.9 * 10^{-12}$ year^{-1}	$5.2 * 10^{-3}$ year^{-1}	$1.6 * 10^{-4}$ year^{-1}
10	$1.5 * 10^{-23}$ year^{-1}	$5.2 * 10^{-3}$ year^{-1}	$5.8 * 10^{-5}$ year^{-1}
100	$6.0 * 10^{-229}$ year^{-1}	$5.2 * 10^{-3}$ year^{-1}	$2.8 * 10^{-5}$ year^{-1}
1000	0.0 year^{-1}	$5.2 * 10^{-3}$ year^{-1}	$2.7 * 10^{-5}$ year^{-1}

Table 6.3: Failure probability with increasing number of elements

6.5. Conclusion

Statistical dependency, between failure mechanisms, within space, etc, can be of large influence on the assessment of a flood defence. In Section 6.4 the effects of dependency in series and parallel systems were explored and explained. Several method applied within the WBI2017 to account for dependency were explored; the failure probability budget and the length effect factor. Both of these solutions introduce (and even rely) on a certain amount of conservatism [20]. Additionally, the applicability of these methods is more suited for standard flood defences, than for complex systems such as the Eastern Scheldt barrier.

A failure probability budget is conservative, per definition. Additionally the standardized failure probability budget does not take dependency into account and instead, assumes the different failure mechanisms fully independent. This assumption was made to keep the standard failure probability budget safe [33]. The length effect factor is also based on the concept of dike cross-sections and the length effects of mechanisms might be less applicable to a complex barrier, consisting on different types of flood defence.

While these methods are both applicable, both the failure probability budget and the length effect factor are ultimately approximations however, and this means that dependency is not assessed completely accurately with these methods. This in turn causes conservatism as conservative assumptions are made to keep the methods safe. If a more accurate assessment of several failure probabilities with dependence is required, a probabilistic assessment might be better suited.

Often times however, these probabilistic assessment also rely on approximations, as the dependency between event is difficult to quantify. For this reason assumptions of full dependence or full independence are often applied, and the effects of these assumptions for series and parallel system of varying amounts of elements have been shown in Table 6.2 and Table 6.3. A fragility based probabilistic assessment has been shown to offer a third option of assuming full independence in strength and full independence in loading. When deemed applicable, this can reduce the amount of conservatism present in the assumptions, based on the schematization of the system (series or parallel).

7

Comparison semi-probabilistic and probabilistic assessments

As stated in Chapter 1, one of the goals for the WBI2017 has been to introduce probabilistic assessment methods where possible, replacing or complimenting the current semi-probabilistic methods. In this chapter the differences between the two will be explained and shown, by assessing piping with a WBI2017 methodology and a fragility-based methodology. The mechanism piping has been selected as it is a straight-forward mechanism that is well-described and calibrated in the WBI2017.

The goal of this chapter is to show how semi-probabilistic tools can introduce error, and thus conservatism, and research whether a probabilistic tool, such as a fragility-based tool, can negate or circumvent this. First, the differences between a semi-probabilistic assessment and a probabilistic assessment will be explained in Section 7.1. This will be followed with an example assessment, first applying a semi-probabilistic approach in Section 7.2, then applying a fragility-based probabilistic approach in Section 7.3. These two approaches will then be compared quantitatively.

7.1. Differences between semi-probabilistic and probabilistic

The main difference between a probabilistic assessment and a semi-probabilistic assessment is the output, not the input [20]:

A probabilistic assessment calculates a failure probability, usually by assessing the PDF of a limit state, Z. The probability that the limit state is negative (Z<0) equals the probability that the considered system fails. The PDF of the limit state is calculated by assessing the distributions of the underlying variables. This methodology was explained in Chapter 4.

A semi-probabilistic assessment does not assess the distributions of the underlying variables however. Instead, a representative value is chosen for each variable, called the characteristic value [37]. The characteristic value is a value that is deemed safe enough to represent the full distribution. It is often chosen as a percentile value, such as a 5% value for strength parameters and a 95% value for load parameters. The difference between the characteristic values for R and S represents the safety factor, γ_s. This difference can be either relative or absolute, depending on the mechanism under consideration.

$$\gamma_{\text{s,relative}} = \frac{R_{\text{characteristic}}}{S_{\text{characteristic}}} \qquad \text{or} \qquad \gamma_{\text{s,absolute}} = R_{\text{characteristic}} - S_{\text{characteristic}} \tag{7.1}$$

In Figure 7.1, a (fictive) distribution for S and for R can be seen. Both the methodology of a semi-probabilistic assessment (left) and a probabilistic assessment (right) have been annotated.

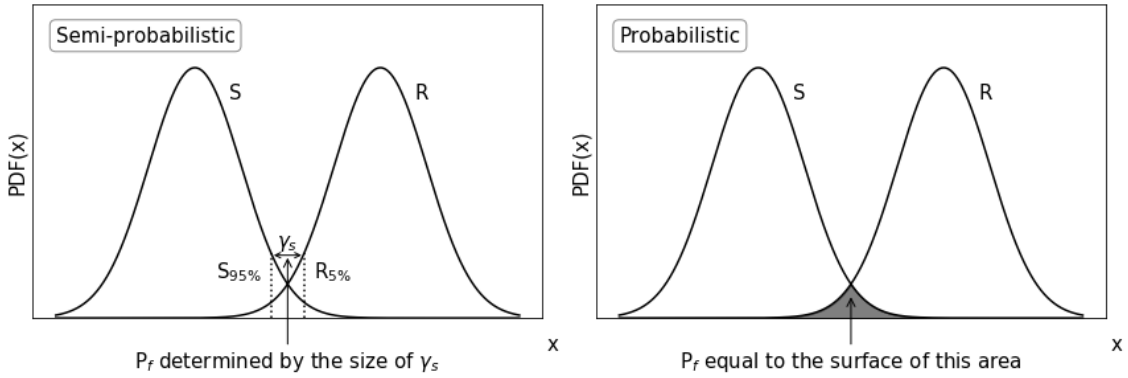

Figure 7.1: PDFs of R and S, with a semi-probabilistic assessment (left) and probabilistic assessment (right)

A probabilistic assessment of Figure 7.1 evaluates the probability P(R<S) and outputs this probability[20]. This can be seen in Figure 7.1 on the right, where the probability P(R<S) has been shaded. A semi-probabilistic assessment of Figure 7.1 evaluates the distributions of R and S with their respective characteristic values (a 5- and 95% value has been selected in Figure 7.1). The difference between these values is the safety factor γ_s. The semi-probabilistic assessment then output a verdict on whether this safety factor is deemed large enough [20]. A difficulty then of course becomes which value of γ_s constitutes 'large enough'.

As can be seen in Figure 7.1, their is no difference in input between a semi-probabilistic and a probabilistic assessment, as a semi-probabilistic assessment starts with the same distributions as a probabilistic assessment. Data collection, for example, is not more or less complicated when a semi-probabilistic assessment is done, and the models applied to calculate a limit state or critical value are the same as well (the same Sellmeijer model can and will be used in a probabilistic and a semi-probabilistic piping assessment to calculate R). Due to the usage of the full distributions, a probabilistic assessment offers more information and is more accurate than the semi-probabilistic assessment however. A semi-probabilistic assessment is an approximation after all. While a probabilistic assessment is more accurate and offers more insight, there are some reasons for applying a semi-probabilistic method instead. The following reasons are described in the WBI2017:

A semi-probabilistic assessment is computationally less demanding, meaning that in terms of computational effort it is easier to apply. Probabilistic assessments can become computationally very demanding, which brings a practical limit to the applicability [20]. Additionally, the output of a semi-probabilistic assessment (pass or fail) is easier to assess and the results of a semi-probabilistic assessment are "*more easily transferable to the wider public*" [20], and probabilistic assessment methodologies are often considered too "*black-box*" [20]. Finally, the semi-probabilistic assessment more closely resembles assessments done in the past, which keeps a certain amount of comparability with previous assessments [12].

As flood risk assessment in the Netherlands has switched to a risk-based approach [35], the output of a regular semi-probabilistic assessment will not suffice anymore however. Dikes are assessed based on a safety norm, which is tied to a maximum allowed probability of failure. As a result a relationship between the safety factor of a system and a failure probability was required [34]. This relationship was found through so called calibration studies [34].

7.1.1. Calibration safety factors

While the current norms set in Dutch flood risk assessment are risk-based, the assessment tools were not, as they were based on semi-probabilistic methods. For this reason, a relation between safety factor and failure probability was needed, which was found through calibration studies [32]. The exact procedure followed can be found in detail in Jongejan, 2017 [34], but the main procedure followed will be explained here. Simply put, for a large amount of test cases, both the semi-probabilistic safety factor and the probabilistic failure probability were evaluated and a relationship was data fitted. This was done on a per-failure-mechanism basis.

The first step in the calibration process was determining test-cases that would be representative in the calibration. These different test-cases were based on a combination of real-life case as well as fictive cases. The

set of these fictive cases was constructed by applying a Monte Carlo-based bandwidth for most variables, to avoid selection bias [32]. For all these test cases, a probabilistic assessment of the mechanism under consideration was performed, to assess the influence of each different stochastic parameter in the assessment. In Figure 7.2, the result of this assessment for piping (sub-mechanism: internal erosion) can be seen.

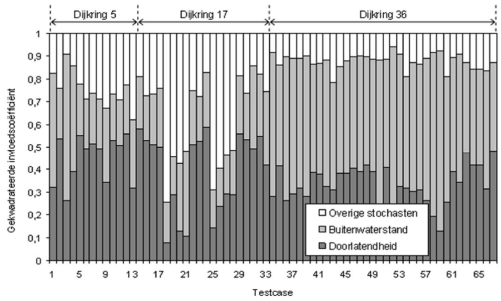

Figure 7.2: The resulting influence factor from the probabilistic analyses of the test-cases for piping (sub-mechanism: internal erosion) (Dutch) [32]

In Figure 7.2 it can be seen that for piping, the outside water level has a large influence factor in most test cases. This created a problem however, as the outside water level to be applied, is determined by the norm (the required safety) of the selected dike section. For example, if a certain dike section has a norm of 1:4000, an outside water level is applied which has a 4000 year return period. As a result of this dependency between water level and norm, the norm is now applied twice; once to calculate S and once to assess whether a failure probability is small enough. To solve for this dependency on the norm, the norm was introduced in the relationship between safety factor and failure probability. This is called the norm-dependent safety factor and it can be seen in the calibration formula for piping, which can be seen in Equation 7.2 (which of course is already calibrated, but it shows the different components of the calibration). All other variables are accounted for in the norm-independent safety factor.

$$P_{f,\text{internal erosion}} = \Phi(-(\ln(\frac{F_{\text{internal erosion}}}{1.04}) + 0.43\beta_{\text{norm}})\frac{1}{0.37}) \tag{7.2}$$

Where:

$P_{f,\text{internal erosion}}$	[-]	Failure probability for internal erosion
$F_{\text{internal erosion}}$	[-]	Safety factor for internal erosion
β_{norm}	[-]	Target reliability index for the considered dike section

The test-case were assessed for different safety factors. For each safety factor assessed, the dimensions of the test case were fine-tuned, such that the test-case would just pass a semi-probabilistic assessment. For each of these safety factors assessed, the failure probability (for the fine-tuned) test case was also computed (with a probabilistic assessment). As the higher safety factors would require larger dimensions, they also imply smaller failure probabilities. This can be seen in Figure 7.3.

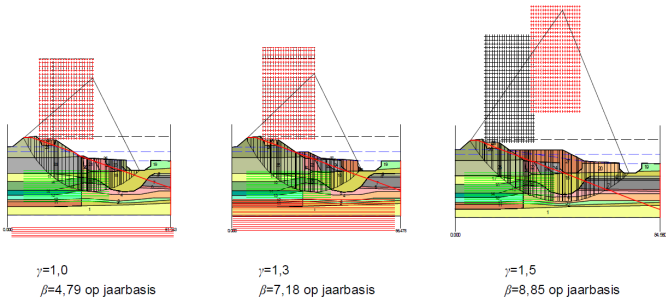

Figure 7.3: Example of a test-case for macro-stability. As the safety factor is increased, the dimensions of the dike need to be increased to pass the semi-probabilistic assessment. As these dimensions are increased, the failure probability of the dike decreases (the reliability index increases) [32] (Dutch)

An example of the result of such a calibration, with an increasing safety factor can be seen in Figure 7.4. A relation is then plot-fitted through this data to compute the calibration relationship, which links the safety factor and the failure probability. In this plot-fitting the fit was made through the 20% quantile of the reliability indices found from the test-cases [34]. This results in a relationship which has an 80% chance of being conservative and a 20% of being optimistic.

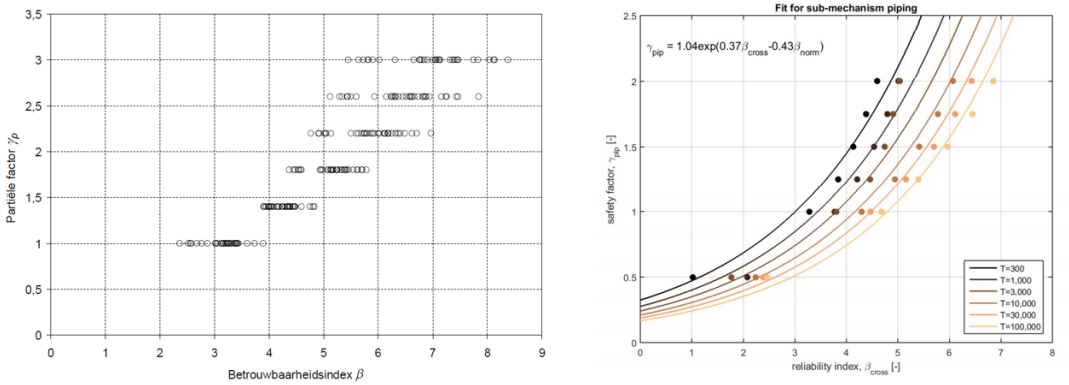

Figure 7.4: Example of the assessment of test cases; the larger the semi-probabilistic safety factor, the larger the reliability index (left)[32] and an example of a plot-fitted relationship (right) [34]

It should be important to notice that the norm-dependency of the characteristic water level has made the calibration relation norm-dependent, as can be seen in Figure 7.4. This has resulted in a safety factor that is thus also norm-dependent. The norm of a dike section is a human creation however, based on the infrastructure and economic/societal risks behind a dike in case of failure [35], yet the failure probability of the dike should not be dependent on the norm. After all, the probability of a dike failing -in reality- is not influenced by the consequences of that failure. This discrepancy between a norm-dependent safety factor and a non-norm dependent failure probability can lead to some non-physical behaviour when assessing, as will be shown in the semi-probabilistic assessment in Section 7.2.

7.2. Semi-probabilistic assessment

In order to show how semi-probabilistic assessments can introduce conservatism, as well as potential non-physical behaviour due to the fitted calibration relationship, a semi-probabilistic assessment will be demonstrated for a fictional case. This assessment follows the WBI2017 methodology to assess the safety of a dike against piping, as described in WBI, appendix III [55] and the so called schematisation manuals (Dutch: schematiseringshandleidingen) [59]. The mechanism piping has been selected as it is a straight-forward mechanism that is well described and calibrated in the WBI2017. Secondly, due to the dependency between the sub-mechanisms, some of dependency discussed in Chapter 6 can be shown. Only an assessment of the sub-mechanisms lift-up and internal erosion will be offered here for simplicity, a full assessment would also include an assessment of the heave sub-mechanism.

Piping under a dike is caused by a water level difference over the dike resulting in a flow through a permeable layer, such as a sand layer for example, under the dike. As stated, two sub-mechanisms are treated here; lift-up and internal erosion. These mechanisms both need to occur for piping to occur, as can be seen in the fault tree in Figure 7.5.

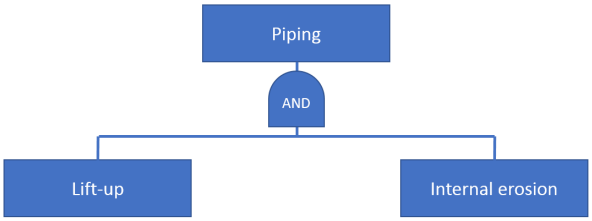

Figure 7.5: Fault tree for piping applied in this chapter

First, a direct path through a permeable layer between the two sides of the dike needs to be present. If a non-permeable layer blocks this path, then the water pressures under this layer need to be large enough to lift the layer and cause cracks in it. This process is called lift-up [69].

Secondly, when a direct path is present, soil particles will start washing away from the exit point of the piping path, since the flow lines have the strongest gradient here. As more of the pipe is formed, the gradients lessen and the pipe formation slows down, until a equilibrium pipe length is eventually formed. This equilibrium piping length is determined by the soil parameters in the permeable layer (such as particle size, friction angle and permeability) and the water level difference over the dike. If the equilibrium piping length is high enough to reach from the exit point to the entry point of the piping path, the pipe can form. This process is called internal erosion [69].

In Figure 7.6 an overview can be seen of the dike schematization to be assessed. When both mechanisms occur, the dike is considered to have failed, i.e. there is no residual strength (time-dependent growth of the pipe, transfer probability leading to crest-reduction, etc.).

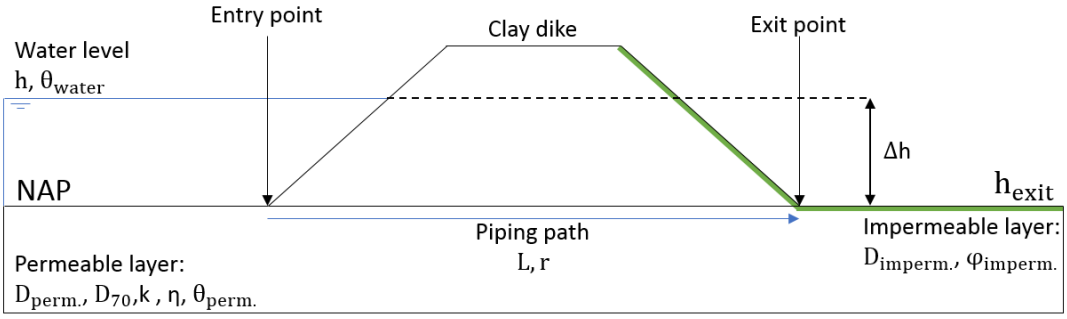

Figure 7.6: The schematization for the piping assessment of a dike

Symbol	Unit	Description	Distr.	Par. 1	Par. 2	Repr. value
Outside water:						
h	[m+NAP]	Outside water level	Gumbel	α=1.04	β=0.43	Norm [34]
γ_{water}	[kN/m^3]	Volumetric weight	Det. [59]	10.27 [59]	-	-
Permeable layer:						
$D_{perm.}$	[m]	Thickness layer	LogN. [34]	μ=20	cov=0.1 [20]	95%-value [34]
d_{70}	[m]	70%-quantile of the grain size	LogN. [34]	μ=2E-5	cov=0.12 [20]	5%-value [34]
k	[m/s]	Permeability of the permeable layer	LogN. [34]	μ=5.8E-5 (5 m/day)	cov=0.5 [20]	95%-value [34]
η	[-]	White's drag coefficient	Det.	0.25 [59]	-	-
$\theta_{perm.}$	[°]	Friction angle	Det.	41 [70]	-	-
$\gamma_{perm.}$	[kN/m^3]	Submerged volumetric weight	Det.	16 [59]	-	-
Impermeable layer:						
$D_{imperm.}$	[m]	Thickness layer	LogN. [34]	μ=0.3	cov=0.3 [20]	5%-value [34]
$\gamma_{imperm.}$	[kN/m^3]	Submerged volumetric weight	Shifted (10) LogN. [34]	μ=10 (av.=20)	cov=0.05 [20]	5%-value [34]
Piping path:						
L	[m]	Length piping path	LogN. [34]	μ =40	cov=0.1 [20]	5%-value [34]
r	[-]	Reduction factor	LogN. [34]	μ=0.05	cov=0.1 [20]	95%-value [34]
h_{exit}	[m+NAP]	Phreatic level at the exit point	Normal [34]	μ=0	σ=0.1 [20]	5%-value [34]

Table 7.1: Variables applied, the marked entries have been assumed, as they are dependent on the case considered. All other distributions, parameters and representative values have been prescribed by the WBI2017

7.2.1. Lift-up

The lift-up sub-mechanism will be assessed by comparing the critical pressure below the impermeable layer with the occurring pressure below the impermeable layer. The ratio between these is used to calculate a stability factor, F_{liftup}, as can be seen in Equation 7.3[55].

$$F_{liftup} = \frac{\Delta\phi_{c,u}}{\Delta\phi} \tag{7.3}$$

Where:

$\Delta\phi_{c,u}$	[m]	The critical pressure
$\Delta\phi$	[m]	The occurring pressure

The critical pressure is given by the weight of the impermeable layer, which is given by Equation 7.4[55]:

$$\Delta\phi_{c,u} = \frac{D_{\text{imperm.}}(\gamma_{\text{imperm.}} - \gamma_{\text{water}})}{\gamma_{\text{water}}} \tag{7.4}$$

Where:

$D_{\text{imperm.}}$	[m]	The thickness of the impermeable layer
$\gamma_{\text{imperm.}}$	[kN/m^3]	The submerged volumetric weight of the impermeable layer
γ_{water}	[kN/m^3]	The volumetric weight of water

The occurring pressure is given by Equation 7.5[55]:

$$\Delta\phi = (h_{\text{norm}} - h_{\text{exit}})r \tag{7.5}$$

Where:

h_{norm}	[m]	The water level at norm
h_{exit}	[m]	The phreatic level at the exit point
r	[-]	Reduction factor, discounting the reduced water pressures between entry- and exit point

All variables except the norm are described in Table 7.1. If a norm is assumed of 1:100, a representative water level with a 99%-value is applied. For all other variables the representative value from Table 7.1 can be applied. As such, all distributions are replaced with representative values and this is now a semi-probabilistic assessment. Applying Equation 7.3, Equation 7.4 and Equation 7.5, a safety factor of 0.80 is then computed for the mechanism lift-up.

7.2.2. Internal erosion

The sub-mechanism internal erosion will be assessed by comparing the critical water level difference over the dike with the occurring water level difference over the dike. This ratio will then be applied to calculate a stability factor, $F_{\text{internal erosion}}$, as can be seen in Equation 7.6, in which a reduction is applied caused by the impermeable layer [55].

$$F_{\text{internal erosion}} = \frac{\Delta h_c}{h_{\text{norm}} - h_{\text{exit}} - 0.3D_{\text{imperm.}}} \tag{7.6}$$

Where:

$D_{\text{imperm.}}$	[m]	The thickness of the impermeable layer

The critical water level difference over the dike is the water level difference for which the equilibrium piping length is equal to the length of the piping path. As such, it is the largest water level difference for which internal erosion does not occur yet[1]. Depending on the shape of the piping path (purely horizontal or with

[1] Internal erosion is always implied when a piping path and head difference are present. Therefore 'starts to occur' should here be seen as the sub-mechanism starting to occur with enough intensity to imply failure, rather than the process itself starting.

vertical components), several formulae can be used to calculate the critical head difference. A piping path is assumed that is purely horizontal and therefore the so called Sellmeijer formulae can be applied. The Sellmeijer formulae use the soil properties to calculate the critical head difference and can be found in Equation 7.7, Equation 7.8 and Equation 7.9[59].

$$\Delta h_c = \alpha c \frac{\gamma_{\text{perm.}}}{\gamma_{\text{water}}} \tan(\theta_{\text{perm.}})(0.68 - 0.10\ln(c))L \tag{7.7}$$

$$\alpha = \frac{D_{\text{perm.}}}{L}\left[\frac{0.28}{(\frac{D_{\text{perm.}}}{L}^{2.8}-1)}\right] \tag{7.8}$$

$$c = \eta d_{70}(\frac{1}{\kappa L})^{\frac{1}{3}} \tag{7.9}$$

Where:

$\gamma_{\text{perm.}}$	[kN/m^3]	The submerged volumetric weight of the permeable layer
γ_{water}	[kN/m^3]	The volumetric weight of water
θ	[°]	The internal friction angle of the permeable layer
L	[m]	The horizontal piping distance
$D_{\text{perm.}}$	[m]	The thickness of the permeable layer
η	[-]	White's drag coefficient
d_{70}	[m]	The 70%-quantile of the grain size
κ	[m^2]	The intrinsic permeability (=1.35E-7*k)

The occurring water level difference is given by the outside water level at norm, and the phreatic level. Applying the assumed norm of 1:100, a safety factor of 0.86 can be computed.

7.2.3. Stability factor to verdict

From the stability factors a failure probability can be computed by applying the calibration relation. These formulae were found with the calibration process, described in Subsection 7.1.1. The calibration formulae for lift-up and internal erosion can be found in Equation 7.10 and Equation 7.11 [34].

$$P_{f,\text{liftup}} = \Phi(-\frac{\ln(\frac{F_{\text{liftup}}}{0.48}) + 0.27\beta_{\text{norm}}}{0.46}) \tag{7.10}$$

$$P_{f,\text{internal erosion}} = \Phi(-\frac{\ln(\frac{F_{\text{internal erosion}}}{1.04}) + 0.43\beta_{\text{norm}}}{0.37}) \tag{7.11}$$

Where

$P_{f,\text{liftup}}$	[year^{-1}]	The failure probability for the sub-mechanism lift-up
$P_{f,\text{internal erosion}}$	[year^{-1}]	The failure probability for the sub-mechanism internal erosion
β_{norm}	[-]	Target reliability index of cross-section at norm
Φ	[-]	Standard normal probability density function

By applying Equation 7.10 and Equation 7.11 on the computed safety factors of 0.80 and 0.86 respectively, the failure probabilities of the sub-mechanisms can be computed. The failure probability of the piping mechanism is then computed by assuming the two sub-mechanisms as a fully dependent parallel system. The failure probability of such a system is equal to the smallest failure probability of the elements in the system, as can be seen from Figure 6.3. It can also be in Figure 6.3 that this is a conservative assumption.

$$\text{For norm} = 1:100, \quad \beta_{\text{norm}} = -\Phi^{-1}(1/100) = 2.33 \tag{7.12}$$

$$F_{\text{liftup}} = 0.80, \qquad P_{f,\text{liftup}} = 6.52E-3 \quad \text{per year} \tag{7.13}$$

$$F_{\text{internal erosion}} = 0.86, \qquad P_{f,\text{internal erosion}} = 1.44E-2 \quad \text{per year} \tag{7.14}$$

$$P_{f,\text{piping}} = \text{Min}(P_{f,\text{liftup}}, P_{f,\text{internal erosion}}) = 6.52E-3 \quad \text{per year} \tag{7.15}$$

The maximum allowed failure probability of dike-section is determined by the norm, as well as the allocated space of the failure mechanism in the failure probability budget. If the standard failure probability space for piping of 0.24 is applied (as seen in the standard failure probability budget seen in Table 6.1). As such, a 1:100 norm implies a maximum allowed failure probability for piping of 2.40E-3 per year. As the failure probability for piping was computed in Equation 7.15 to be 6.52E-3, the dike fails the semi-probabilistic assessment for a 1:100 norm. The term 'for a 1:100 norm' is important, as many factors have been influenced by this assumption of a 1:100 norm. After all, the norm determines; firstly, the outside water level, which is the main loading variable, secondly, the relationship between safety factor and failure probability and thirdly, the maximum allowed failure probability. The semi-probabilistic assessment has been computed for a varying norm, to assess the influence of this norm on the compute failure probability as well as the final verdict. These assessment results can be seen in Table 7.2.

Norm	β_{norm}	h_{norm}	F_{liftup}	$P_{f,\text{liftup}}$	$F_{\text{I.E.}}$	$P_{f,\text{I.E.}}$	$P_{f,\text{piping}}$	$P_{f,\text{max}}$	Verdict
1/10	1.28	2.00	1.20	2.97E-3	1.27	2.17E-2	2.97E-3	2.4E-2	Pass
1/30	1.83	2.48	0.97	4.59E-3	1.03	1.76E-2	4.59E-3	8.0E-3	Pass
1/100	2.33	3.00	0.80	6.52E-3	0.86	1.44E-2	6.52E-3	2.4E-3	Fail
1/300	2.71	3.47	0.69	8.34E-3	0.75	1.20E-2	8.34E-3	8.0E-4	Fail
1/1.000	3.09	3.98	0.60	1.03E-2	0.65	9.82E-3	9.82E-3	2.4E-4	Fail
1/3.000	3.40	4.45	0.54	1.20E-2	0.59	8.11E-3	8.11E-3	8.0E-5	Fail
1/10.000	3.72	4.96	0.49	1.37E-2	0.53	6.50E-3	6.50E-3	2.4E-5	Fail
1/30.000	3.99	5.43	0.44	1.51E-2	0.48	5.27E-3	5.27E-3	8.0E-6	Fail
1/100.000	4.26	5.94	0.41	1.64E-2	0.44	4.14E-3	4.14E-3	2.4E-6	Fail

Table 7.2: Semi-probabilistic assessment for a varying norm (Norm and probabilities in [year^{-1}], h_{norm} in [m+NAP])

It can be seen from Table 7.2 that the norm, a completely non-physical attribute, has an influence on the probabilities of failure. Nonetheless, since the norm also determines the maximum allowed probability of failure, a verdict can still be rendered. The dike section is rendered safe for less-strict norms and unsafe for stricter norms, which makes sense, as a higher norm implies a stricter assessment. When looking at the failure probabilities for lift-up and internal erosion in Table 7.2 however (which have been marked), something unexpected seems happen. For the sub-mechanism lift-up, a stricter norm leads to a higher failure probability. For the sub-mechanism internal erosion however, a stricter norm leads to a lower failure probability. This results in a failure probability for piping, which is maximal for a norm 1:1000, with lower failure probabilities with stricter and less-strict norms. For both sub-mechanisms, the safety factor is lowered with stricter norms, which is expected as the only variable influence by the norm in the safety factor is the outside water level. This outside water level increases with increasing norm. The strange behaviour of the failure probabilities must then be caused by the calibration relationship. To get insight into what is happening, both the calibration relationships have been plotted in Figure 7.7, as well as the safety factors/failure probabilities.

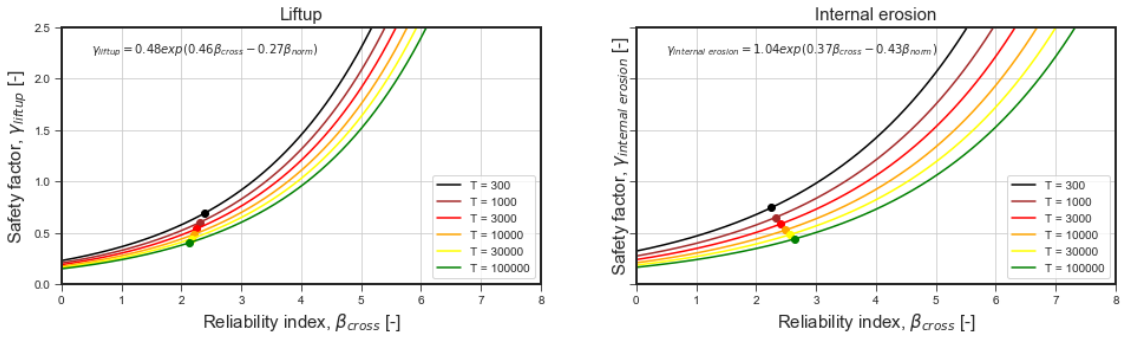

Figure 7.7: Calibration relationship for lift-up (left) and internal erosion (right)

In Figure 7.7 it can be seen that as the safety factor is lowered for lift-up, the reliability index is lowered as well, and a lower reliability index implies a higher failure probability. For internal erosion however, a lower safety factor has increased the reliability index, due to the low gradients of the curves. As an increased reliability index implies a lower failure probability, the lower safety factor has implied lower failure probabilities. Clearly, this behaviour is non-physical.

7.3. Fragility-based probabilistic assessment

As shown in Section 7.2, the semi-probabilistic approach as described in the WBI2017 can be used to compute the failure probability for piping. Nonetheless, some non-physical behaviour was seen, which is primarily due to the norm-dependency of the calibration relationship. As a comparison, a fragility-based probabilistic assessment will be done in this section. Theoretically, this should result in a failure probability that is less conservative, as the methodology is more accurate.

As the fragility-based methodology is applied, the strength and loading terms are described in separate steps. The conditional failure probabilities are computed with a subset sampling algorithm, explained in Subsection 4.3.3. The distributions applied in this section will be exactly the same as in the semi-probabilistic assessment, meaning that Table 7.1 will be used, as well as the schematisation seen in Figure 7.6. After all, there is no difference in input between the semi-probabilistic and the probabilistic assessment.

7.3.1. Limit state functions

To evaluate the limit state functions R and S need to be determined. The expressions for R and S can be determined from the formulae of the stability factors: Equation 7.3 and Equation 7.6. In these formulae R was divided by S after all to calculate the safety factor. Instead of the characteristic values, the entire distribution are now applied however and the failure probability is equal to P(Z<0).

$$Z_{\text{liftup}} = R_{\text{liftup}} - S_{\text{liftup}} = \Delta\phi_{c,u} - r\,h_{\text{outside}} \tag{7.16}$$

$$Z_{\text{internal erosion}} = R_{\text{internal erosion}} - S_{\text{internal erosion}} = \Delta h_c - h_{\text{outside}} \tag{7.17}$$

Where:

$\Delta\phi_{c,u}$	[m]	The critical pressure as calculated with Equation 7.4
r	[-]	Reduction factor, discounting the reduced pressures between entry- and exit point
Δh_c	[m]	The critical head difference calculated with the Sellmeijer formulae
h_{outside}	[m+datum]	Outside water level

First a loading range is determined. In this example the loading parameter S, which represents the outside water level, has been defined as a linearly spaced vector; minimum 0, maximum 10 and 101 vector entries. These are the conditional loading scenarios considered.

$$\overline{S} = \langle\, 0.0,\ 0.1,\ \ldots,\ 9.9,\ 10.0 \,\rangle \tag{7.18}$$

For every entry in vector $\overline{S}$, a subset sampling algorithm evaluates the conditional failure probability. This conditional failure probability is equal to the probability this entry s is larger than R:

$$\text{for s in } \overline{S}: \quad P_{\text{f,liftup,conditional,s}} = P(R_{\text{liftup}} - s < 0) = P(\frac{\Delta\phi_{c,u}}{r} < s) \tag{7.19}$$

$$\text{for s in } \overline{S}: \quad P_{\text{f,internal erosion,conditional,s}} = P(R_{\text{internal erosion}} - s < 0) = P(\Delta h_c < s) \tag{7.20}$$

The fragility curve is then defined as the set of conditional failure probabilities, $P_{\text{f,conditional}}$, matching vector $\overline{S}$. For both the sub-mechanisms a fragility curve can be constructed, by plotting vector $\overline{S}$ (representing outside water level) against these conditional failure probabilities. These fragility curves can be seen in Figure 7.8. The gradients of the curves are an indication of the uncertainty. A fully deterministic assessment would lead to a jump (infinite gradient) in the curve at the load where the system fails. From the curves in Figure 7.8 it can be concluded that the sub-mechanism lift-up has more uncertainty than the sub-mechanism internal erosion[2].

[2] This also means that for the low loading tail, the conditional failure probabilities of lift-up are much higher than for internal erosion (which is not really visible from Figure 7.8). For example, the conditional failure probabilities for h=1.0m+NAP are 2.59E-14 for internal erosion and 3.01E-7 for lift-up. This can be of large influence on the final failure probabilities as these low end tails are weighted very heavily by the PDF of the load, due to their higher probability of occurrence. This is confirmed by Equation 7.21 and Equation 7.22, where the failure probability for internal erosion is over twice as high as the failure probability for lift-up, even though the fragility curves of the sub-mechanisms have roughly the same average.

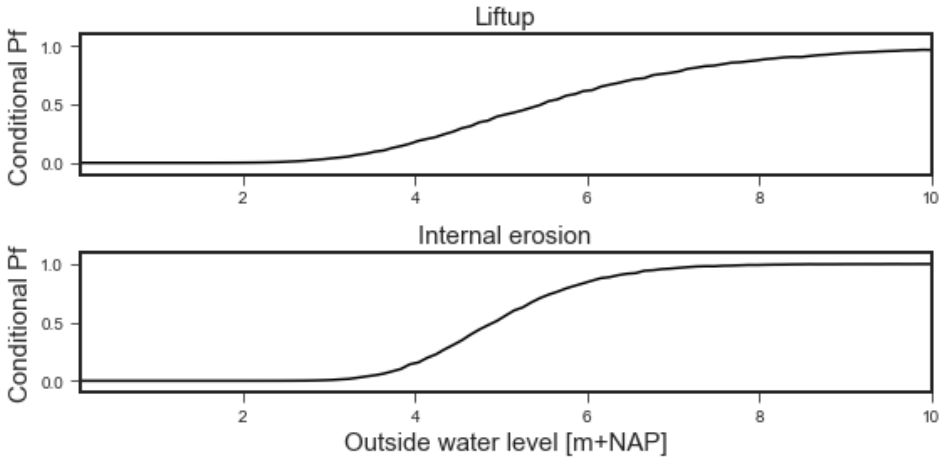

Figure 7.8: Fragility curves for the sub-mechanisms lift-up and internal erosion

7.3.2. Loading term: integration

The loading has been modelled as a Gumbel distribution, as can be seen in Table 7.1. The PDF of this loading can be seen Figure 7.9.

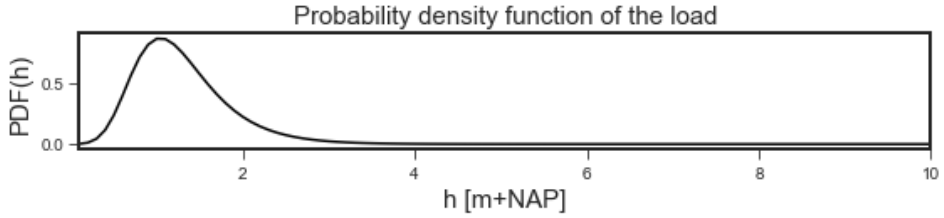

Figure 7.9: PDF for the loading

As was shown in Chapter 6, the dependence can be controlled by the manner in which integration is done. Both fragility curves can be integrated independently. If the curves are integrated this leads to[3]:

$$P_{f,\text{liftup}} = \int_0^{\infty} P_{f,\text{conditional,liftup}}\ \text{f}(h)\ \text{dh} = 1.56\text{E-}3\ \text{year}^{-1} \tag{7.21}$$

$$P_{f,\text{internal erosion}} = \int_0^{\infty} P_{f,\text{conditional,internal erosion}}\ \text{f}(h)\ \text{dh} = 6.29\text{E-}4\ \text{year}^{-1} \tag{7.22}$$

If the parallel sub-mechanisms are considered fully independent this would lead to a (as can be seen in Figure 6.3, optimistic) failure probability for piping of:

$$P_{f,\text{piping}} = P_{f,\text{liftup}} * P_{f,\text{internal erosion}} = 9.72\text{E-}7\ \text{year}^{-1} \tag{7.23}$$

If the parallel sub-mechanisms are considered fully dependent this would lead to a (as can be seen in Figure 6.3, conservative) failure probability for piping of:

$$P_{f,\text{piping}} = \text{Min}(P_{f,\text{liftup}}, P_{f,\text{internal erosion}}) = 6.29\text{E-}4\ \text{year}^{-1} \tag{7.24}$$

[3]The integration has only been applied for positive water levels. Since the outside water level can be negative when below NAP, integration could have been applied on $[-\infty,\infty]$. When the outside water level is lower than the inside ground level however, piping can not occur. These types of checks need to be made whenever abstract mathematical models are used, to ensure that the behaviour that is modelled is still physically sound (or even possible). Especially when (normal) distributions are applied, results can quickly become non-physical as the tails extent to (minus) infinity.

If the parallel subsystems are to be considered independent in strength and dependent in loading, the conditional failure probabilities can be considered instead of the actual failure probabilities (as was shown in Chapter 6). As such, the overlap of the conditional failure probabilities becomes:

$$P_{f,\text{conditional, piping}} = P_{f,\text{conditional,liftup}} * P_{f,\text{conditional,internal erosion}} \tag{7.25}$$

These conditional failure probabilities can then be used to construct a new fragility curve for the mechanism piping, which includes both the sub-mechanisms liftup and internal erosion. This can be seen in Figure 7.10.

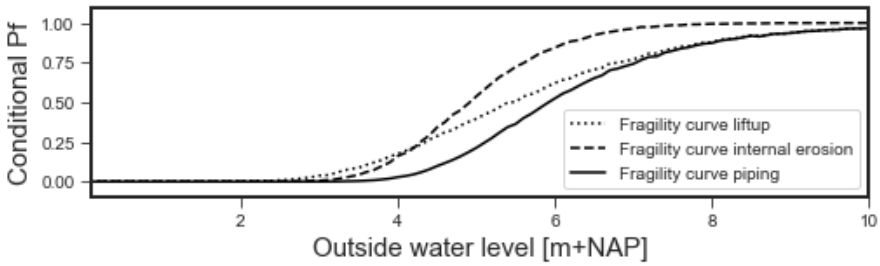

Figure 7.10: Fragility curve for the combined parallel sub-mechanisms liftup and internal erosion

Integration of the full fragility curve leads to a failure probability that is less conservative than the fully dependent failure probability:

$$P_{f,\text{piping}} = \int_0^{\infty} P_{f,\text{conditional,piping}} \,\text{PDF}(h)\,\text{dh} = 1.23\text{E-}4\ \text{year}^{-1} \tag{7.26}$$

Additionally, since a fully probabilistic assessment has been done, more information about the limit state function can be collected, for example the importance factors. Importance factors can be calculated analytically, through a FORM analysis, or through perturbation methods, such as a Taylor expansion [9]. The importance factors for lift-up and internal erosion have been drawn in Figure 7.11 and Figure 7.12 respectively. The importance factors indicate the relative influence that each parameter has on the limit state function[4]. As such, it can offer great insight into the process, as the importance of variables can also show whether failure mechanisms are dependent. In Figure 7.12 it can be seen that the permeability of the permeable layer is a large influence on the mechanisms. In Figure 7.11, the reduction factor (which is likely related to the permeability) can also be seen to be important. This importance on the same physical attributes in the soil will causes dependence between the sub-mechanisms, and as such, an assumption of independence between the strength parameters would be too optimistic.

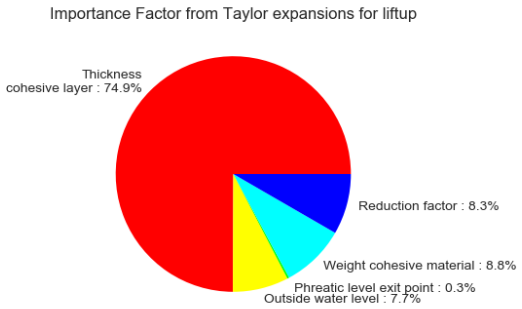

Figure 7.11: Importance factors lift up

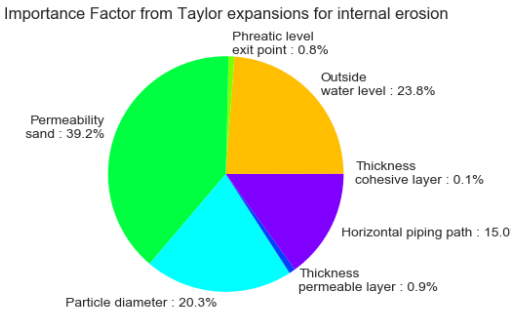

Figure 7.12: Importance factors internal erosion

[4]The influence factors take the underlying distribution of a variable into account. The volumetric weight of water could greatly influence the failure probability for piping, for example. This variable has a very small variance however, and as such, hardly influences failure.

7.4. Comparison semi-probabilistic and probabilistic assessments

When assessing whether the computed failure probability complies with a norm in a probabilistic assessment, all failure mechanisms will need to be computed. The computed failure probabilities per failure mechanism can then be combined in a series system and compared to the norm, where an assumption of full dependence in strength and load has been made to keep the results comparable. To avoid having to compute the failure probabilities for all failure mechanisms, and to allow for a direct comparison between the semi-probabilistic assessment and the fragility-based assessment, the fragility-based assessment will be compared to the norm multiplied with the allocated failure space (0.24) from the failure probability budget (as is also done in the semi-probabilistic assessment). This can be seen in Table 7.3. Since the failure probability in a fragility-based assessment is independent on the norm, it is constant over all norms considered. It can be seen that the fragility-based assessment complies with significantly stricter norms when compared to the semi-probabilistic assessment.

Norm	$P_{f,Semi\text{-}probabilistic}$	$P_{f,Fragility}$	$P_{f,max}$	Verdict semi-probabilistic	Verdict probabilistic
1/10	2.97E-3	6.29E-4	2.40E-2	Pass	Pass
1/30	4.59E-3	6.29E-4	8.00E-3	Pass	Pass
1/100	6.52E-3	6.29E-4	2.40E-3	Fail	Pass
1/300	8.34E-3	6.29E-4	8.00E-4	Fail	Pass
1/1.000	9.82E-3	6.29E-4	2.40E-4	Fail	Fail
1/3.000	8.11E-3	6.29E-4	8.00E-5	Fail	Fail
1/10.000	6.50E-3	6.29E-4	2.40E-5	Fail	Fail
1/30.000	5.27E-3	6.29E-4	8.00E-6	Fail	Fail
1/100.000	4.14E-3	6.29E-4	2.40E-6	Fail	Fail

Table 7.3: Comparison of verdicts in a semi-probabilistic and a fragility-based assessment

7.5. Conclusion

This chapter has shown how semi-probabilistic methods compare to fully probabilistic methods, specifically a fragility-based methodology. It has been shown that in terms of input (the variables and their distributions) as well as in terms of modelling (the formulae applied) there is no difference between the methods. The main difference between the methods is found in the output. A semi-probabilistic assessment offers a verdict, and the WBI2017 applies a calibrated relationship to compute a failure probability, which brings conservatism. A probabilistic assessment offers a direct failure probability, which is more accurate. It was shown in this chapter that this leads to lower failure probabilities, due to the decreased conservatism. Nonetheless, the probabilistic assessment might be considered less practical, both when considering the complexity of the assessment and the computational effort required.

Some problems with the semi-probabilistic assessment have been highlighted. These were mainly caused by the norm-dependency and the effort to compute a failure probability from a (norm-dependent) stability factor. The calibration process that is applied for this conversion is essentially an empirical process. This means that a formula has been plot-fitted through data. This leads to inaccuracies, which ultimately leads to conservatism. This can also lead to some non-physical behaviour as it was shown that increasing the norm can lead to lower failure probabilities for a dike. Due to the norm-dependency found in the failure probability, the failure probability is not the 'real-life' failure probability of the dike (as this is norm-independent), which might be confusing to administrators. This can be considered strange, as one of the main reasons for applying a semi-probabilistic method was that probabilistic methods were considered 'black box'[20]. Finally, it was shown how a fragility-based method offer increased more insight, both through the fragility curves and through post-sampling analyses, such as determining the importance factors. The fragility-based method was also shown to offer more influence on the dependency, which was already theorized in Chapter 6.

The semi-probabilistic methodology applied in the WBI2017 works however, as was shown and thus it can be applied as detailed assessment to assesses dikes for piping. The fragility-based assessment can offer a probabilistic custom assessment, to be applied when the detailed assessment fails and a less conservative assessment is required, or when additional insight into the process is preferred.

8

Failure mechanism I: Height of structure

In Chapter 6 and Chapter 7 the fragility-based assessment method was investigated and compared the methodology with methods prescribed in the WBI2017. The next part of the report will focus on the application of the fragility-based methodology, in order to assess the Eastern Scheldt barrier.

In this chapter the Roompotsluis will be assessed on the aspect of retaining height. Both the lock itself and the coupure in which it is situated will be assessed , and through this assessment will attempt to show the flexibility that a fragility based methodology offers. This will start with a description of the failure mechanisms, from which limit state functions will be defined. These limit state functions will then be applied to compute the fragility curves for the lock. As multiple loading variables play a role, these curves will be expanded into a 3d surface, which will be integrated into a failure probability. The chapter will end with some comparisons between the fragility based assessment and an earlier safety study.

A description of the lock can be found in Chapter 2. Due to the low height of the lock, both the bottom protection behind the lock as well as the stones on the coupure will be assessed. Failure will be defined as failure of any stone, meaning no form of transfer probability is taken into account.

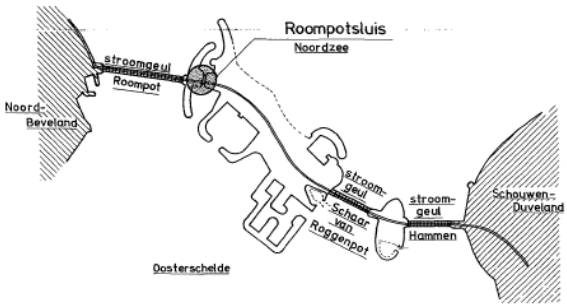

Figure 8.1: Location of the Roompotsluis [85]

Figure 8.2: The Roompotsluis seen from the sea side [68]

8.1. Failure mechanism

The height of a structure can be considered insufficient when either the discharge over the structure is large enough to endanger the storage capacity of the basin behind the structure, or when the discharge over the structure causes dangerous erosion. Discharge over a structure can occur through two distinct mechanisms; overtopping and overflow.

Overtopping describes the process of wave overtopping. Each wave impacting the structure discharges water over the structure. This water then flows over the structure to the Eastern Scheldt. This discharge is very variable, as every wave discharges a large amount of water, while between each wave there is zero discharge. A schematisation of the overtopping mechanism can be seen in Figure 8.3.

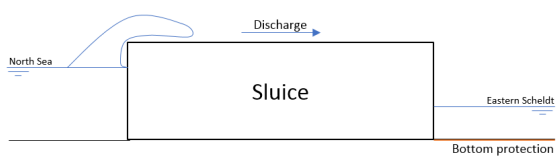

Figure 8.3: Overtopping when $h_{\text{North Sea}} < h_{\text{lock}}$

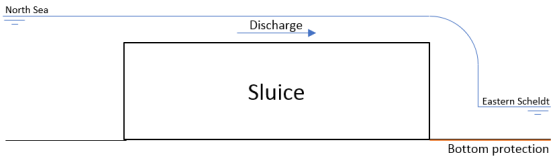

Figure 8.4: Overflow when $h_{\text{North Sea}} > h_{\text{lock}}$

Overflow describes the flow of water when the water level exceeds the height of the structure. As the water level on the North Sea side is higher than the water level on the Eastern Scheldt side, a flow occurs. This discharge is a lot more constant. A schematisation of the overflow mechanism can be seen in Figure 8.4.

Due to the size of the Eastern Scheldt barrier, as well as the discharge through the barrier due to leakage in closed conditions, the discharge over the Roompotsluis is considered to be insignificant for storage capacity problems in the Easter Scheldt basin. Other failure besides failure of the bottom protection can become an issue however. When the water levels outside become high enough for significant plunging flow into the lock, the safety of the lock can no longer be guaranteed, due to vibrations in the doors, etc. [74]. This water level is selected as an upper limit, for which the lock will always fail (this also saves on computational effort). The rest of the assessment of the height of the structure will consist of an assessment of the stability of the stones on and behind the coupure only. The location of these stones can be seen in Figure 8.5 and Figure 8.6.

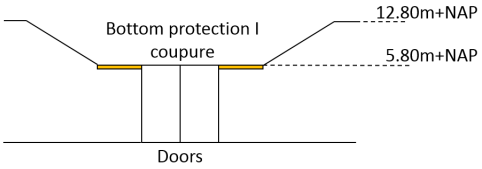

Figure 8.5: Front view of the lock, showing the lower height of the coupure with regard to the height of the dike (not to scale)

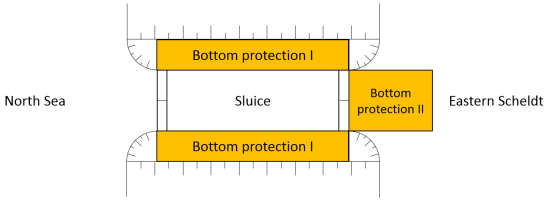

Figure 8.6: Top view of the lock, with the locations of the bottom protection to be assessed highlighted (not to scale)

In total 5 different sub-mechanisms can thus be distinguished; failure of the two types of bottom protection by two different mechanisms as well as failure of the doors. These can be seen in the fault tree in Figure 8.7.

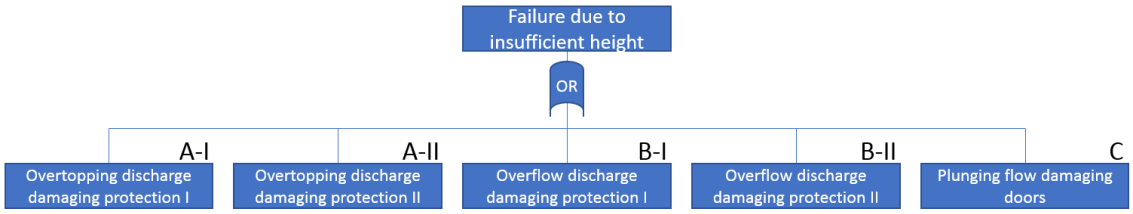

Figure 8.7: Fault tree applied in the assessment of the height of the lock, with the different sub-mechanisms numbered

8.2. Assessment

The assessment of the stability of the stones on and behind the coupure consists of a comparison between the critical flow velocity over the stones (R) and the occurring flow velocity over the stones (S). The critical flow velocity over a stone can be calculated with a stability formula. The occurring flow velocity is highly dependent on the water level outside the lock, with overtopping and overflow (or both) occurring at various different realizations of the outside water level, as was shown in Figure 8.3 and Figure 8.4. This makes a (conditional) fragility based assessment useful, as it can assess with different limit state functions for different deterministic water levels. This will be discussed in Subsection 8.2.2. The variables applied in this section can be found in Table A.1 in Appendix A.

8.2.1. Strength term: critical discharge

The critical discharge over a stone is calculated with the Pilarczyk formula. This formula combines various design formulae [16] and can be used to calculate the needed dimensions of granular material as well as non-granular material (block mattresses or gabions for example) against current attack. Rewriting it allows for the calculation of a critical flow velocity for a certain stone dimension. The Pilarczyk formula, rewritten to evaluate critical flow velocity, can be seen in Equation 8.1[74].

$$D = \frac{\varphi_{sc}}{\Delta} \frac{0.035}{\psi_{cr}} k_h k_{sl}^{-1} k_t^2 \frac{U^2}{2g} \quad \rightarrow \quad U = \sqrt{\frac{2g\Delta D \psi_{cr} k_{sl}}{0.035 \varphi_{sc} k_h k_t^2}} \tag{8.1}$$

Where:

U	$[m/s]$	Depth averaged flow velocity
g	$[m/s^2]$	Gravitational acceleration
Δ	$[-]$	Relative density
D	$[m]$	Thickness of the element
Ψ_{cr}	$[-]$	Shear stress parameter
k_{sl}	$[-]$	Slope factor
φ_{sc}	$[-]$	Stability constant
k_h	$[-]$	Depth parameter
k_t	$[-]$	Turbulence factor

Plunging flow

When the water level on the North Sea exceeds the height of the doors of the lock, water will flow into the lock. The height of the doors of the lock are the same as the height of the coupure, 5.80m+NAP [85]. When this happens, the water will plunge over the doors into the lock. Plunging flow is difficult to describe mathematically [80]. A maximum water level has been determined for which the safety of the lock doors due to plunging can no longer be assessed. At discharges over a lock door of $1 m^3/s$ or more, damaging effects to the doors can start to occur, such as vibrations [74]. This maximum discharge occurs around a water level that is 0.6m higher than the lock door [58]. At this water level the lock door will be considered as failed and thus the lock fails.

8.2.2. Loading term: occurring discharge

The type of occurring discharge is determined by the outside water level. This means that for a varying water levels outside, a varying limit state functions can be determined. As such, a fragility curve method is very applicable, due to the deterministic selection of the outside water level. When the water level on the North Sea is below the height of the structure (5.80m+NAP), only overtopping waves causes a discharge. When the water level on the North Sea is at or above the height of the structure, both overtopping and overflow cause a discharge. When the water level on the North exceeds the height of the structure by 0.60m, the structure fails. Two limit state functions there need to constructed; one for overtopping and one for overtopping plus overflow.

Overtopping
The overtopping discharge is given by Equation 8.2[1][2]:

$$q_{ot} = \sqrt{g H_s^3} \exp(-2.61 \frac{h_{str} - h_{NS}}{H_s}) \tag{8.2}$$

Where:

q_{ot}	$[l/s/m]$	Average discharge due to overtopping
g	$[m/s^2]$	Gravitational acceleration
H_s	[m]	Significant wave height
h_{str}	[m+NAP]	Height structure
h_{NS}	[m+NAP]	Water level North Sea

This formula only calculates the average discharge however. For the bottom protection behind the lock this is sufficient. For the assessment of the stones on the coupure a flow velocity has to be computed, which is difficult for overtopping waves. After all, what is the water depth of an overtopping wave? There are empirical tables available for the relation between discharge and water level. These are based on field test and can be used to assess for a critical discharge.

A more quantitative approach is preferred however. In the original design of the barrier, the maximum flow velocity over the stones was assumed to be equal to the maximum orbital velocity of the incoming waves [84]. This assumption will be followed here. The maximum horizontal particle velocity of a wave for all water depths (deep, intermediate and shallow) is given by Equation 8.3 [28]:

$$\hat{u_x} = \omega a \frac{\cosh k(d+z)}{\sinh kd} \tag{8.3}$$

Where:

$\hat{u_x}$	$[m/s]$	Maximum orbital velocity of a wave
ω	[rad/s]	Angular frequency
a	[m]	Amplitude of the wave
k	$[m^{-1}]$	Wave number
d	[m]	Water depth
z	[m]	Height in the water column

For a probabilistic assessment, the term kd is difficult to determine for intermediate water depths, as an iterative calculation is required [28]. An approximation will be applied and can be seen in Equation 8.4[22]:

$$kd \approx \frac{\alpha + \beta^2 (\cosh \beta)^{-2}}{\tanh \beta + \beta (\cosh \beta)^{-2}} \quad \text{with} \quad \alpha = k_0 d \quad \text{and} \quad \beta = \alpha (\tanh \alpha)^{-0.5} \tag{8.4}$$

Where:

k_0	$[m^{-1}]$	Wave number in deep water
d	[m]	Water depth

This approximation can also be used to to apply the so called dispersion relationship between the angular frequency, $\omega = \frac{2\pi}{T}$ and the wave number, $k = \frac{2\pi}{L}$ [28]:

$$\omega^2 = gk \tanh(kd) \tag{8.5}$$

This relationship can be used to write the wave period (T) and the wave length (L) as a single variable.

[1] There are coefficients added to this formula when a nose is present on the structure or when waves come in under an angle. These are not applied here and therefore they are not displayed in the formula.

Overflow
When the water levels on the North Sea are above the height of the structure (5.80m+NAP), overflow will start to occur. The discharge caused by this overflow can be calculated with Equation 8.6[75]:

$$q_{of} = 0.55\sqrt{-g(h_{str} - h_{NS})^3} \tag{8.6}$$

Where:

q_{of}	[l/s/m]	Discharge over the structure
g	$[m/s^2]$	Gravitational acceleration
h_{str}	[m+NAP]	Height structure
h_{NS}	[m+NAP]	Water level North Sea

8.2.3. Limit state functions

With the formulas for strength (critical discharge) and load (occurring discharge) known a limit state function can be set up. This limit state function will evaluate the bottom protection at two location, the stones on the coupure and the stones behind the lock. The limit state function is build up from 3 scenarios: overtopping only, overtopping+overflow and plunging flow, with the scenario determined by the outside water level compared to the height of the structure. The numbering from Figure 8.7 has been included as to offer quick reference to which limit state function is for which mechanism.

For the stones on the coupure, the occurring flow velocities are compared to the critical flow velocities[2]. When the water level on the North Sea is lower than the height of the structure, only overtopping occurs. If the maximum orbital velocity of the waves exceeds the maximum flow velocity for the stones, the structure fails:

$$\text{Mechanism A-I:} \quad Z = u_{\text{max,Pilarczyk}} - \hat{u}_x \tag{8.7}$$

$$Z = \sqrt{\frac{2g\Delta D_c \psi_{cr} k_{sl}}{0.035\varphi_{sc} k_t^2}} - \omega a \frac{\cosh k(d_{NS} + z)}{\sinh k d_{NS}} \quad \text{for } h_{NS} < h_{str} \tag{8.8}$$

When the water levels on the North Sea is higher than the height of the structure, both overtopping and overflow occur. If the flow velocity due to the maximum orbital velocity *and* the flow due to overflow exceeds the maximum flow velocity for the stones, the structure fails:

$$\text{Mechanism B-I:} \quad Z = u_{\text{max,Pilarczyk}} - \hat{u}_x - \frac{q_{of}}{h_{NS} - h_{str}} \tag{8.9}$$

$$Z = \sqrt{\frac{2g\Delta D_c \psi_{cr} k_{sl}}{0.035\varphi_{sc} k_t^2}} - \omega a \frac{\cosh k(d_{NS} + z)}{\sinh k d_{NS}} - \frac{0.55\sqrt{-g(h_{str} - h_{NS})^3}}{h_{NS} - h_{str}} \quad \text{for } h_{NS} > h_{str} \tag{8.10}$$

For the stones behind the lock the traditional model is applied, where the occurring discharge over the structure is compared to the critical discharge over the structure. When the water level on the North Sea is lower than the height of the structure, only overtopping occurs. If the average discharge due to overtopping behind the structure exceeds the critical average discharge for the stones behind the structure (maximum flow velocity multiplied by the water depth), the structure fails:

$$\text{Mechanism A-II:} \quad Z = d_{ES} * u_{\text{max,Pilarczyk}} - q_{ot} \tag{8.11}$$

$$Z = d_{ES}\sqrt{\frac{2g\Delta D_b \psi_{cr} k_{sl}}{0.035\varphi_{sc} k_h k_t^2}} - \sqrt{gH_s^3}\exp(-2.61\frac{h_{str} - h_{NS}}{H_s}) \quad \text{for } h_{NS} < h_{str} \tag{8.12}$$

[2]The term k_h can be ignored in Pilarczyks formula, when the local velocity is used instead of the average velocity. As such when the orbital velocity is applied to assess the stones on the coupure, the term is ignored[74].

When the water levels on the North Sea are higher than the height of the structure, both overtopping and overflow occur. If the average discharge caused by these mechanisms exceeds the critical average discharge for the stones behind the structure, the structure fails:

$$\text{Mechanism B-II:} \quad Z = q_{\text{max,Pilarczyk}} - q_{ot} - q_{of} \tag{8.13}$$

$$Z = d_{ES}\sqrt{\frac{2g\Delta D_b \psi_{cr} k_{sl}}{0.035\varphi_{sc} k_h k_t^2}} - \sqrt{gH_s^3} - 0.55\sqrt{-g(h_{str} - h_{NS})^3} \quad \text{for } h_{NS} > h_{str} \tag{8.14}$$

When the water levels on the North Sea exceed the height of the structure by more than 0.60m, the doors will be considered to fail:

$$\text{Mechanism C:} \quad Z < 0 \quad \text{for } h_{NS} > h_{str} + 0.60 \tag{8.15}$$

8.3. Fragility curves

From the derived limit state functions, it can be seen that three main loading parameters influence the limit state: outside water level, wave height and wave length (in the form of the wave number, k). Different choices can be made with regards to the variables chosen as deterministic for the fragility analysis.

8.3.1. Water level and wave height

When only the outside water level and wave height are selected as deterministic parameter, a 2 dimensional fragility curve can be constructed. In Figure 8.8 several of these fragility curves are displayed, for the stones on the coupure ($P_{\text{f,coupure}}$), the stones behind the lock ($P_{\text{f,behind}}$) and the total series system, where: $P_{\text{f,total}} = \text{Max}(P_{\text{f,coupure}}, P_{\text{f,behind}})$. The behaviour of the lock can now be seen in Figure 8.8.

When wave heights are low (H_s = 3.0m) the lock will only fail when the threshold of height of the structure + 0.60m is reached (at h_{NS} = 6.40m). Even at higher wave heights, the bottom protection behind the lock never causes failure, as the lock doors will fail before before the bottom protection behind the lock fails.

When the wave height is increased (H_s = 4.0m), the fragility curve of the stones on the coupure starts to change. First the overflow starts to add increased failure probabilities for water levels between h_{NS} = 5.80m and h_{NS} = 6.40m, as overflow only occurs between these values (while not failing the doors). When the wave height is increased further (H_s = 5.0m and 6.0m), the orbital velocity starts to add to the failure probability as well. Interestingly this effect is strongest for low water levels. As such, when waves are the highest (6.0m) a higher water level, while still low enough as to cause no overflow, leads to lower failure probabilities then a lower water level. This is caused by the increased orbital velocity at low water levels. To show the cause of this the orbital velocities of a 10s period wave have been displayed in Table 8.1. These orbital velocities have been calculated with Equation 8.3 and Equation 8.4.

	H_s = 3.0m	H_s = 4.0m	H_s = 5.0m	H_s = 6.0m
h_{NS} = 2.0m +NAP	1.663	2.217	2.771	3.326
h_{NS} = 4.0m +NAP	1.496	1.995	2.493	2.992
h_{NS} = 6.0m +NAP	1.372	1.830	2.287	2.745

Table 8.1: Maximum orbital velocities for a 10s period wave [m/s]

It can be seen from Table 8.1, that for similar wave heights a lower water level leads to a higher maximum orbital velocity[3]. This higher orbital velocity increases the conditional failure probability in high wave, low water level scenarios. This leads to the situation where for these conditions there is an optimum water level where the lock is safest, with rising failure probabilities for both higher and lower water levels.

[3]This only holds if no wave breaking occurs. When the water depth is low enough for the waves to start breaking (for the significant wave height this is approximately at $H_{s,\max}/d = 0.45$[28]), the wave height will decrease with decreasing water depth. This is not taken into account in the fragility curve however. In the fragility curve only the strength terms are taken into account after all. The effects of physically impossible combinations of loads will be integrated out as these have no probability of occurrence.

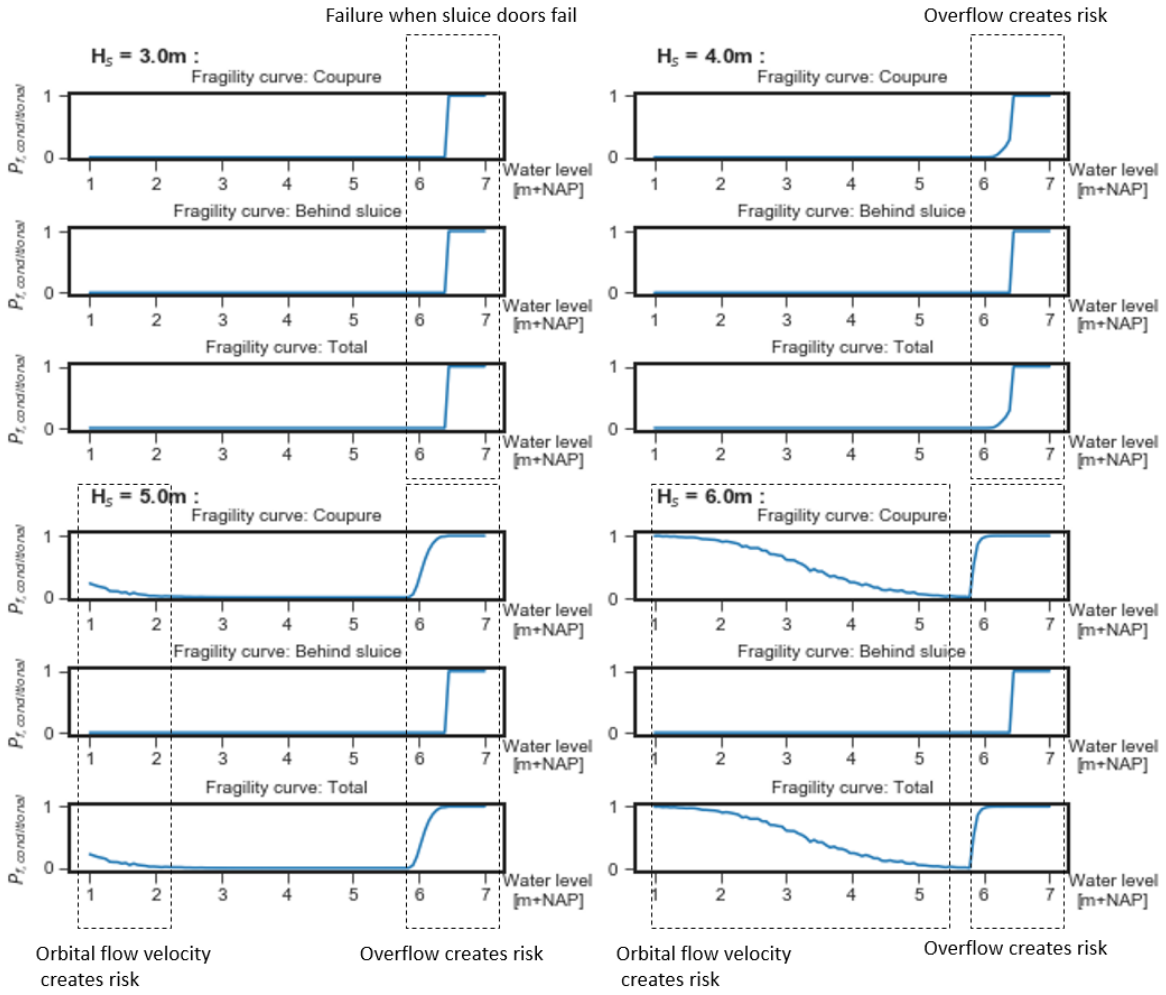

Figure 8.8: Fragility curves with deterministic water levels and wave height

It should be noted that the limit state functions for the protection on the coupure (mechanisms A-I and B-I) are based on the orbital velocity of the waves and as such, an implicit assumption is made that the waves can load these stones. If the water level is low enough that waves may not reach the stones on the coupure, this is a very conservative assumption. When looking at the different situations in Figure 8.8 it can be seen that the failure probability due to orbital velocity starts to rise for wave heights of over 4.0m. The assumption that the waves can load the stones (located at 5.80m+NAP) during low water levels becomes a lot less conservative as a result, but it is still an important assumption, as it is not fully physical. The water level and wave height can be plotted against the conditional failure probability in a 3-dimensional plot. This can be seen in Figure 8.9. The 2-dimensional fragility curves from Figure 8.8 can be seen as slices from this so called fragility surface, which can also be seen in Figure 8.9. By combining the two failure mechanisms into a single fragility surface, the loading parameter(s) will be considered fully dependent, as was further explained in Chapter 6.

Choosing the parameters on which the fragility analysis is applied, determines the amount of hidden dependency. Each parameter not on the axis (and thus not taken into account as fragility) is fully independent. This makes sense from a theoretical standpoint: dependency in loading should not be evaluated in the fragility step, but in the integration step. In the fragility analysis leading to Figure 8.9, the wave period was not considered with fragility. As such, it was given a independent distribution. The water level and wave height were taken into account with fragility, and during the integration step, their dependence can be taken into account. As the limit state function changes with the water level, assessing the water level with fragility can offer a large advantage. As the water level is deterministic in each probabilistic analysis, the limit state function does not change during this calculation. It is therefore possible to apply intelligent sampling methods, which greatly reduces the computational effort. These types of intelligent Monte Carlo simulation (in this

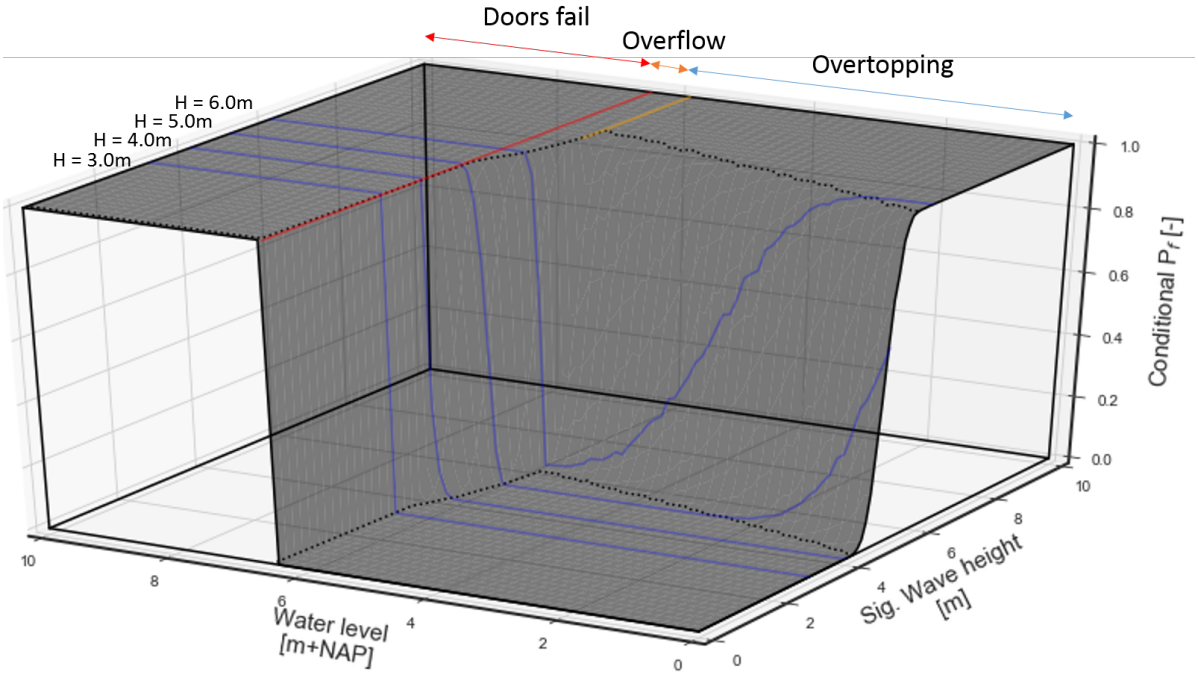

Figure 8.9: Fragility surface of the Roompot lock for the mechanism height structure

report subset sampling was applied) rely on a constant limit state function. If the water level was not considered with fragility, each Monte Carlo simulation would have to start with a sample of the water level, which would then imply a limit state function. This would still make a probabilistic analysis possible, however only with a Crude Monte Carlo simulation. Given the low failure probabilities considered for some combination of loading parameters («1E-10) this can be computationally demanding.

8.3.2. Loading parameters: water level, wave height and wavelength

If all three variables are applied conditionally, several 3d surfaces could be constructed, as can be seen in Figure 8.10.

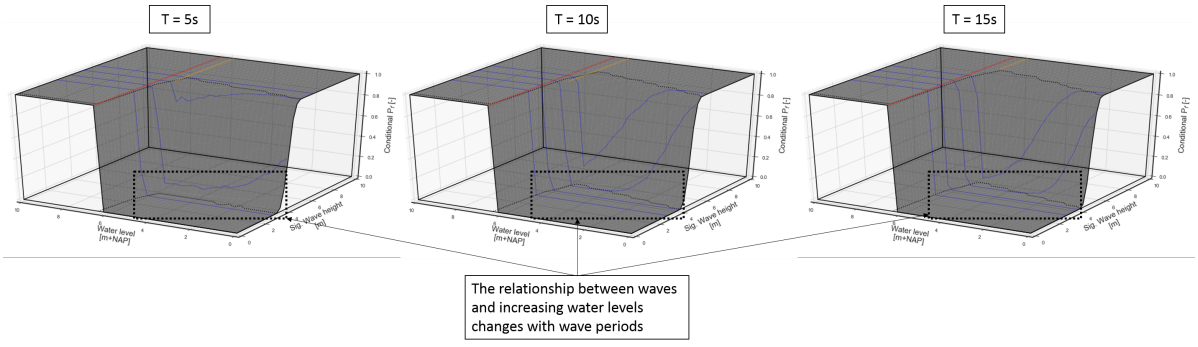

Figure 8.10: 4D fragility surface, plotting wave level, wave height and wave period against conditional failure probability

This type of 4D representation can present difficulties however. One of the main advantages of a fragility curve based methodology is the insight that it offers, including the readability of curves. The shape of the curves gives a quick insight into the behaviour of the structure. In Figure 8.10, this readability is reduced. The second difficulty introduced by higher dimensional fragility surfaces is the integration. When these multi-dimensional fragility surfaces need to be integrated into a failure probability, integration of higher dimensional shapes is required. Integration of higher dimensional shapes is often computationally demanding or highly inaccurate.

The multidimensional fragility analysis is not without potential uses however. The most notable advantage comes when the dependency in hydraulic conditions on a structure can be accounted for in the loading PDF. When a bivariate PDF of these three loading conditions is known (with dependency taken into account), the dependency of these loading conditions is discounted perfectly. Although the surface is less readable, more insight is (potentially) gained into the effects of the extra loading variables. In Figure 8.10, the varying effects of all three loading parameters can be seen. The effect of a rising water level can be seen to be different for waves with a 5 second period, when compared to waves with a 10 and 15 second period, as the influence of the water level on the waves (during overtopping) changes. As such, the multidimensional fragility surface still offers increased insight.

8.4. Integration over load

The integration of the fragility surfaces over the probability density will yield the failure probabilities. Multi-dimensional integration is computationally demanding (as well as intuitively difficult), and as such, the 3d fragility surface from Figure 8.9 will be integrated only. The probability density functions of the outside water level as well as the wave height are thus required[4].

The PresPeil2017 model has been developed by the ESB-administration to perform probabilistic calculations on data from the Eastern Scheldt barrier. Water level calculations for the Eastern Scheldt water system are performed with the hydraulic model IMPLIC, and stored in the FSmax422 database [19]. The Eastern Scheldt water system is the only water system in the Netherlands, which uses this hydraulic model to calculate water levels[40]. The wave calculations have been performed with SWAN [19]. With PresPeil2017, the exceedance curves of the hydraulic boundaries of the barrier can be extracted from the database. Additional information regarding the IMPLIC model and the PresPeil2017 model applied can be found in Appendix E. The exceedance curve (EC) of a stochastic variable displays the probability that the realization of the variable exceeds a given value. This means that it is the inverse of the cumulative density function (CDF or F_X), discussed in Chapter 4. As the CDF is the integral of the probability density function (PDF or f_X), taking the derivative of the CDF leads to the PDF.

In Figure 8.11 and Figure 8.12, the EC, CDF and PDF of the outside water level and the significant wave height can be seen. The water level has been determined for the location 'Roompot Buiten', which is located outside of the Roompot barrier. The water level along the Roompot barrier is assumed constant in Prespeil2017, meaning that there is no spatial variation along the barrier. There is no output location for the lock and therefore this assumption will be extended to the lock in this report. The wave height has been determined for the location R16, which is the middle of the Roompot barrier. The waves attacking the Roompot lock will likely be lower due to the more sheltered location, so this is a conservative approach[5].

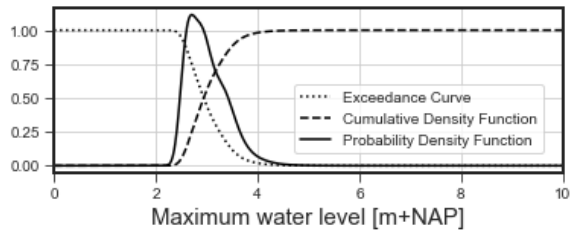

Figure 8.11: Maximum yearly water levels

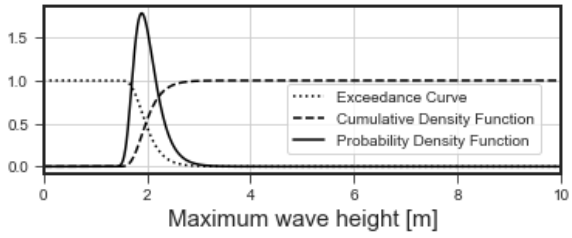

Figure 8.12: Maximum yearly wave heights

From PDF of the water level and wave height (the so called marginals) a bivariate (also sometimes referred to as composed or joint) PDF can be constructed, which is a PDF into multiple dimensions. When two independent probability density function are combined, the bivariate PDF is the product of the marginal PDFs [87], as seen in Equation 8.16.

[4] Increases in wave height and orbital velocity, due to standing wave patterns have not been included in this analysis

[5] The lock is protected by wave breakers, but these are not designed to withstand design storm conditions [84]. Nonetheless, the lock is located in a less deep area of the Eastern Scheldt when compared to the middle of the Roompot barrier. As such this assumption of conservatism will still be valid.

$$f_{\underline{x1},\underline{x2}}(x,y) = f_{\underline{x1}} * f_{\underline{x2}} \tag{8.16}$$

The water level and wave height are, most likely, not independent however. While the moment of maximal water level and maximal wave attack will likely both occur during a storm event, they will not always occur at the same time. This dependency was already used in the determination of the boundary conditions in the original design of the barrier. The boundary conditions were modelled as a 3d PDF of water level (inside and outside) and the wave energy [87][43]. PresPeil2017 allows for the extraction of the conditional exceedence probability during storms. An example of this is the wave height during maximum water level. In Figure 8.13 the PDF of the independent wave height and the wave height at maximum water level can be seen.

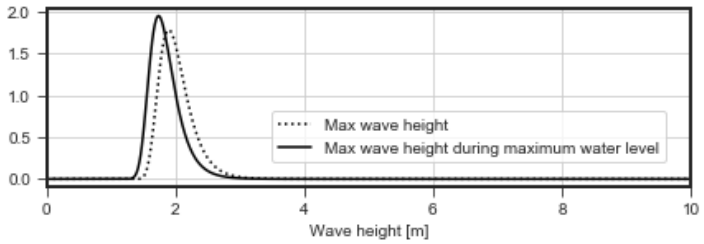

Figure 8.13: Comparison of the independent wave height and the wave height during maximum water level

It can be seen that the wave height during maximum water level is lower than the independent wave height. Applying the independent wave height would thus be a conservative approach. Additionally, the difference between the two PDF's indicates that the assumption of independence would have been incorrect. After all, when two events, A and B (or realizations of water level and wave height), are independent, $P(A) = P(A|B)$ should hold. Since the PDF's in Figure 8.13 are not identical, this does not hold. The maximum water level and the wave height *at maximum water level* will be assumed independent however[6]. Under this assumption the maximum water level and the wave height *during maximum water level* can be used as independent marginals for the bivariate PDF. This can be seen in Figure 8.14, where the bivariate PDF has been calculated with Equation 8.16. In Figure 8.14 also lines of equal probability have been displayed, to give a better indication of the shape of the low distribution tails.

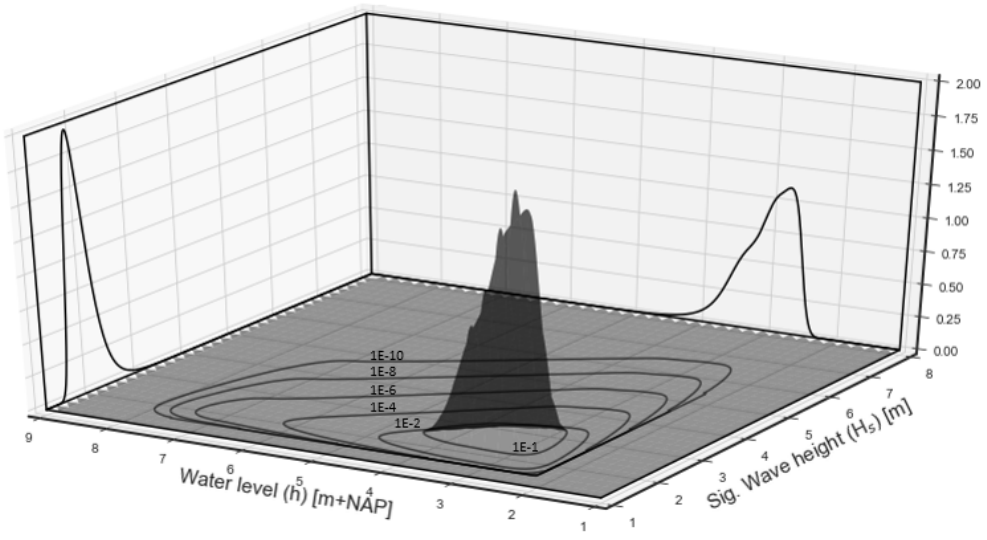

Figure 8.14: Bivariate PDF of yearly maximum water level and wave height during maximum water level

[6]Since water level and wave height are always linked, they are dependent, even when assessing the wave height during maximum water level.

The bivariate PDF from Figure 8.14 can be multiplied with the fragility surface from Figure 8.9 and integrated over both the loading marginals. This can be seen in Equation 8.17[7].

$$P_f = \int_0^{\infty} \int_{-d}^{\infty} P_{R<S|S}\, f(h, H_s)\, \mathrm{dh}\, \mathrm{dH}_s = 7.14\text{E-}6 \text{ per year} \tag{8.17}$$

If a 1:30.000 year norm is considered, overtopping and overflow are allowed a 24% share, according to the standard failure probability budget[8]. This means that the maximum allowed failure probability for overtopping and overflow is 8E-6. As such, the lock would just pass this norm.

By multiplying the fragility surface from Figure 8.9 with the PDF from Figure 8.14 insight into the relative influence of each failure mechanism can be gained. After all, this is the part of Equation 8.17 that is integrated into the failure probability. This can be seen in Figure 8.15, where the different mechanisms (Doors failing, overflow and overtopping) have been drawn for clarity. Additionally, a projection of the fragility surface has been plotted on the ground.

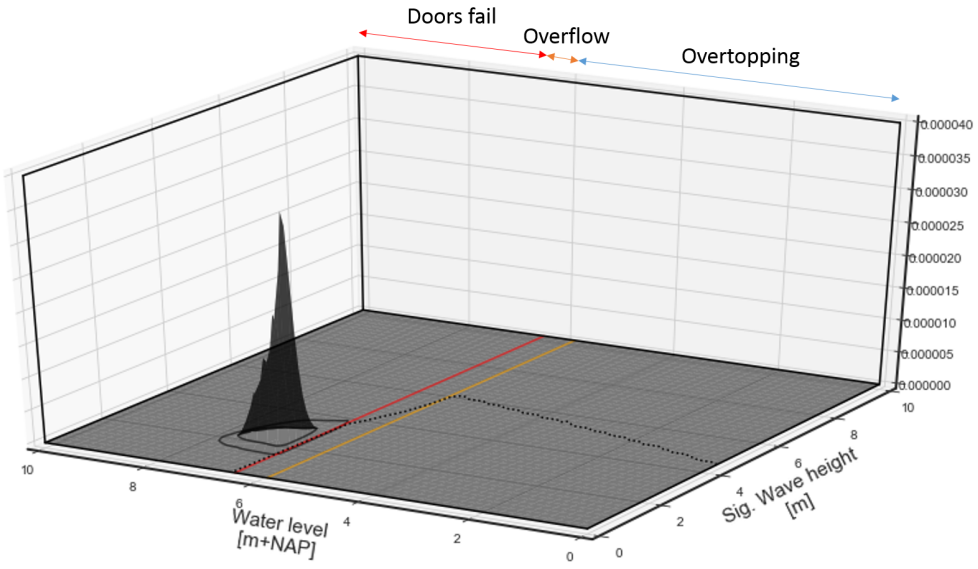

Figure 8.15: Conditional failure probability multiplied with PDF

From Figure 8.15 it can be seen that most of the failure probability is introduced by the water level exceeding the maximum allowed water level set for the doors. This is interesting, as it shows that the rock protection, both behind the lock and on the coupure, is not the most likely vulnerability of the lock, as failure of the doors is much more likely.

8.4.1. Comparison previous assessment round (VTV2006)

During the previous assessment round (the ARCADIS study [68]) the lock was assessed semi-probabilistic. As such, a quantitative comparison might be difficult, but some comparisons can be drawn nonetheless. The semi-probabilistic assessment had as possible outputs/verdicts: good, sufficient or insufficient.

Lock doors and bottom

For the assessment of the height of the lock, only the situation of overtopping was considered. This choice was due to the VTV2006, which describes the normative situation (overtopping or overflow), by comparing

[7] The water level will be integrated over the interval [−d,∞], while the wave height will be integrated over the interval [0,∞] to keep the calculation physically sound. After all, the water level cannot be lower than the bottom depth in front of the structure, while the wave height cannot be negative. Since the bivariate PDF should already have these limits taken into account, this step is redundant. It is nonetheless included here to keep the physics visible.

[8] The usage of a failure probability budget is not necessary, but it allows for the comparison whether a single mechanism would pass the norm. In a real assessment all failure probabilities of all mechanisms would be added and this would be compared with the norm.

the design water level with the retaining height of the structure [51]. As the retaining height (5.80m+NAP) was higher than the design water level (5.18m+NAP) plus a safety margin (0.30m), only overtopping was considered to be relevant. When looking at Figure 8.14 however, it can be seen that overflow (which occurs above water levels of 5.80m+NAP) can occur with a probability of approximately 1E-4 per year, which is not negligible. The ARCADIS study can therefore be assumed to be too optimistic (unsafe), as overflow adds considerably to the discharge into the lock. The discharge due to overtopping was calculated to be 1000 l/m/s which was deemed safe as the design overtopping discharge into the lock was 1100 l/m/s. As such the lock was given the verdict: 'good'.

Stones behind the lock
The stones behind the structure were not assessed for overtopping and/or overflow. Instead they assessed for the situation where the lock fails to close. As such a direct comparison between the assessments is not possible. From Figure 8.8 it can be seen that the stones behind the structure never show any failure probability (at least not under the limit water level of 6.40m+NAP). It can be concluded that the stones are sufficiently safe and that an assessment under the condition of a lock failing to close was indeed more relevant.

Stones on the coupure
The stones on the coupure were assessed by comparing the critical flow velocity of the basalton blocks with the maximum occurring flow velocity over the stones. This maximum occurring flow velocity was selected to be 2 m/s, which was taken from the original design of the barrier [84]. In the original design this maximum occurring flow velocity was selected as it was the orbital velocity of the design waves. As such this maximum occurring flow velocity is also only relevant for overtopping scenarios. As mentioned above, this is an underestimation of the flow velocities, as the probability of overflow situations is non-negligible. Therefore the ARCADIS study can again be assumed to be too optimistic as it gave the verdict 'good'.

8.5. Conclusion

This chapter has shown the application of a fragility based method for assessment of the height of the Roompotsluis. Several conclusions can be drawn:

By taking a conditional approach, a non-constant limit state can be applied. This allows the combination of several different failure mechanisms in a single probabilistic assessment. Since the limit state function per deterministic scenario is constant however, this still allows for the application of an intelligent Monte Carlo simulation, such as the subset sampling applied in this chapter.

In this chapter it was also shown how a fragility curve can be extended into a multi-dimensional fragility surface. By extending the variables over which fragility is applied, the insight into the structure is increased. In Figure 8.9, an oddly shaped safe region of combinations of water level and wave height was shown, limited by several different effects on all sides. In this way fragility based assessments can offer additional insight into the processes. This lines up perfectly with wishes voiced by Rijkswaterstaat during the original reconnaissance study [12].

It was shown to be possible to take two failure mechanisms (overtopping and overflow) into account, including the dependence in loading. While during the previous assessment round a choice in prevailing mechanism was necessary (let alone taking the dependence into account), a fragility based methodology has been shown to offer this flexibility. Furthermore, a limit for the water level was added to model the lock doors, while it was also shown how additional loading parameters could be taken into account with fragility.

It should be kept in mind that the results in this chapter have been based on several assumptions. Most notably, the flow velocity over the stones on the coupure has been estimated using the orbital flow velocity of the waves. This assumption has lead to the behaviour seen in Figure 8.10; where lower water levels can lead to higher failure probabilities. Within this assumption it is not taken into account how higher water levels lead to an increase in overtopping, as more waves can reach the top of the structure. This would increase failure probabilities for higher water levels and decrease failure probabilities for lower water levels. A more detailed assessment into these overtopping mechanisms is therefor recommended when a more quantitative assessment is required.

9

Failure mechanism II: Failure due to failing to close structure

For most failure mechanisms a basis exists within the WBI2017. The limit states have been well defined as have the formulas behind the strength and loading terms. The Eastern Scheldt barrier, being a complex storm surge barrier, has several unique failure mechanisms as well however. For these mechanisms, no clear guidelines and/or limit states are defined in the WBI2017. This means that a custom assessment will need to be performed. In this chapter such a custom assessment will be applied for the failure mechanism 'failure due to failing to close structure'.

Failing to close a structure can lead to significant flow through a structure when the water level difference over the structure rises. Locks are often constructed in such a way that the doors on both sides cannot open at the same time, or with double doors. This makes sure that the lock is not 'stuck' in an open state when high water conditions approach. In the WBI2017 a guideline to assess the probability that a regular structure fails to close is proposed in the form of a questionnaire [71]. With the questionnaire the probability of failing to close a structure can be estimated, but this type of estimation is not applicable to the Eastern Scheldt barrier. The general fault tree for the mechanism can be applied however and can be seen in Figure 9.1. The following sections will explain the different branches.

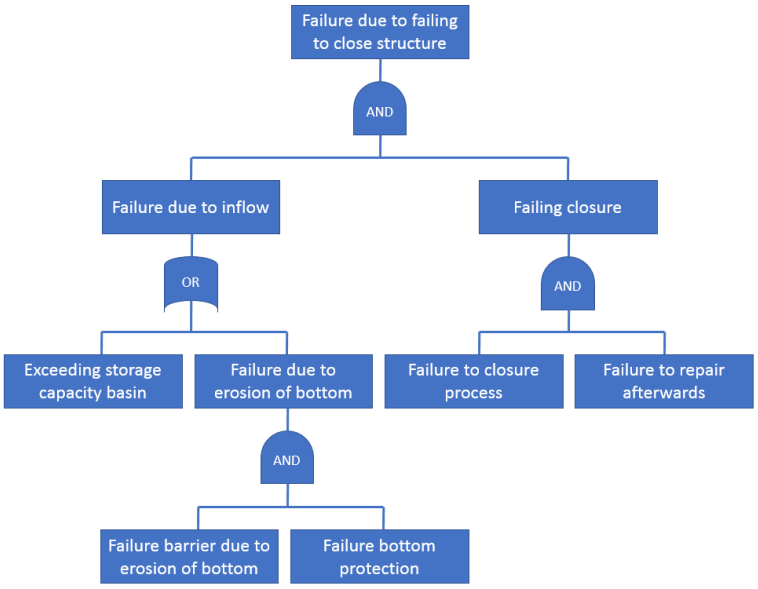

Figure 9.1: Fault tree failure mechanism failure due to failing to close structure [56]

9.1. Failure closure

The branch 'failing closure' describes the probability that a closure will fail and thus that the gate of a structure is open when it should be closed. The Eastern Scheldt barrier has 2 closing strategies; manned and unmanned. When an outside water level 2.75m+NAP is expected, a crisis team will be assembled, 10 hours before high water. This team will determine whether the barrier will be closed [12]. This is described as a manned closure. If some part of this strategy fails, for example the forecast, assemblage of the team or human operation of the barrier, an emergency closure will take place automatically at a water level of 3.00m+NAP [12]. This is called the unmanned closure. The type of closure is of influence for the probability of a failing closure, as an automatic closure has a larger probability of failure. This difference in failure probability is caused by the effects of potential human intervention. An example would be an administrator who can walk to the gate which failed to close and try a manual closure on site, after a computer-related failure to close has occurred [24]. In the safety assessment of the Eastern Scheldt barrier 9 different closure scenarios are considered. These all described different failures of the closing process, dependent on the amount of doors that has failed to close. A total of 18 scenarios are thus taken into account (9 failure states times 2 closure strategies), which can be seen in Table 9.1. The failure of certain groups of gates was taken as a single scenario to keep the amount of scenarios limited (for example, the closure of either 3, 4 or 5 gates is all taken as a single scenario: 5 gates open).

9.1.1. Failure to closure process

From Table 9.1 it can be seen that there is an approximate probability of 1.4% per manned closure request and an approximate probability of 6% per unmanned closure request of 1 or more gates failing to close. It can also be seen from Table 9.1 that the probability of a full failure of all gates is larger than the probability of 75% of the gates. If 75% of the gates fail, this is likely caused by a larger problem with the barrier, not by 47 individual gates failing independently. As such there is a larger probability of the entire barrier failing to close, than only 75% [25].

Scenario	Manned	Unmanned
0 (No gates fail)	9.86E-01	9.40E-01
1 (1 gate fails)	1.18E-02	5.41E-02
2 (2 gates fail)	3.81E-04	1.83E-03
5 (3, 4 or 5 gates fail)	1.88E-04	2.00E-03
10 (6-10 gates fail)	5.88E-04	9.72E-04
16 (25% of gates fail)	3.77E-04	6.07E-04
31 (50% of gates fail)	1.70E-04	2.31E-04
47 (75% of gates fail)	7.12E-08	9.47E-08
62 (All gates fail)	2.05E-05	7.53E-04

Table 9.1: Probability of failure to close on request [12]

This report will only consider failure of one gate, in the manned scenario, and will consider the failure of gates to be independent. As an assumption the failure probability of the closure process will be taken as 1.4%. This failure probability will then be split evenly over the different gates. In reality, the closure of some gates will have a higher failure probability than others and the failure of gates is to some degree dependent. Each gate is then considered to have an independent and exclusive 2.3E-4 failure probability per closure request, which is of course a very rough assumption.

9.1.2. Failure to repair afterwards

The failing of a gate is always detected and the dangers to the bottom protection, when a gate fails, are known to the inspectors [24]. As such, when a gate fails, close inspection of the bottom protection and detection of subsequent damages will follow [24]. The possibility of repairing this damage on time is dependent on many factors and is not considered within the scope of this report. An assumption is made that repairs can occur when the first flood period has passed, while no repairs are possible during this first flood period. This leave a period of approximately 6.25 hours during which damage can occur.

9.2. Failure due to inflow

Inflow can lead to failing of a structure by exceeding either the maximum storage capacity of the basin, or by exceeding the maximum discharge over the bottom protection.

9.2.1. Exceeding storage capacity basin

When the Eastern Scheldt barrier is fully functioning and closed, it is far from water tight [40]. A cumulative flow surface of 1250m^2 exists at all times and as such a discharge will still occur over the barrier, even when closure does not fail. This indicates that a discharge does not necessarily imply failure of the barrier. As this report looks at technical failure of the Eastern Scheldt barrier (and considering the size of the Eastern Scheldt barrier) exceeding storage capacity will not be considered in this report[1].

9.2.2. Failure barrier due to failure bottom protection

In the original design a scour hole was predicted to occur at the downstream end of the bottom protection [84], as will always occur at the end of a bottom protection [61]. Any scour hole needs to be kept far enough from the structure as to not endanger it. Damage to a bottom protection can cause a scour hole to develop closer to a structure however. This is the mechanism through which failure of a bottom protection leads to failure of a structure. Traditionally, this formation of a dangerous scour hole has been taken to always occur; the transfer probability between failure of bottom protection and failure of the structure was set to 1 [13]. This means that a failing bottom protection always eventually implies a failing barrier. In this chapter the formation of a scour hole will be assessed conditional however; dependent on the loading scenario under which the bottom protection fails.

9.3. Fault tree applied

The fault tree from Figure 9.1 can be simplified when the aforementioned neglected sub-mechanisms are removed. The resulting fault tree can be seen in Figure 9.2. Two probabilities are to be computed; the failure probability of the bottom protection and the failure probability of the barrier due to erosion of the bottom (the transfer probability). Both will be taken into account conditionally and then integrated over the PDF of the load.

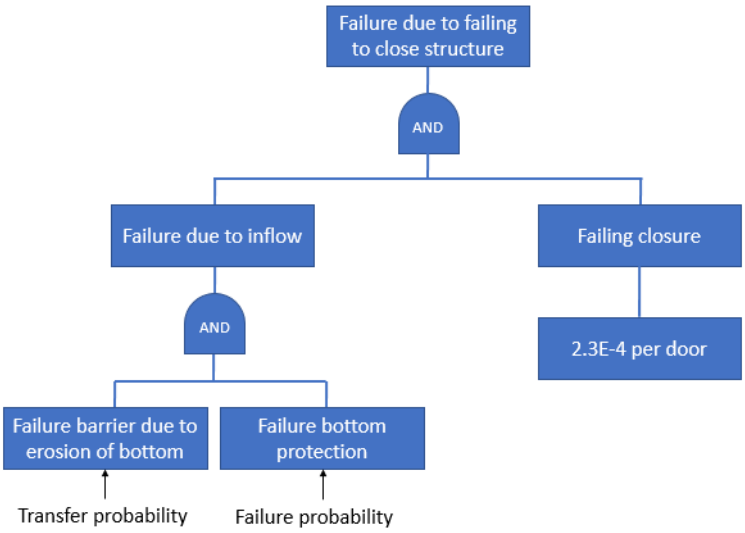

Figure 9.2: Fault tree applied in this chapter

[1] It should however not be forgotten that the main function of the Eastern Scheldt barrier is not to exist, but to keep water levels in the Eastern Scheldt basin below a certain threshold. As such, by neglecting the storage capacity of the basin, the primary function of the barrier is now technically neglected!

9.4. Failure probability: failure bottom bottom protection

The bottom protection behind the barrier is assessed by comparing the critical flow velocity with the occurring flow velocity. Therefore, first a schematization of the flow will need to be made. With this schematization, the local flow velocity over the stones of the bottom protection can be computed from the hydraulic conditions on the outside of the barrier.

9.4.1. Occurring discharge through the barrier

The flow gates of the Eastern Scheldt barrier will be modelled as a weir. A weir is an overflow structure, which regulates the amount of water flowing over it. Within hydraulic engineering, two types of weir are distinguished: broad-crested and sharp-crested, depending on the shape of the weir and the resulting flow lines. The length of the weirs (in flow-wise direction) makes the Eastern Scheldt barrier weirs broad-crested. Additionally, a gate can close the weir. As such, both overflow and underflow can occur, depending on the upstream water level (H_1), the downstream water level (H_2) and the gate opening (H_0), as seen in Figure 9.3.

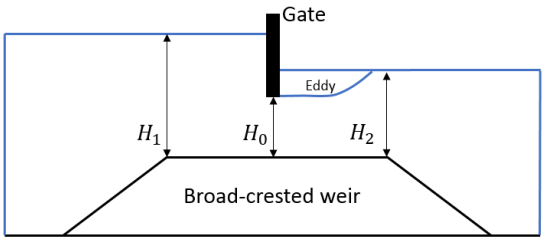

Figure 9.3: Parameters influencing the type of discharge

In the 1-dimensional flow model (IMPLIC) applied by the Eastern Scheldt barrier administration 7 discharge formulae are applied, these will also be applied here [63]. The main differences between the formulae are whether the flow is supercritical or subcritical and whether underflow or free surface flow occurs. The applied discharge formulae can be found in Appendix B.

Supercritical or subcritical flow
Whether the flow is supercritical or subcritical depends on the Froude number. The Froude number is a dimensionless number indicative of the ratio between the inertia and the gravitational acceleration. The main difference between super- and subcritical flow lies in the fact that in supercritical flow no information can travel upstream [8]. As such, the discharge formulae and the formulae determining the flow surface are all independent of H_2. The discharge formulae for supercritical flow are thus only governed by the upstream water level, H_1. When subcritical flow occurs, information from downstream can travel upstream and the discharge depends on the downstream water level. The discharge formulae for subcritical flow are therefore governed by the water level difference, ΔH.

Underflow or free surface flow
Flow over a gated weir can occur in two regimes: underflow (Dutch: verdronken uitstroming) and free surface flow (Dutch: vrije uitstroming). The different flow regime influence the contraction coefficient [10], as can be seen in Figure 9.4 and the formulae in Appendix B, and the type of flow which occurs is determined by the up- and downstream water levels.

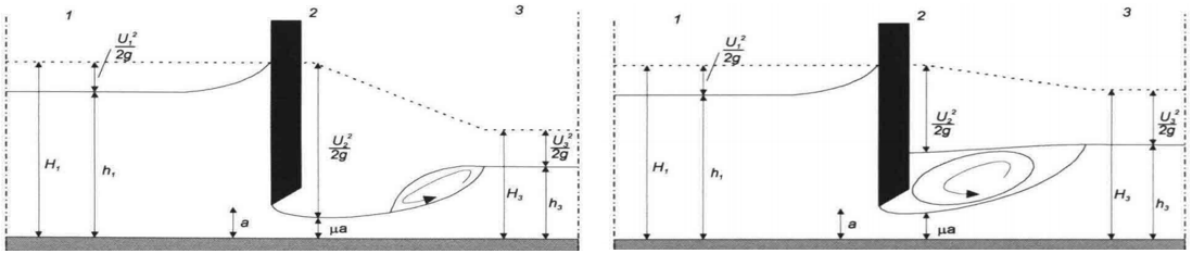

Figure 9.4: Free surface flow (left) and underflow (right) [10]

The discharge formulae applied use the water level difference[2] as the main hydraulic loading parameter. In Table 9.2 the occurring discharge and flow velocities through gates 1 (R01, with the highest sill height) and 16 (R16, with the lowest sill height) of the Roompot barrier can be seen. Interestingly, although the discharge greatly varies between the gates, the average flow velocity does not.

Water level difference [m]	1.0	2.0	3.0	4.0	5.0	6.0	7.0
Discharge through R01 [m^3/s]	962	1361	1667	1925	2152	2357	2546
Flow velocity through R01 [m/s]	4.4	6.3	7.7	8.9	9.9	10.8	11.7
Discharge through R16 [m^3/s]	2012	2846	3485	4024	4499	4928	5323
Flow velocity through R16 [m/s]	4.4	6.3	7.7	8.9	9.9	10.8	11.7

Table 9.2: Discharge and flow velocity through gate R01

9.4.2. Flow patterns behind the weir

The discharge over the weir can be calculated with the formulae described in Appendix B, and the flow velocities have been shown to be constant over the different gates. As such, the assumption will be made that the flow patterns behind a gate are independent on which gate is opened[3]. If a flow of water with excess velocity enters into a large body of (stagnant or low velocity) water, jet flow can occur [61]. Jet flow can be described as going through two distinct phases: flow development (where the mixing layers grow) and fully developed flow. These two phases can be seen in Figure 9.5.

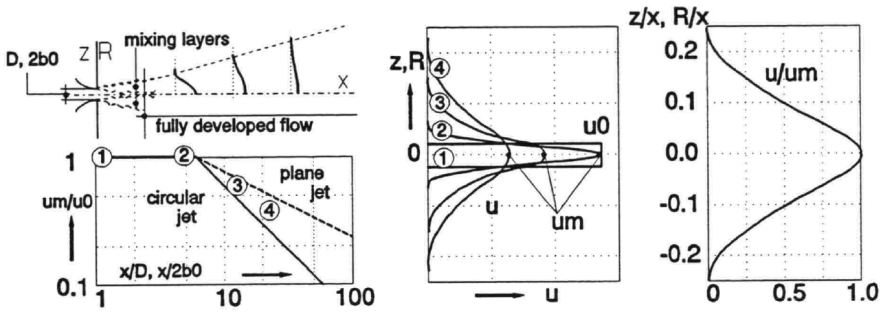

Figure 9.5: Phases of jet flow (left) and the development of the flow velocities (middle and right) [61]

As jet flow exits the orifice (the nozzle, which in this case is the space between the door and the sill, H_0), the surface area of the flow does not grow at first. Rather, in this region of flow development, the mixing layers (which form between the moving jet and the stagnant body of water of the Eastern Scheldt) grow, both into the jet and into the body of stagnant water. In the middle line of the jet, surrounded by penetrating mixing layers, the flow velocity remains undisturbed (u_0). This region of undisturbed flow is cone shaped, due to the penetration of the mixing layers in the downstream direction and is known as the potential cone.

At a distance of approximately $6H_0$[48] from the nozzle the mixing layers will reach the middle of flow (and each other). At this point the flow is fully developed, and will start to spread out over the water depth and width, which decreases the flow velocity in the downstream direction; the core of the jet is said to be fully consumed [48]. Until this point of full flow development the flow velocity of the jet, u_m, can be modelled as constant, at u_0. After the flow is fully developed however the velocity profile starts spread out, following a Gauss curve. Both these flow profiles can be seen in Figure 9.5 [61].

[2] Supercritical flow will almost never occur here. Nonetheless it is taken into account in the discharge formula. After all, the likelihood of occurrence is irrelevant for the fragility curve. When supercritical flow occurs the outside water level is computed by adding the maximum regulated inside water level to the water level difference, which is used in the computation. As such, the water level difference over the barrier is still the defining hydraulic load.

[3] This does not yet include the limited cross-section of the flow near the edges of the Eastern Scheldt, caused by physical barriers present there. This will be discussed in Subsection 9.4.4.

9.4.3. Flow schematizations

Whether the flow through a gate of the Eastern Scheldt barrier behaves as a jet greatly influences the flow pattern behind the barrier. After all, when jet-like behaviour is displayed, the flow will not spread out directly behind the barrier. This will increase the load on this area close to the barrier. Two scenarios will therefor be considered; an optimistic flow scenario and a conservative flow scenario.

Optimistic scenario: instant flow spreading
When the flow shows no jet-like behaviour, the flow will start to spread immediately after exiting the orifice. As such the flow follows the bottom contours and widen with an assumed angle of 1:6, similar to the jet after development. As the average flow velocities are applied, the Pilarczyk formula can be applied. The schematization of this model can be seen in Figure 9.6, and it functions as an optimistic lower limit (for the resulting failure probabilities).

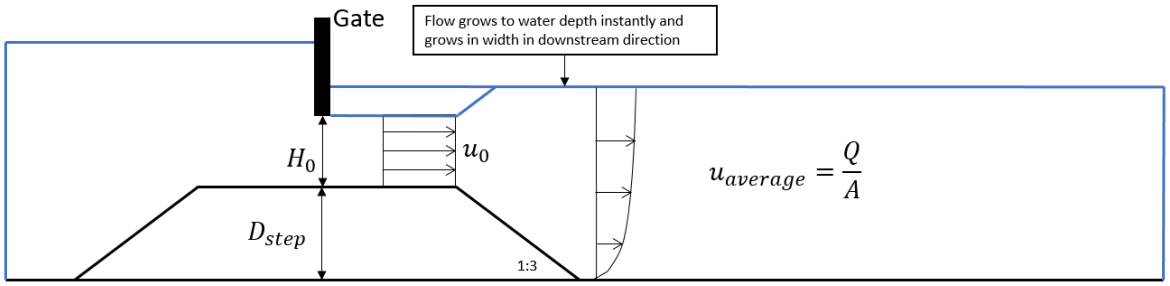

Figure 9.6: Optimistic schematization of the flow pattern behind the weir

Conservative scenario: undeveloped jet pushed against the bottom
If the flow through the gate develops as a jet, the flow velocities stay very high during the flow development phase (as the flow doesn't spread out). Eddie formation can cause this flow to divert, as the increase in turbulence 'pushes' the flow lines away from the eddy. As the gates of the Eastern Scheldt barrier can cause an eddie above the flow, as seen in Figure 9.3, this eddie can force the flow downwards, against the bottom. This is a conservative assumption, as the bottom gets loaded more heavily. A schematization of this model can be seen in Figure 9.7, and it functions as a conservative upper limit (for the resulting failure probabilities).

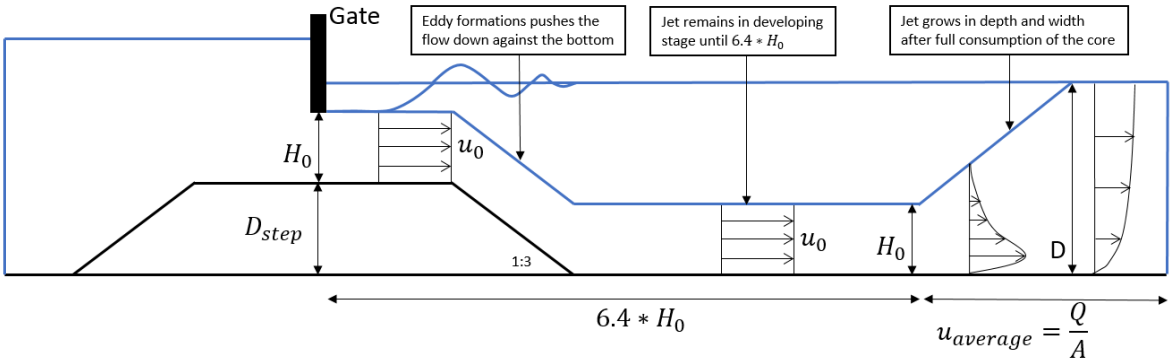

Figure 9.7: Conservative schematization of the flow pattern behind the weir

The flow velocities remain equal to the flow velocity through the gate, u_0, for the first $6.0*H_0$ meters (flow development) and are computed by dividing the discharge by the cross-section of the flow after the flow is fully developed. The cross-section of the flow is H_0 times the gate width until the point of flow development, after which the depth grows to water depth with an angle 1:6 while the width grows with an angle 1:6 as well (unless hindered by the edge of the grid, which simulates the southern dike and northern wave breaker blocking flow). As the local flow velocities are applied over the area of flow development, a correction will here be applied in the Pilarczyk formula, though not taking the depth parameter into account [16]. Over the area of fully developed flow, the average flow velocities are applied and as such the Pilarczyk formula can be applied normally.

The schematizations in Figure 9.6 and Figure 9.7 function as optimistic and conservative limits to the model, with the 'true' flow pattern most likely somewhere in-between. With a discretized (and thus 'deterministic') outside water level (on the basis of fragility), the discharge formulae in Appendix B and the flow schematizations from Figure 9.6 and Figure 9.7, the average flow velocities for all locations behind the barrier can be computed. As such, the loading on the stones behind the barrier can be described by the water level difference over the barrier, Δh. The water level difference can thus be expressed in terms of occurring flow velocity, to be compared with the strength term, the critical flow velocity.

9.4.4. Critical flow velocity

The critical flow velocity is determined with the Pilarczyk formula, which can be seen in Equation 9.1[16].

$$D = \frac{\varphi_{sc}}{\Delta}\frac{0.035}{\psi_{cr}}k_h k_{sl}^{-1}k_t^2\frac{U^2}{2g} \quad \rightarrow \quad U = \sqrt{\frac{2g\Delta D\psi_{cr}k_{sl}}{0.035\varphi_{sc}k_h k_t^2}} \tag{9.1}$$

Where:

U	$[m/s]$	Depth averaged flow velocity
g	$[m/s^2]$	Gravitational acceleration
Δ	$[-]$	Relative density
D	$[m]$	Thickness of the element
Ψ_{cr}	$[-]$	Shear stress parameter
k_{sl}	$[-]$	Slope factor
φ_{sc}	$[-]$	Stability constant
k_h	$[-]$	Depth parameter
k_t^2	$[-]$	Turbulence factor

The slope factor and depth parameter are dependent on the bathymetry behind the barrier. As such a schematization of the water depths in the Eastern Scheldt basin is required to apply Equation 9.1. The water depths of the Eastern Scheldt are obtained with SonarChart [44]. An image of the applied bathymetry behind the barrier can be seen in Figure 9.8. The line at 'Distance from barrier = 0' indicates the height of the weir. The variables applied in Equation 9.1 will be discussed below.

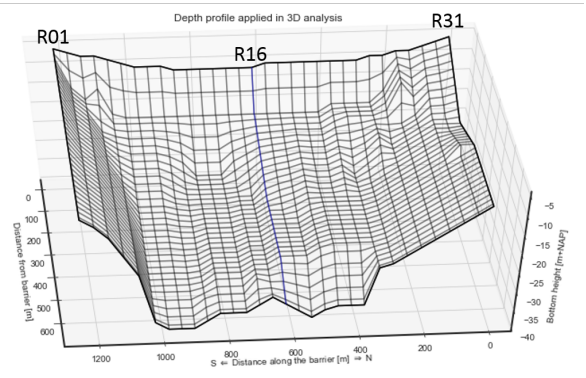

Figure 9.8: Bathymetry behind the barrier, with the gates named and R16 marked blue

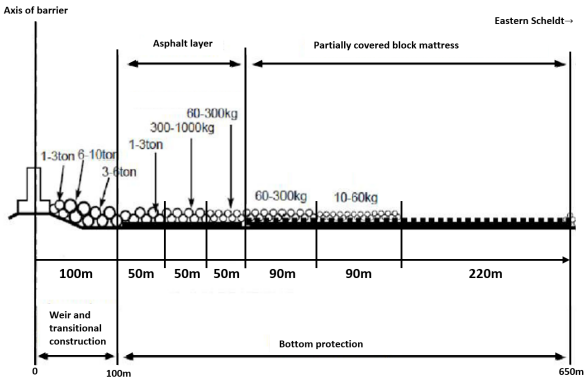

Figure 9.9: Overview of the barrier, transitional construction and bottom protection original: [13], edit: Fiolet, 2018

Stone size and relative density

The stones sizes behind the barrier vary with distance from the barrier, as can be seen in Figure 9.9. A distinction can be made between the so called transitional construction (covering the area between the weir and 100m from the weir) and the bottom protection (beyond 100m from the weir), both can be seen in Figure 9.9. In the original design, the area behind the transitional construction was protected with an asphalt layer and a block mattress partially covered in rocks. The asphalt layer was covered in rocks during reinforcements in the 90s [67]. The critical flow velocity will be determined for the rocks covering the asphalt layer, while the

layer itself will be considered as already failed[4]. An overview of the different rock classes found behind the barrier and the distributions applied to described them, can be found in Appendix D. The relative density is described with a normal distribution, with mean 1.65 and coefficient of variance of 0.1, truncated to avoid negative values. It is assumed that the shift in mean introduced by this truncation is negligible.

Shear stress parameter
The critical shear stress (or Shields parameter[61]) is determined by the maximum allowed transport of bottom material. De Boer, 1998 [17] devised an empirical formula to compute the amount of material transported as a function of time and critical shear stress parameter. This formula can be seen in Equation 9.2 and Equation 9.3 [17].

$$\phi = 7.8E3\Psi_{cr}^{7.5} \quad \rightarrow \quad \Psi_{cr} = \sqrt[7.5]{\frac{\phi}{7.8E3}} \quad \text{for} \quad \Psi_{cr} < 0.1 \tag{9.2}$$

$$\text{with} \quad \phi = \frac{q_s}{\sqrt{\Delta g d_{n,50}^3}} \tag{9.3}$$

where:

q_s	[m^3/s]	The discharge of rock material

Equation 9.2 and Equation 9.3 can be used to calculate a discharge of material per running meter from a shear stress parameter. As discussed in Subsection 9.1.2, the time a gate is open is limited by the duration of flood, approximately 6.25 hours. As such, the maximum allowed volume of material allowed to be transported out of the bottom protection, before it is considered failed can be divided by 6.25 hours to compute a discharge of material per second, q_s. Failure of the bottom protection will be defined as the removal of at least 5 stones per running meter. As bottom protection layers are composed of at least two layers of stones [61], the removal of less than three stones will be assumed to not never expose the bottom, while the removal of three or more stones can potentially expose the bottom. An assumption is made that the removal of 5 stones exposes the bottom in such a way that the bottom protection can be considered as failed. The sensitivity of this very rough assumption will be assessed in Appendix G. The time available for this erosion has been assumed to be a normal distribution (N(3.125,0.75), truncated to not allow negative values or values above 6.25). The critical shear stress parameter can then be calculated with Equation 9.4, as a function of the stone diameter.

$$q_s = \frac{N * d_{n,50}^3}{T * 3600} \quad \text{and thus} \quad \Psi_{cr} = \sqrt[7.5]{\frac{q_s}{7.8E3\sqrt{\Delta g d_{n,50}^3}}} = \sqrt[7.5]{\frac{N d_{n,50}^{3/2}}{2.8E7 T \sqrt{\Delta g}}} \tag{9.4}$$

where:

N	[-]	The number of stones per running meter that is allowed to be removed in time T
T	[hours]	Time during which the bottom protection is loaded
$d_{n,50}$	[m]	Nominal stone diameter ($\approx d_{50}/1.2$ [61])

It should be noted that this approach for the critical shear stress parameter will lead to high shear stress parameters. Shear stress parameters will usually be in the range 0.03-0.035 when describing the points at which the first stones start to move, while a shear stress parameter of 0.05-0.055 describes limited movement [16]. The critical shear stress has been calculated for each rock class and can be seen in Table 9.3.

Stone class	6-10 ton	3-6 ton	1-3 ton	300-1000 kg	60-300 kg	10-60 kg	blocks, d_{50}=0.17m
Ψ_{cr}	0.096	0.093	0.088	0.081	0.074	0.066	0.061

Table 9.3: Average critical shear stress per stone class, as the diameter of stones per class, time T, and Δ are defined as distributions, so is the critical shear stress.

[4]Current assessments for the bottom protection consider the asphalt layer by introducing an 80% failure probability for it. This estimate is not based on any physics however [24], and will not be considered in this report. Nonetheless, it can easily be added to the model by multiplying the conditional failure probabilities by 0.8, as the condition of the layer can be considered independent of any other variables.

As can be seen in Table 9.3, the shear stress parameters applied are higher than usual, describing huge amounts of movement. This is considered justified by the extreme circumstances of failure due to failing closure. When a gate has failed, the bottom protection will need to be repaired regardless. As such, any damage to the bottom protection is allowed so long as its function, of protecting the bottom, is fulfilled. The protection of the bottom only needs to last for approximately 6 hours to fulfill this function.

Slope factor
The bathymetry can be used to determine the slope factor, by calculating the partial derivatives of the bathymethry in x and y direction (parallel and perpendicular to the barrier respectively). The slopes in x direction are found to be negligible in comparison to the slopes in the y direction (as can be seen by comparing the axis in Figure 9.8). The formula for the slope factor can be seen in Equation 9.5.

$$k_{\mathrm{sl}} = \frac{\cos\Psi\sin\beta + \sqrt{\cos^2\beta\tan^2\phi - \sin^2\Psi\sin^2\beta}}{\tan\phi} \tag{9.5}$$

Where:

Ψ	[°]	The angle made by the flow to the upslope direction
β	[°]	The angle of the sloping embankment with the horizontal
ϕ	[°]	The angle of repose of the material

Stability constant
The stability constant describes the influence of transitions. The different possible flow situations can be seen in Figure 9.10. It is assumed that no transitions experience direct flow against the layer. This leads to a stability constant of 0.75 for the rock layers and 0.5 for the mattresses [74].

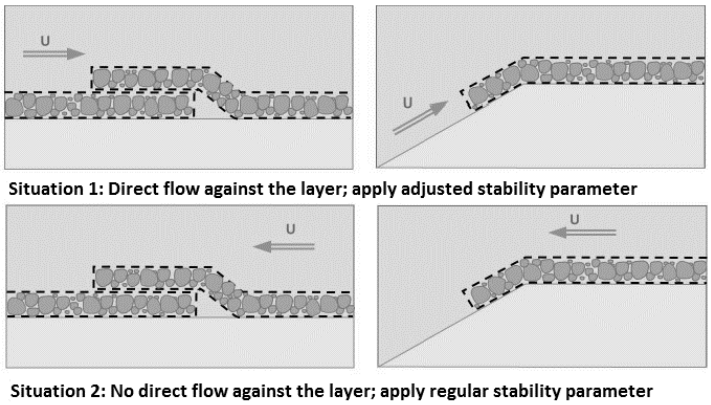

Figure 9.10: Stability constant under different situations [74]

Depth parameter
The depth parameter is dependent on whether the flow is fully developed or not. It is assumed that the flow is not fully developed over the entire grid. The formula for the depth parameter can be seen in Equation 9.6. When, instead of the average velocity, the local flow velocity is applied in the Pilarczyk formula, the depth parameter needs to be corrected to 1.0 [74]. This correction will be applied in the conservative scenario, where the jet is in the flow development phase.

$$k_h = (1 + h/D)^{-0.2} \tag{9.6}$$

Where:

h	[m]	Water depth
D	[m]	Stone size

Turbulence factor
The turbulence factor is an indicator for the amount of turbulence. Some rough estimates will be applied here, as a full description of the turbulence is outside the scope of this report. In Figure 9.11 a description

of the turbulence factor by Pilaczyk, 1995 can be seen. The turbulence factor, k_t^2, is assumed to be 2 at the barrier and then decreases linearly to 1, at a distance of 5 times the (average) bottom depth. The turbulence factor remains 1 further downstream. The sensitivity of this assumption is assessed in Appendix G.

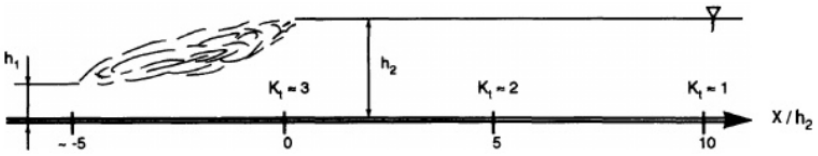

Figure 9.11: Turbulence factor (Pilarczyk, 1995 applies K_t instead of k_t^2, these represent the same however)[47]

Critical flow velocity per location

Applying Equation 9.1, the critical flow per location behind the barrier can be computed. In Figure 9.12, the critical flow velocity along a single line, perpendicular to the barrier. This line has been drawn in Figure 9.8 and is located behind the middle gate of the barrier (R16). It can give an indication of how the critical flow velocity behind the barrier develops with distance from the barrier. Although the flow lines behind each gate are different, they roughly follow the same pattern as Figure 9.12. Figure 9.12 has been drawn by applying the conservative scenario. This influences the critical flow velocity through the depth parameter, k_h.

Figure 9.12 has been computed with Monte Carlo simulation, where the critical flow velocity has been simulated for every location behind gate R16. The PDF of the critical flow velocity has been constructed with Kernel Density Estimation (KDE). KDE is a statistical tool capable of smoothing a curve through data, to approximate the PDF of the underlying distribution (for more on KDE, see Cator, 2006 [14]).

The critical flow velocity has been drawn with 5% and 95% uncertainty bounds, as it is computed with probabilistic input parameters, described with distributions. As such, the output parameter, the critical flow velocity, is described with a distribution as well. For each point along the flow line, a full fragility curve can thus be constructed by integration of the PDF at that location. This can be seen in in the subplots of Figure 9.12.

It can be seen that as the distance from the barrier is increased, the (average) critical flow velocity is decreased. This makes sense, as the stones sizes of the bottom protection are decreased with distance from the barrier (as can be seen in Figure 9.9). The stones situated in the approximate 100/150m near the barrier do not show this reduction with distance, however. The critical flow velocity is instead increased with distance, due to 3 factors:

First, the stones in this region lie on a slope, as can be seen in Figure 9.8. This is reflected in the slope factor, k_{sl}, lowering the critical flow velocity. Secondly, the jet that develops near the barrier, as seen in the conservative flow scenario, leads to the usage of the local flow velocity instead of the average velocity. As a result the depth parameter, k_h, is neglected (the depth factor increases the critical flow velocity, as the local flow velocities near the bottom are usually lower than the average flow velocities). Finally, the turbulence is assumed higher near the barrier. This is reflected in a higher turbulence factor, k_t. Together, these three factors lower the critical flow velocity in the vicinity of the barrier.

Interestingly however, both the second and third reason are qualitatively better described as loading parameters instead of strength parameters. After all, they describe the local, turbulent flow that loads the bottom protection. In fact, due to the usage of the depth parameter in Equation 9.1, the different flow scenarios now also have different strength parameters. This shows how the concepts of strength and load are really arbitrary distinctions and only the limit state (the difference between R and S) matters when computing failure probabilities. It also shows that assumptions regarding independence in strength or load, as demonstrated in Chapter 6, should be made carefully.

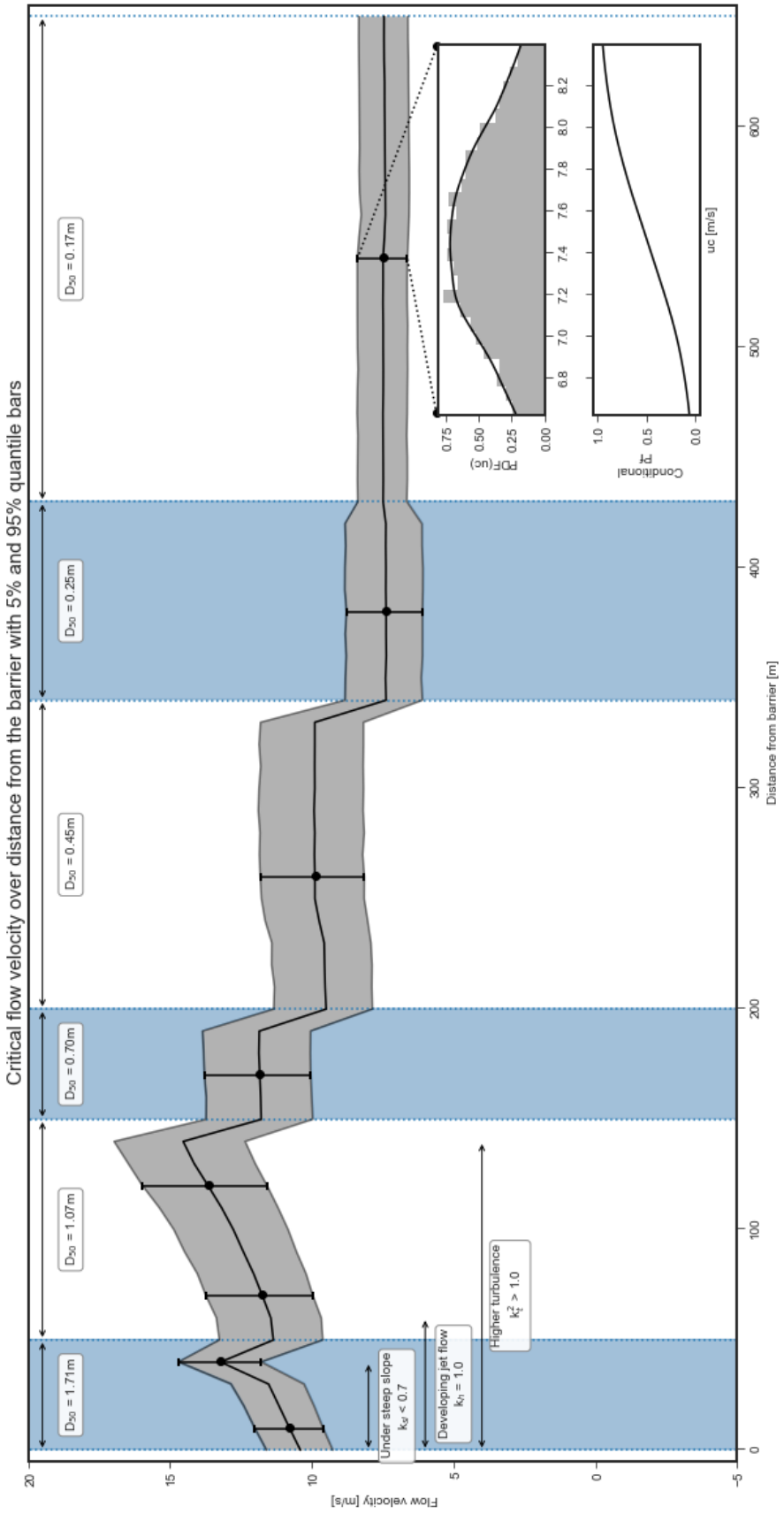

Figure 9.12: Critical flow velocity of the stones behind R16

9.4.5. Conditional failure probability

By comparing the probabilistic critical flow velocity, visible in Figure 9.12, with the discretized water level difference over the barrier and the resulting flow velocities behind the barrier, the conditional failure probability per location can be computed. Failure of the bottom protection occurs when the occurring flow velocity at a location exceeds the critical flow velocity at that location. As such, the conditional failure probability at each location can be computed with Equation 9.7.

$$P_{\text{f,conditional}} = P(R < S) = P(u_{\text{crit}} < u_{\text{occurring}}) \tag{9.7}$$

Where:

u_{crit}	[m/s]	Critical flow velocity, computed with Equation 9.1
$u_{occurring}$	[m/s]	Occurring flow velocity at location x,y, as seen in Figure 9.6 and Figure 9.7

In Figure 9.13, both the occurring flow velocity (both for the optimistic and the conservative scenario), the critical flow velocity and the conditional failure probability behind gate R16 (given that its open) for a water level difference of 3.0m have been drawn. The average critical flow velocity is drawn, but the critical flow velocity is still a distribution, as is shown in Figure 9.13 with the error bars indicating the 5- and 95% values. The flow in the optimistic scenario can be seen to only cause failure probabilities to rise near the barrier (which is barely visible). The flow in the conservative scenario can be seen to develop in a different pattern however. In the conservative scenario, when a water level difference of 3.0m is present over the barrier and R16 open, it can be seen that the bottom protection at a distance of approximately 50m from the barrier starts to become more vulnerable than the bottom protection near the barrier itself. This is caused by the jet flow (plotted in red), which do not decrease with distance from the barrier, until after a distance of approximately 60m. The bottom protection at a distance of 50m and beyond has a lower stone diameter than the stones near the barrier (1.07m and 1.71m respectively).

Even when considering the lower average stone diameter however, the average critical flow velocity at this distance is still larger than near the barrier (plotted in green). As can be seen by looking at the error bars however, the uncertainty in critical flow velocity is also larger. This is caused by the wider grading of rock class 1-3 ton (where d_{85}/d_{15}=1.4 [61]) when compared to rock class 6-10 ton (where d_{85}/d_{15}=1.2 [61]). As a result of this increased uncertainty, the conditional failure probability for relatively low water level differences is larger at a distance of approximately 50m from the barrier than at locations closer to the barrier. Nonetheless, the failure probability seems to be high when comparing the flow velocity with the critical flow velocity. It should be remembered however that failure at a certain location is defined as the loss of a certain volume of material from the bottom protection, as described in Subsection 9.4.4, not as the failure of a single stone.

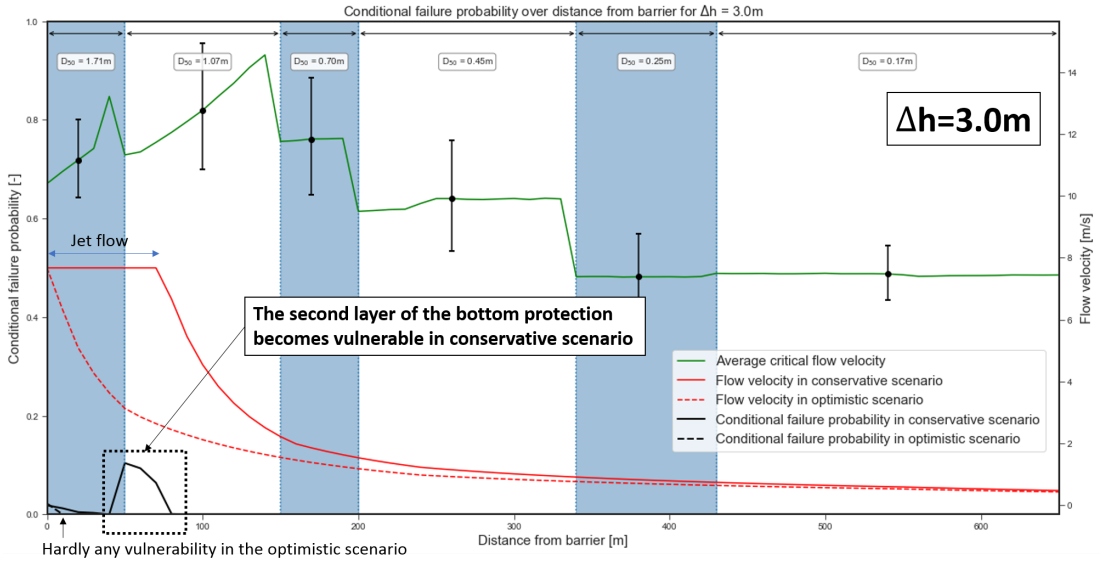

Figure 9.13: Occurring flow velocity, critical flow velocity and the resulting conditional failure probability behind R16, when opened with a water level difference of 3.0m

When the water level difference over the barrier is increased to 4.0m, as can be seen in Figure 9.14, the same effect can be seen. Although the conditional failure probability near the barrier also rises at these conditions, the conditional failure probability at 50m from the barrier in the conservative scenario remains larger. Two peaks in the conditional failure probability thus start to occur; one near the barrier and one at 50m from the barrier. In the optimistic scenario only the locations very close to the barrier show any failure probability.

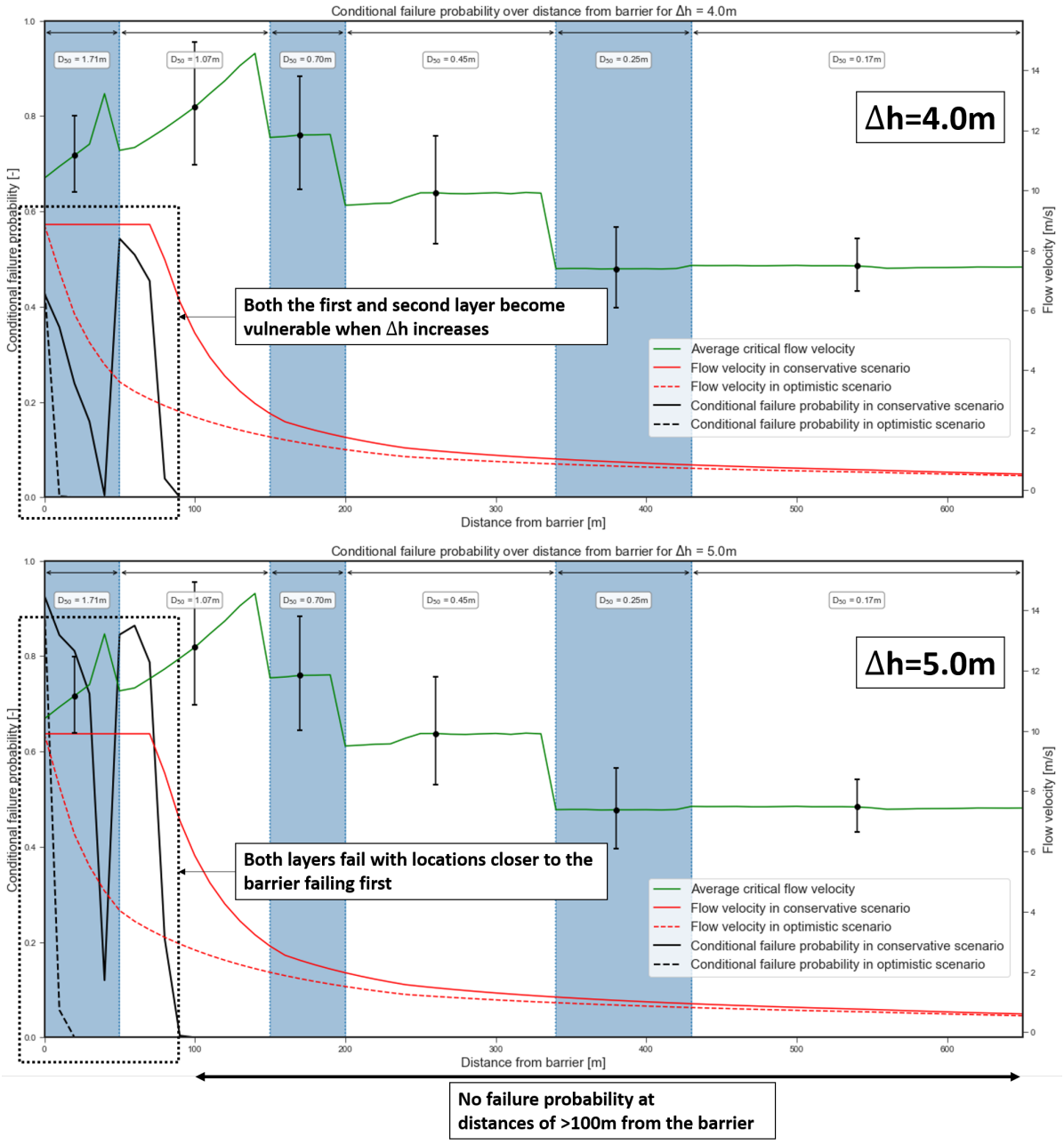

Figure 9.14: Occurring flow velocity, critical flow velocity and the resulting conditional failure probability behind R16, when opened with a water level difference of 4.0m and 5.0m respectively

If the water level difference over the barrier is increased further to 5.0m, both peaks in conditional failure probability increase further in the conservative scenario, with the failure probability near the barrier now higher than at a distance of 50m from the barrier. In the optimistic scenario the failure probability grows only at the location very close to the barrier. For none of these conditions (Δh=3.0, 4.0 and 5.0m) any substantial conditional failure probability starts to emerge at distances further than 100m from the barrier (for gate R16) in either scenario.

Similar to gate R16, the conditional failure probability behind all gates can be computed by comparing the distribution of the critical flow velocity with the occurring flow velocity under varying water level differences. This can be seen in Figure 9.15, where the conditional failure probability behind all gates has been computed for several loading conditions, under the assumption that the gate is open when these loading conditions occur. For clarity, only the first 100m behind the barrier have been plotted here, but all locations behind the barrier have been computed.

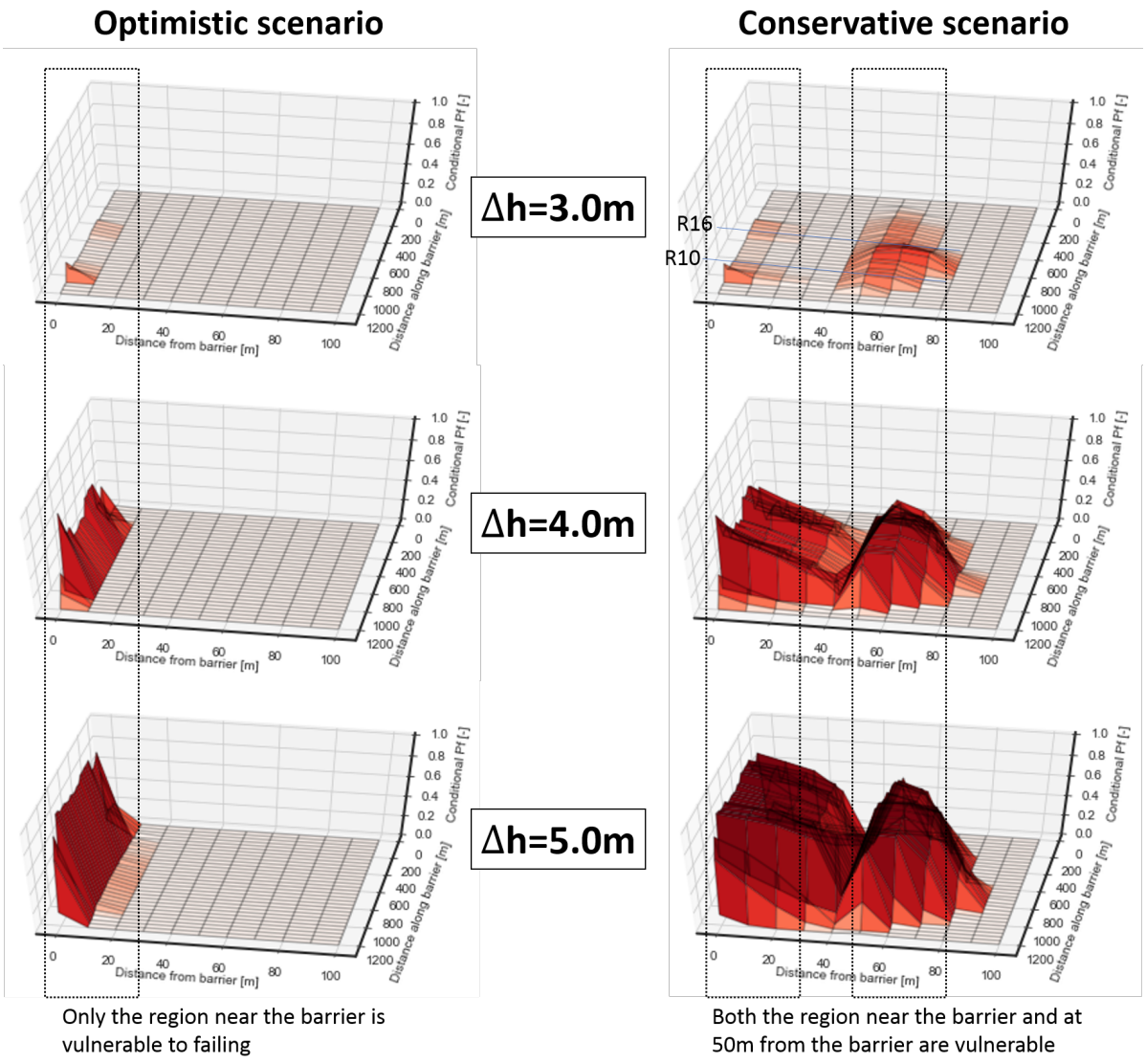

Figure 9.15: Conditional failure probability behind all gates for increasing water level differences

The effects seen behind gate R16 in Figure 9.13, where the region at 50m from the barrier is vulnerable in the conservative flow scenario, can also be seen for other gates. Interestingly however, only the gates around the middle of the barrier and slightly to the south of the middle of the barrier (most notable between gates R10-R16) show this behaviour for lower loading conditions.

If the bathymetry of the basin is consulted, as seen in Figure 9.8, it can be seen that these gates feature the lowest sill heights along the barrier. As a result, the jet that forms will remain in the flow development stage longer. After all, the length of the flow development region is linearly related to the height of the orifice. While in flow development, the flow velocities in the jet remain very high, as can be seen in Figure 9.13, where the flow velocity in the conservative scenario remains constant over the first approximate 60 meters from the barrier. When the jet development phase takes long enough for the jet to reach the second layer of bottom protection, which is made with smaller stones, high (conditional) failure probabilities can occur.

In the optimistic scenario no such effects can be seen. For every gate considered, the failure probabilities are the highest near the barrier. This is not unexpected, as the cross-sectional surface of the flow is the smallest at these locations. Nonetheless, some differences between the gates can be seen, especially when looking at the lower loading scenarios. Notably, when a water level difference of 3.0m is present and gate R5 (at 1060m along the barrier) is open, a relatively high conditional failure probability can be seen (both in the optimistic and conservative scenario). This can again be explained by the bathymetry, as seen in Figure 9.8; right behind gate R5 the steepest slopes can be found. As a result, this is the only location where a slope factor of <0.6 is applied. This leads to a critical flow velocity that is approximately $\sqrt{0.6}$ times smaller, which in turn leads to a high conditional failure probability at this location.

9.5. Transfer probability: failure barrier given failure bottom protection

Traditionally, the probability of failure of the bottom protection would be considered as the probability of failure of the Eastern Scheldt barrier [13]. This means that the conservative assumption has been made, in which the failure of the barrier due to erosion of the bottom after failure of the bottom protection (the transfer probability, as seen in Figure 9.2) equals 1. A fragility-based methodology can make this transfer probability a function of the discretized loading conditions. This makes sense as, for example the growth of a scour hole is dependent on the load conditions under which the initial failure of the bottom protection (which exposed the soil to the flow) occurred. If a relation can be constructed between load S and the consequence of failure due to scour, the transfer probability can be made conditional. The main model to assess this scour can be seen in Figure 9.16.

A scour hole in itself is not dangerous, as long as it does not threaten the stability of a nearby structure. This is the main goal of a bottom protection; to move the scour hole (that inevitably forms at the end of the protection) far enough from any structure [61]. In order for a scour hole to be sufficiently far from a structure, the gradient of a potential slide line has to remain below a certain threshold value [29]. The gradient of this line can be computed geometrically, and is dependent on two variables: the depth of the scour hole and the distance between the scour hole and the structure.

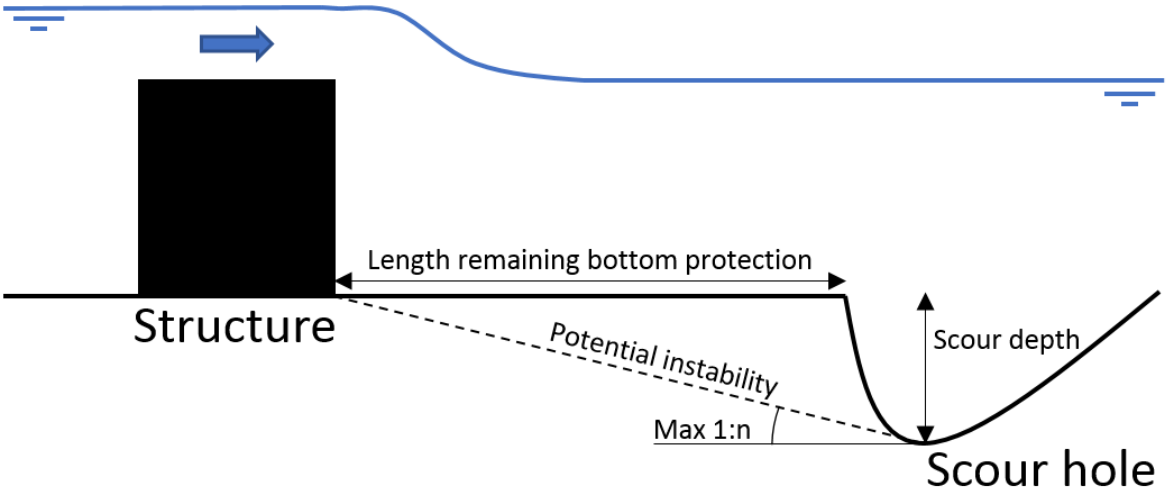

Figure 9.16: The maximum allowed scour depth is a function of the location of the scour hole and the maximum allowed gradient, 1:n

9.5.1. Conditional scour depth

Scour is a time dependent process, ultimately leading to an equilibrium scour depth [82]. As explained in Subsection 9.1.2, the time during which scour can occur is limited by the duration of a single flood period. The time available for the transport of material from the bottom protection and the time available for the transport of bottom material added together is thus limited at 6.25 hours. Time-dependent scour can be computed with Equation 9.8 [29].

$$\mathrm{h}_{\max}(t) = \frac{(\alpha \overline{u} - u_c)^{1.7} h_0^{0.2}}{10\Delta^{1.7}} t^{0.4} \tag{9.8}$$

where:

$h_{\max}(t)$	[m]	Maximum scour that can occur in time t
α	[-]	Amplification factor for the velocity
$\overline{u}$	[m/s]	Mean velocity in front of a scour hole
u_c	[m/s]	Critical flow velocity of the material
h_0	[m]	Water depth
Δ	[-]	Relative density of the material
t	[hrs]	Time

Amplification factor
The amplification factor, α, is an indicator for, among other thing, the amount of turbulence present in the flow. The factor acts as an increase in the effective flow velocity and can be computed with Equation 9.9 as a function of the relative fluctuation intensity, or relative turbulence [61].

$$\alpha = 1.5 + 5r_0 \tag{9.9}$$

Where:

r_0	[-]	The relative fluctuation intensity at the upstream end of a scour hole

This relative fluctuation intensity, r_0 can be difficult to compute, especially when considering highly turbulent, non-stationary, non-uniform flow (which can might be expected in the high velocity jets that can occur for high water level differences over the barrier). Additionally, a probabilistic quantification of these turbulent fluctuations is a research field in itself, and is considered outside the scope of this report. This report will therefor apply a rough estimate regarding the turbulence, based on the applied turbulence factor, as seen in Subsection 9.4.4. The Rock Manual, 2012, [16] offers a relationship between the turbulence factor, k_t, applied in the Pilarczyk formula, and the relative turbulence, which can be seen in Equation 9.10.

$$k_t = \frac{1+3r_0}{1.3} \qquad \rightarrow \qquad r_0 = \frac{1.3k_t - 1}{3} \tag{9.10}$$

For a turbulence parameter of k_t^2=2.0 (applied close to the barrier) this implies a relative turbulence of 0.28, while a turbulence parameter of k_t^2=1.0 (applied further away from the barrier) implies a relative turbulence of 0.1.

Time
The time during which the scour hole can grow is dependent on the total amount of time during which the bottom is loaded (which is assumed in Subsection 9.4.4 to be 6.25 hours). Additionally, this time is divided into a duration during which the bottom protection is loaded, and a duration during which the bottom is exposed. As such, the time during which the bottom is exposed can be defined as 6.25-T, where T is the time during which the bottom protection is eroded, as defined in Subsection 9.4.4.

Other parameters
The critical velocity of the soil material been assumed to be described with a normal distribution with mean 0.5 and a coefficient of variance of 0.1. The relative density of the material has been assumed to be described with a normal distribution with mean 1.65 and a coefficient of variant of 0.1. Both distributions have been truncated to not allow for negative values, and the resulting shift in moments this truncation introduces has been assumed to be negligible.

Potential conditional scour depth

The conditional scour depth can then be computed by applying Equation 9.8. As several inputs of the formula are described with distributions, the output will be described with a distribution as well. A Taylor expansion has been applied to compute the mean and variance of the output parameter, the conditional scour depth [9]. The conditional scour depth has been assumed to be normally distributed, with this mean and the standard deviation (which is equal to the square root of the variance). As this scour can only occur after the bottom protection has failed and is conditional on the load, it will be referred to as potential conditional scour. The potential conditional scour is the scour that would occur at a given location, given that the bottom protection has failed at that location, for the conditional loading scenario considered.

When the middle gate, R16, is considered as an example, the potential conditional scour depth for a water level difference of 3.0m over the barrier can be seen in Figure 9.17, as a function of the distance from the barrier. The scour has been plotted for locations up to 200m from the barrier for clarity, but all locations are taken into account in the computation. In order to keep the different graphs (conditional failure of the bottom protection, conditional scour, etc.) comparable, the different components of the bottom protection have also been displayed, but of course they do not influence the scour depth. After all, the scour process has been assumed to only be able to start after the stones in the bottom protection are eroded. The scour has been drawn with 5% and 95% quantile values as bounds.

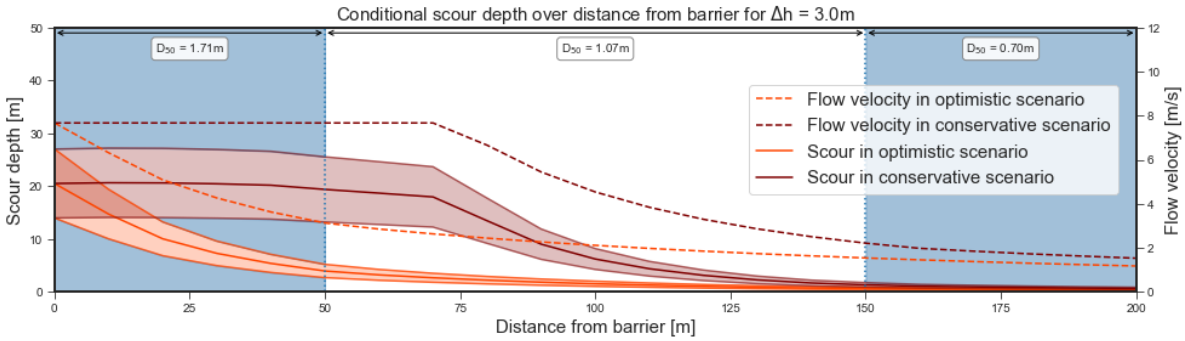

Figure 9.17: The scour that potentially occurs behind gate R16 when a water level difference of 3.0m occurs

Both the optimistic and the conservative flow scenario have been considered. While the conservative flow scenario does not lead to deeper maximum scour hole formation near the barrier, the probability of a deep scour hole at a larger distance from barrier is significantly increased. This is caused by the flow velocities, which remain high during flow development. While the flow velocities do not decrease during flow development, the scour can be seen to (slightly) decrease over this region however. This is caused by the decrease in turbulence with distance from the barrier. The turbulence decreases the amplification factor, which reduces the potential scour. In the conservative scenario it can be seen that the potential scour remains large for locations beyond 50m from the barrier. These same locations have been shown to be vulnerable to failure of the bottom protection in Figure 9.13. This can be explained by the dependence on the same flow velocity for both mechanisms.

When the water level difference over the barrier is increased to 4.0m and to 5.0m, the scour depth increases, both in the optimistic and the conservative scenario. This makes sense as the flow velocities increase with an increase in water level difference. The general behaviour of the potential scour does not change however, with the same scour depth near the barrier in both scenarios and a scour depth that stays high for the locations located in the flow development region in the conservative scenario. The potential conditional scour for 4.0m water level difference over the barrier and 5.0m water level difference over the barrier can be seen in Figure 9.18.

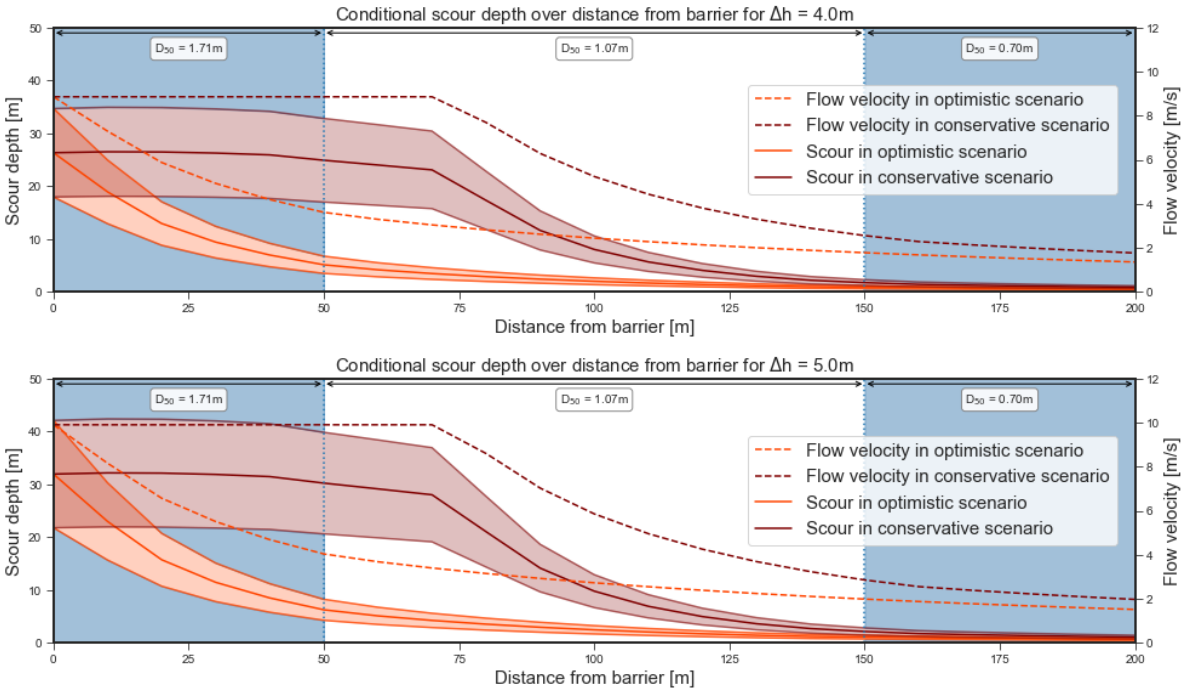

Figure 9.18: The scour that potentially occurs behind gate R16 when a water level difference of 4.0m or 5.0m occurs

The potential conditional scour can be computed for all gates, as was done for gate R16. As such, any differences in potential scour along the length of the barrier can be investigated. This can be seen in Figure 9.19. To keep clarity, only the mean potential conditional scour depth has been plotted, but the scour depth is still described with a distribution for all locations.

In the optimistic scenario, failure of gate R27, can be seen to lead to larger scour depths. Behind this gate, the water depth remains relatively low, due to the high bottom height, as can be seen in Figure 9.8. This low water depth decreases the scour depth as can be seen from Equation 9.8. The lower water depth also increases the flow velocities however. As the cross-sectional surface of the flow is decreased, the flow velocity is kept higher. While the water depth can be found in Equation 9.8 to be raised to the power of 0.2, the flow velocity is raised to the power of 1.7. As a result, the scour depth is more strongly influenced by the increase in flow velocity, than decrease in water depth. This leads to an increase in scour depth behind gate R27. In the conservative scenario, the potential scour depth remains high over the flow development region, caused by the high flow velocities. As such, failure of one of the gates with higher sills will not always lead to large scour depths. For these gates with higher sills, the flow development region of any potential jet is short after all. This might be interesting, as it implies that failure of the bottom protection behind these gates with higher sills has less severe consequences than failure of the bottom protection behind one of the middle gates. This will be further investigated in Subsection 9.5.2.

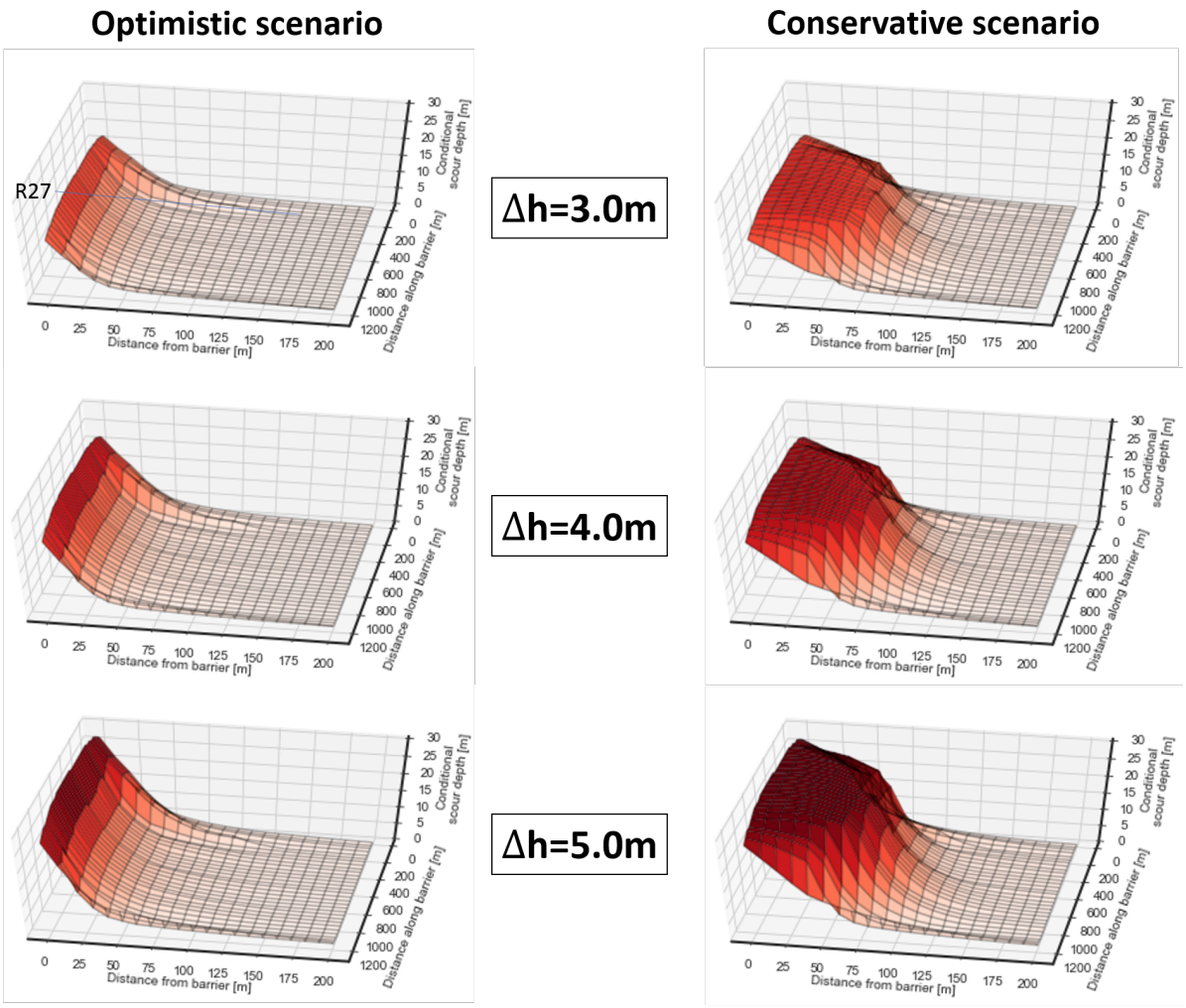

Figure 9.19: Mean potential conditional scour depth for all gates

9.5.2. Conditional scour hole instability

As aforementioned, the existence of a scour hole is not in itself a problem, if the scour hole can be kept far enough away from the barrier. If a scour hole becomes unstable and sliding, or flow sliding, occurs, this sliding can not be allowed to reach the structure. A maximum allowed gradient between the scour hole and the barrier can be drawn, as indicated in Figure 9.16.

This maximum allowed gradient is equal to the gradient of a scour hole that has become unstable, which for normal slides is 1:6 [29]. Flow slides will not be considered in this report. The maximum allowed gradient will be described with a distribution, with a mean 1:6 and an assumed (large) standard deviation of 0.05. The sensitivity of this assumption will be assessed in Appendix G. For each location behind the Eastern Scheldt barrier the maximum allowed scour depth can then be computed by multiplying the distance between the location and the barrier with this maximum gradient. As both the maximum allowed scour depth and the occurring scour depth are now described with a distribution, the transfer probability can be described as with the limit state function seen in Equation 9.11.

$$Z = R - S = \underbrace{h_{\text{scour,max}}}_{\text{Conditional on location}} - \underbrace{h_{\text{scour}}}_{\text{Conditional on load and location}} \quad \text{and} \quad P_{\text{transfer}} = P(Z < 0) \tag{9.11}$$

The maximum allowed scour is not conditional on the loading, but the occurring scour is. The transfer probability is therefore conditional on the loading and will be named the conditional transfer probability. The conditional limit state function will thus need to be solved for each discretized loading scenario (as well as for each location), as seen in Equation 9.12.

$$\text{for} \quad S_i = s_1, s_2, ..., s_n: \quad P(\text{transfer}|S_i) = P(R - S_i < 0) = P(h_{\text{scour,max}} - h_{\text{scour}|S_i} < 0) \tag{9.12}$$

The potentially occurring scour was computed in Subsection 9.5.1, and thus only the maximum allowed scour is required to compute the transfer probabilities. As this maximum allowed scour depth is independent from the loading and thus constant, both over loading conditions as well as over the two flow scenarios. Additionally, there is no difference in the maximum allowed scour depth along the barrier. The maximum allowed scour depth can be seen in Figure 9.20. The maximum allowed scour depth is uncertain due to the gradient being described with a distribution, and this uncertainty therefore grows with distance. Only stability of a scour hole with respect to the Eastern Scheldt barrier has been considered.

The stability of the soil between the piers, which constitute the first approximately 20m from the barrier have not been included when computing the transfer probability. These 20m closest to the barrier are situated between the piers of the barrier, as can be seen in Figure 2.5. The sill and bottom protection at these locations is composed of several layers of different types of bottom protection, including the top layer, several secondary and filter layers, filter mattresses, and a bottom layers that has been compacted. As such, the model, of erosion of the rock of the bottom protection exposing the bottom and subsequently scour was deemed too simplistic. A more thorough assessment of these layers, as well as the potential occurrence and consequences of the instability of a scour hole is recommended for these locations.

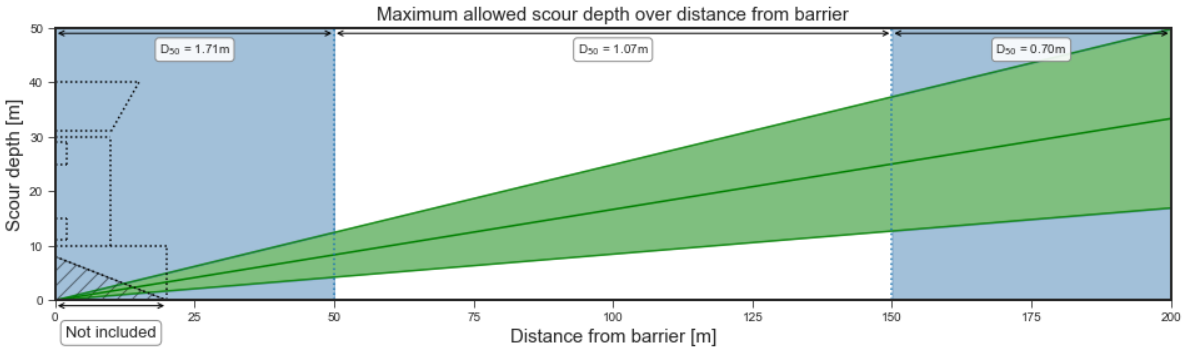

Figure 9.20: The maximum allowed scour depth is a function of the deterministic location and a probabilistic gradient. The locations within 20m of the barrier have not been included. The barrier drawn is for illustration purposes, and not to scale.

In Figure 9.21 and Figure 9.22 the maximum allowed scour, potentially occurring scour and the resulting potential transfer probabilities are drawn, conditionally, for the optimistic and conservative scenario respectively. After all, while the maximum allowed scour is independent on the load, the potentially occurring scour is not. The barrier has been drawn schematically (and not to scale) as well[5].

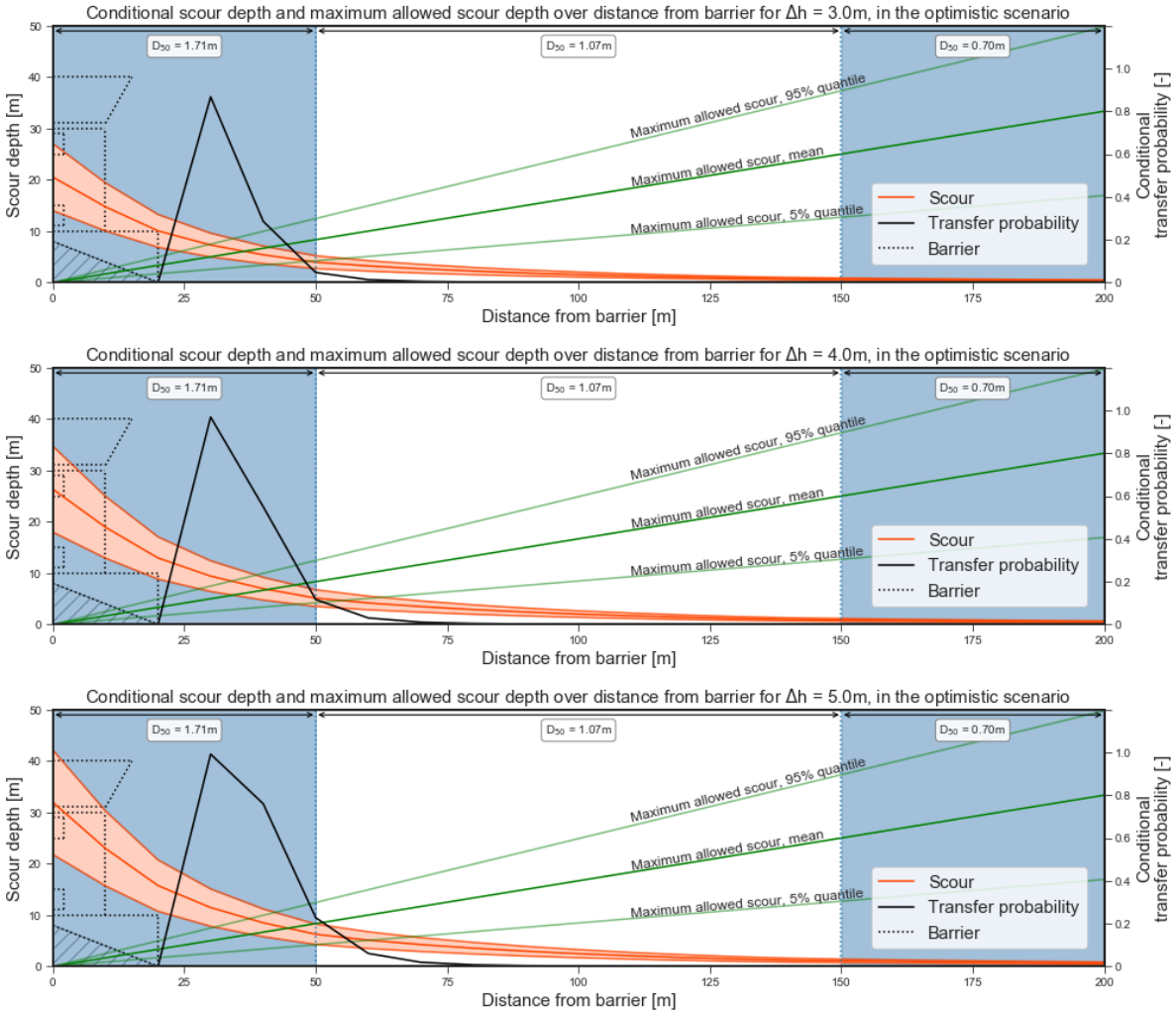

Figure 9.21: Conditional scour, maximum allowed scour and the resulting transfer probability, behind R16, in the optimistic scenario

Interestingly, in both the optimistic and the conservative scenario, the dependence of the transfer probability on the loading conditions seems limited. The transfer probability in the optimistic scenario can be seen to peak around the barrier and then diminish, while the conservative scenario leads to conditional transfer probabilities which remain higher at larger distances from the barrier. An increase in the water level difference over the barrier only slightly influences these transfer probabilities. The independence on loading implies that the transfer probabilities are mostly influenced by the maximum allowed scour depth (and thus the gradient).

[5]When looking at Figure 9.21 and Figure 9.22, the caissons on which the piers are build are displayed, stretching out 20m from the axis of the barrier. The maximum allowed scour depth gradient starts in the axis of the barrier however and not at the end of these caissons. These caissons are located 'behind' the sill (from the perspective in these images) and are partially buried, which can be seen in Figure 2.4 more clearly. To avoid the necessity of applying more complex forms of geo-technical failure to account for this partially buried structure, as well as sliding into an additional dimension, a simplification was made, where the maximum allowed scour depth is computed as function of the distance from the axis of the barrier only. The geo-technical stability directly at the sill, and around the piers requires a more complex assessment, not deemed within the scope of this report. As such, the locations in the first 20m can be part of the instability caused by a slide, but slides cannot initiate in these locations.

In the optimistic scenario, the conditional transfer probabilities in the region beyond 50m from the barrier can be seen to be small. This implies that failure of the bottom protection in this region will not lead to enough scour to endanger the barrier. In the conservative scenario however, a larger region can be seen (from approximately 20-100m from the barrier) where the transfer probabilities are very high. This suggests that failure of the bottom protection in this region will always lead to enough scour to threaten the barrier. Unsurprisingly, this is the approximately the region where the jet flow is in development and causes high flow velocities.

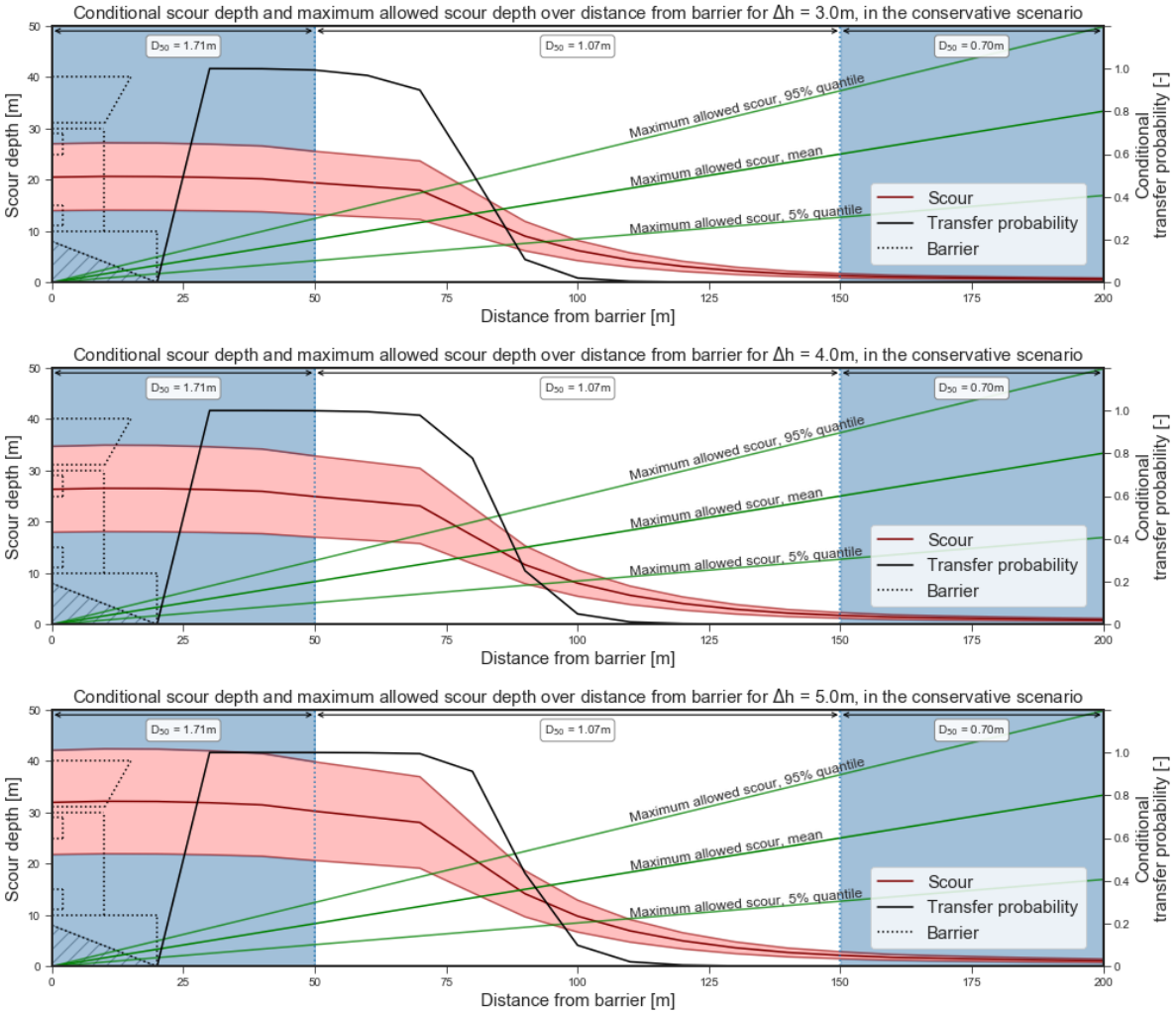

Figure 9.22: Conditional scour, maximum allowed scour and the resulting transfer probability, behind R16, in the conservative scenario

9.6. Conditional failure per location to conditional failure of the barrier

With the conditional failure probability of the bottom protection, as well as the conditional transfer probability per location known, the conditional failure probability of the barrier per open gate can be computed[6]. Failure of the barrier is a parallel system, composed of two elements; failure of the bottom protection and transfer towards the barrier. If the conditional probability of these two elements is considered independent, these probabilities can be multiplied, to compute the conditional failure probability of the barrier. As can be seen in Figure 6.3, this would be an optimistic assumption. Physically speaking, these two processes are independent in strength. After all, the movement resisting strength of a stone in the bottom protection is

[6]Failure of the barrier is now defined as failure of the bottom protection multiplied with the transfer probability. As such, a distinction can be made between conditional failure of the bottom protection (without transfer probability taken into account) and conditional failure of the barrier (with transfer probability taken into account).

independent of the scour resisting strength of the soil below. The models applied for the calculation of the strength have applied the turbulence of the flow within the strength part of the computation however! While the strength thus is physically speaking independent, the turbulence (not usually seen as a strength parameter) has already introduced dependence. Nonetheless, this report will continue under an assumption of independence in strength between the failure probability of the bottom protection and the transfer probability. By multiplying the conditional failure probability of the bottom protection, per location, with the conditional transfer probability, per location, the conditional failure probability of the barrier, per location, can then be computed. This conditional failure probability of the barrier represents the probability that the bottom protection fails, and that the scour of the soil beneath this bottom protection endangers the barrier. These probabilities are still conditional however. This can be seen in Figure 9.23 for the middle gate, R16.

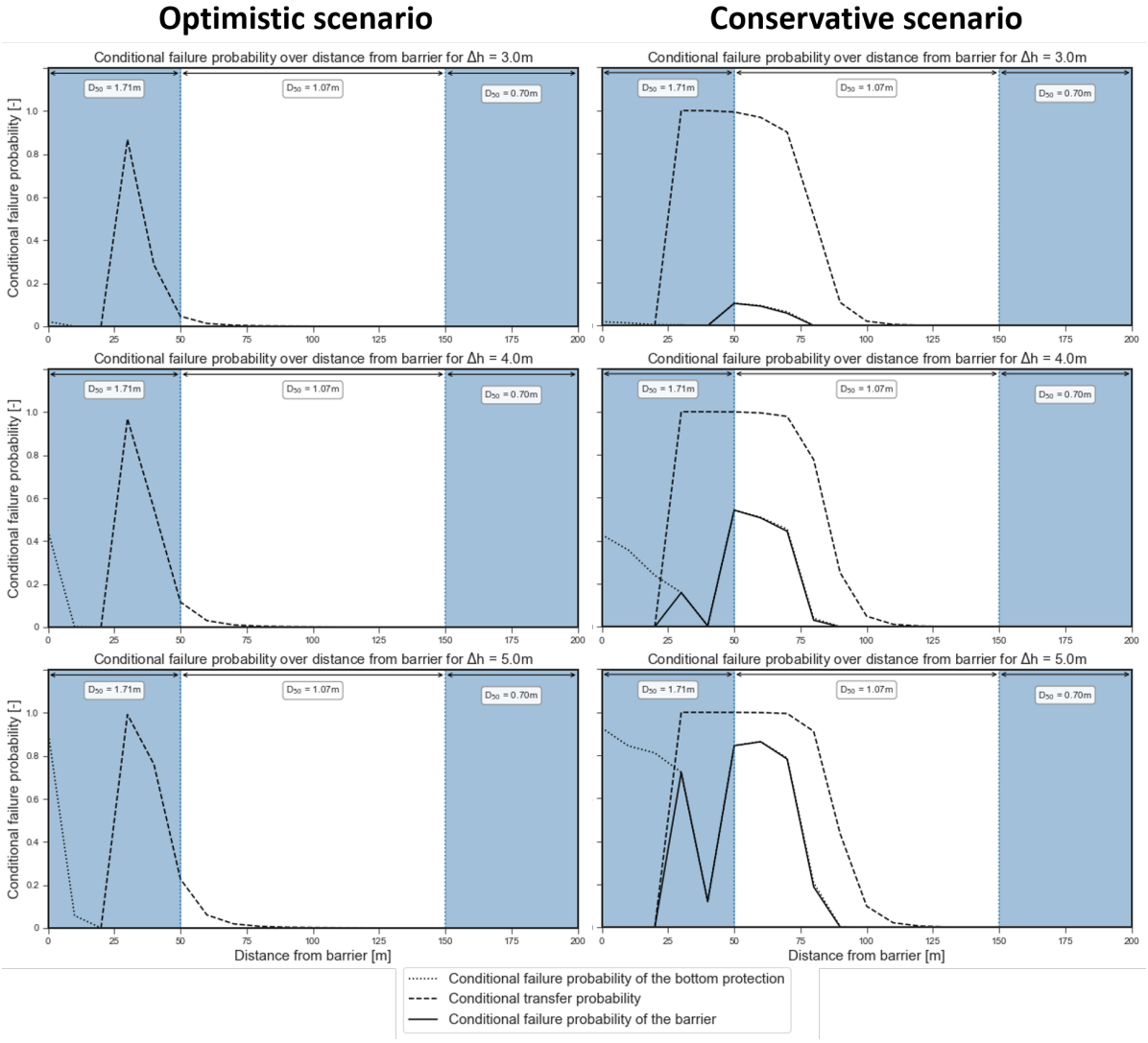

Figure 9.23: The conditional failure probability of the bottom protection multiplied with the conditional transfer probability gives the conditional failure probability of the barrier. These graphs represent gate R16.

It can be seen in Figure 9.23, that in the optimistic scenario the failure probability of the barrier is very low (to the point of not being visible in the plot). This is caused by fact that the conditional failure probability is negligible for locations where the transfer probability is significant and vice versa. In the conservative scenario the failure probability of the barrier is highest for the locations at approximately 50m from the barrier. At these locations the failure probability of the bottom protection is high due to the smaller stone diameter. At the same time, these locations are close enough to the barrier that a potential scour hole can quickly grow deep enough to endanger the barrier. For gate R16, it thus appears that only in the conservative flow scenario the barrier can be endangered.

The conditional failure probability of the bottom protection and the conditional transfer probability can be multiplied for all locations, to compute the conditional failure probability of the barrier for all locations.

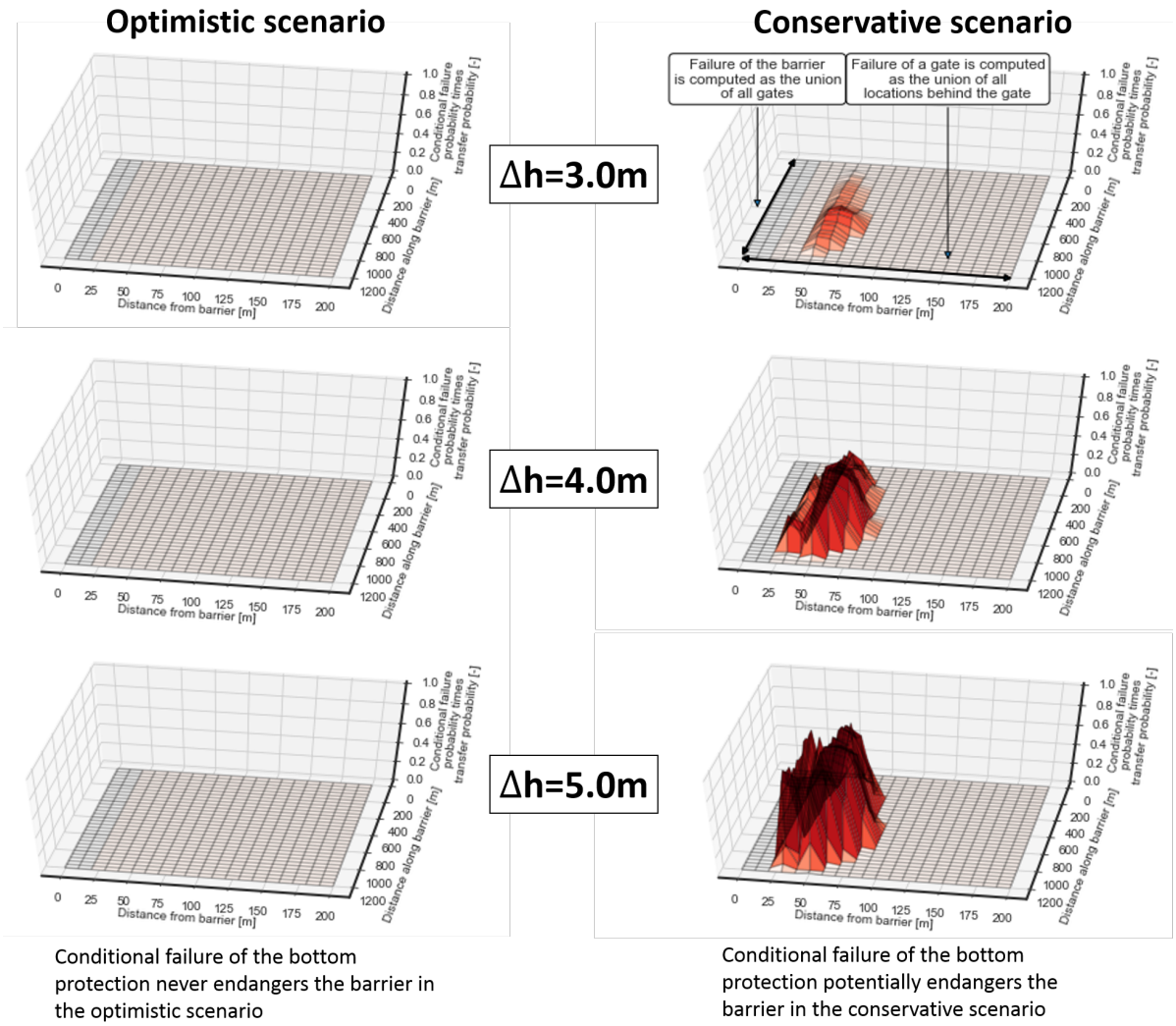

Figure 9.24: The conditional failure probability multiplied with the transfer probability for all locations behind every gate

As can be seen in Figure 9.24, failure of the bottom protection in the optimistic scenario can be seen to never causes danger to the barrier. In the conservative scenario locations at a distance of 50m from the barrier will endanger the barrier first. For low water level differences, failure of gates with deeper sills lead to larger failure probabilities for the bottom protection and barrier, due to the longer flow development of the jet flow that would occur. This longer jet flow development region would allow high flow velocities to reach the (weaker) second layer of bottom protection. If the water level difference is increased, locations behind more of the gates will potentially start to fail, while the conditional failure probability behind the gates on the ends of the barrier (with higher sills) will remain lower.

As the conditional failure probability at every location now implies the failure of the barrier, the different locations can be seen as a series system, where the different locations behind a gate form the elements. After all, when a gate is open, failure at any location behind that gate now implies the failure of the barrier. Additionally, failure of the barrier behind a single gate implies failure of the barrier as a whole. The different gates can thus also be seen as a series system, where the different gates form the elements. In Figure 9.24 both of these series systems can be seen, while in Figure 9.25 the fragility curves for failure behind each gate has been computed. Each curve represents the conditional failure of the barrier given that that specific gate has failed to close. As such, the fragility curve marked R21 represents the conditional failure of the barrier given that

gate R21 is open when a water level difference is present over the barrier. Only several gates have been plotted in Figure 9.25 to keep the graph readable, but the fragility curve behind every gate has been computed.

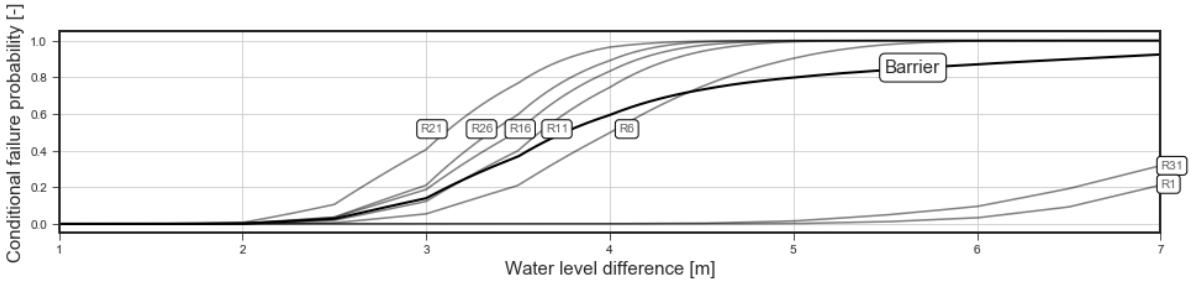

Figure 9.25: Fragility curve of the individual gates and the entire barrier in the conservative scenario

The fragility curves in Figure 9.25 have been drawn for the conservative scenario. These curves indicate that the gates with deeper sills (say R10-R27) are most vulnerable when opened. This is not unexpected, as both the conditional failure probability of the bottom protection and the conditional transfer probabilities where shown to be higher behind these gates. The gates at the end of the barrier; R1 and R31, appear to not be very vulnerable, due to the limited length of the development region of the jet flow. As stated before, failure behind a single gate now represents failure of the barrier. The fragility curve of the barrier, which represents the failure probability when any gate is open while a water level difference is present over the barrier, can thus be computed by taking the union of the fragility curves of all the gates. As only the failure of a single gate is considered (exclusively, all with a 1/31 share of the probability of any gate failing) the law of total probability can be applied to compute the union, as can be seen in Equation 9.13.

$$\text{for} \quad S_i = s_1, s_2, ..., s_n : \quad P_{\text{f,barrier}}|S_i = \sum_{j=1}^{31} \frac{1}{31} P_{\text{f,gate=j}}|S_i \tag{9.13}$$

At first glance it might seem strange that the fragility curve of barrier implies lower conditional failure probabilities than some individual gates. If gate R21 is considered for example, it can be seen to have much higher conditional failure probabilities than the barrier as a whole. It should be kept in mind however that as the failing closure per gate is considered to be exclusive from failing another gate, the fragility curve of the barrier is an average of the curves of the gates. After all, when a gate has failed there is a probability of 1/31 of it being (the very vulnerable) gate R21, but also a 1/31 probability of it being (the not very vulnerable) gate R1. Figure 9.25 has been computed under the assumption that a gate is open, and as such the fragility curve tends to 1. In Subsection 9.1.1 the failure probability of a closure request was calculated to be 2.4E-4 per gate. If the 31 gates of the Roompot section are considered there is an approximately 7.13E-3 probability of one of the gates failing to close on request. By taking the probability of a gate failing to close into account, the fragility curve per closing request can be computed. This fragility curve can be seen in Figure 9.26.

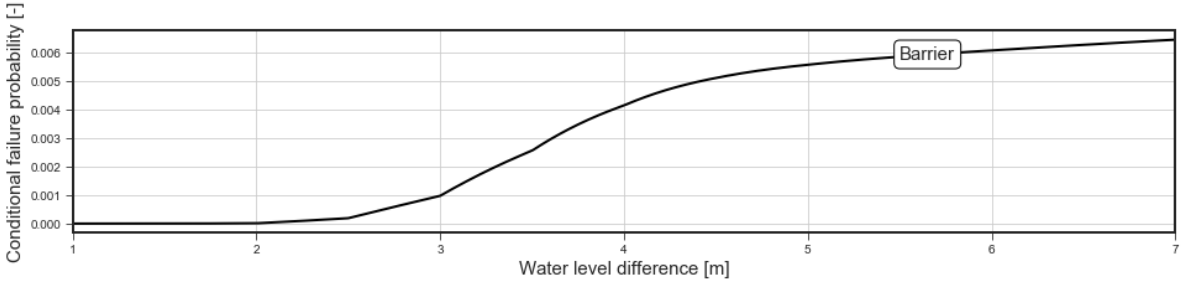

Figure 9.26: Fragility curve of the entire barrier in the conservative scenario per closure request

From Figure 9.26, it can be seen that the fragility curve tends to 7.13E-3. This makes sense as the conditional failure probability of the barrier is now limited by the probability of a gate failing. After all, when the water level difference over the barrier becomes large enough, the failure of the barrier is determined by the probability of an open gate (as an open gate then always implies failure of the barrier).

9.7. Integration

The fragility curve of the barrier can be integrated over the PDF of the water level difference to compute the failure probability of the barrier. This integration can be done over Figure 9.25 or over Figure 9.26 as the only difference is the (constant) probability of a gate failing. The failure probability of the mechanism 'failure due to failing closure' has to be presented as a probability per closure request [12]. As such, the water level difference per closure request is required for the computation. The Prespeil model allows for the extraction of the probability density of the maximum water level difference per year, which can be seen in Figure 9.27.

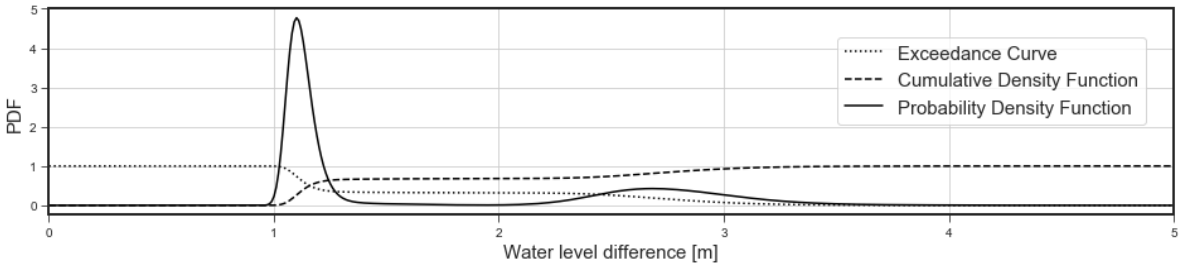

Figure 9.27: PDF, CDF and exceedance curve of the maximum water level difference per year over the barrier

This PDF of the water level difference shows two distinct peaks. These are caused by the maintenance strategy of the barrier when it is closed, as the water level on the Eastern Scheldt is maintained at 1.00m+NAP alternating 2.00m+NAP. This alternating is done to keep the wave attack which occurs on the dikes along the Eastern Scheldt (due to the fetch over the large Eastern Scheldt basin the wave attack can still be significant even when the barrier is closed) from loading the same spot on the dikes. The PDF of the water level difference clearly shows this alternating strategy. Additionally, it can be seen that a water level difference under 1.0m hardly occurs. This can be explained by the fact that the barrier is not closed until a water level of 3.00m+NAP is predicted, while a maximum water level of 2.00m+NAP is maintained on the Eastern Scheldt.

It will be assumed that Figure 9.27 can also be applied as the water level difference per closure request. As the barrier closes with an average frequency of once per year [12], the maximum water level difference per year and the maximum water level difference per closure will likely be similar. After all, when the barrier is open, no water level difference will exist over the barrier. Integration of the PDF then computes the failure probability, which can be seen in Equation 9.14, while the resulting failure probability of the barrier can be found in Table 9.4. These failure probabilities have been computed for both the optimistic and the conservative scenario. Additionally, the failure probabilities have been computed with the transfer probabilities set to 1 for every location. As such the effect, of taking the transfer probabilities into account conditionally, can be gauged. It can be seen that the failure probability in the conservative scenario is of course much larger than in the optimistic scenario (by a factor 1E7).

$$P_{\text{f,barrier}} = \int_0^{\infty} \underbrace{P(f|S_i)}_{\text{Fragility curve barrier}} \underbrace{P(S_i)}_{\text{PDF}(S)} \, \mathrm{d}S \tag{9.14}$$

	Failure probability given failed gate	Failure probability per closure request	Failure probability per closure request if $P_{transfer}$=1	Reduction due to $P_{transfer}$
Optimistic scenario	3.90E-9	2.78E-11	4.50E-11	38.4%
Conservative scenario	3.44E-2	2.45E-4	2.54E-4	3.74%

Table 9.4: Failure of the barrier under various conditions

From Table 9.4, it can be seen that the conditional failure probabilities are always lowered by the transfer probabilities. This makes sense of course as the conditional transfer probability will always be valued between 0 and 1. In the optimistic scenario the application of the conditional transfer probabilities reduces the failure probability by almost 40%, as the failure probability per closure request is reduced from 4.50E-11

to 2.78E-11. In the conservative scenario the application of the conditional transfer probabilities reduce the failure probability by only 4%, from 2.54E-4 to 2.45E-4. The difference between these two reductions can be explained by looking at Figure 9.21 and Figure 9.22.

In the optimistic scenario the conditional failure probabilities of the bottom protection are high at locations where the conditional transfer probabilities are low and vice versa. As a result, the application of the conditional transfer probabilities greatly reduces the failure of the barrier. This implies that in the optimistic scenario, failure of the bottom protection hardly ever leads to failure of the barrier, due to the transfer probabilities.

Alternatively, in the conservative scenario, the conditional failure probabilities of the bottom protection are high at locations where the conditional transfer probabilities are also high. At locations further from the barrier, the conditional transfer probabilities are smaller, but since the system behind a gate is considered a series system, the failure behind a gate is dominated by the largest conditional failure probabilities behind that gate. As such, the smaller failure probabilities of the bottom protection further from the barrier hardly contributing to the overall failure probability and the transfer probabilities do not influence failure of the barrier. After all, a chain is only as strong as the weakest link. This leads to the conditional transfer probabilities barely influencing the failure of the barrier. This implies that in the conservative scenario, failure of the bottom protection almost always leads to failure of the barrier.

The reduction introduced by applying a conditional approach to the transfer probabilities can thus be seen to greatly vary. As the assessment of the barrier in this report is based on several assumptions, a sensitivity analysis was performed to gauge the effects of these assumptions. This sensitivity analysis can be found in Appendix G.

9.7.1. Comparison previous studies

In the original design, the bottom protection was designed to comply with the so called Delta criterion. The Delta criterion stated that the barrier would have to withstand a combination of loads with a combined exceedance frequency of 2.5E-4 per year [84]. When considering the situation of a gate failing to close, a design water level difference over the barrier of 4.15m+NAP was selected. During the design there was no indication of water levels which would be maintained on the Eastern Scheldt however, and as such a minimum water level of -0.70m+NAP was taken into account [67]. Since in this report a water level on the Eastern Scheldt of 2.00m+NAP is assumed, similar outside water levels would lead to a design water level difference of 1.45m with this water level on the Eastern Scheldt. In the conservative scenario, this water level difference implies a conditional failure probability of 8.85E-6 per closure request. As such, this conditional failure probability would take an approximate 4% of the available failure space of the barrier [7].

In the previous assessment round the barrier was assessed by ARCADIS [67] . In this assessment the bottom protection, under the condition of a failed gate was assessed and just passed the assessment, with a failure probability of 6.4E-5 per year. This failure probability was based on the probability of occurrence of the design water level difference. The assessment concluded with a recommendation of further research into the bottom protection under the condition of a failed gate, as well as an assessment of the transfer probabilities, between failure of the bottom protection and failure of the barrier. The failure probability found in this report is higher than the failure probability of the ARCADIS study, but only when considering the conservative flow scenario. Additionally, for this conservative scenario, the transfer probabilities have been shown to be of minor influence on the failure of the barrier.

[7] No space is allocated in standard failure probability budgets for this unique mechanism, so whether this 4% would have been acceptable is difficult to say without computing more failure mechanisms.

9.8. Conclusion

By applying the fragility-based assessment method, the Eastern Scheldt barrier has been assessed on failure due to failing closure. The conditional methodology allowed for a more detailed analysis of the transfer probabilities as a conditional approach could also be applied here. As a result, the failure probabilities of the barrier could be decreased. The barrier was shown to be vulnerable in very specific circumstances. First the flow conditions can be considered. Two flow scenarios have been explored; an optimistic and a conservative scenario, with the effects of applying conditional transfer probabilities very dependent on this choice of scenario.

Optimistic scenario
In the optimistic scenario, the flow exiting the orifice (gate) immediately starts to spread over the depth and width of the basin behind the gate. This results in the flow velocities being strongly reduced with distance from the barrier. Any danger to the top layer of the bottom protection is found in the first 20 meters from the barrier, as can be seen in Figure 9.23. In this region, the conditional transfer probabilities have been assumed to be zero; as various layers of bottom protection form a thick layer above the bottom, while the bottom itself is densified as well. Due to this assumption, failure of the top layer of the bottom protection at these locations will not lead to failure of the barrier. This assumption of a transfer probability of zero will need to be tested in a more detailed assessment however. At locations further from the barrier, where non-zero transfer probabilities exist, the failure probability of the bottom protection is low.

Due to this, the optimistic flow scenario leads to the low failure probability of the barrier of 2.78E-11 per closure request. This failure probability is found to be relatively evenly distributed along the barrier, with gate R04 being most vulnerable during lower water level differences over the barrier.

Conservative flow scenario
In the conservative flow scenario, the flow exiting the orifice (gate) will display jet-like behaviour. Due to this behaviour, the flow will remain in flow development over a distance related to the height of the orifice. During this flow development phase, the flow remains concentrated along the bottom, leading to high flow velocities, at distances further from the barrier. When these high flow velocities can reach the second layer of bottom protection, which starts at a distance of 50m from the barrier, high conditional failure probabilities may occur. This can be seen in Figure 9.23. Additionally, as these flow velocities remain high during flow development, the conditional transfer probabilities are also significantly higher over larger regions.

Whether the flow development region is long enough to reach the second layer of bottom protection is dependent on the gate considered, as the length of the flow development region is linearly related to the height of the orifice. The locations behind gates with lower sills are therefore significantly more vulnerable to failure. As a result of these deeper sills, the bottom protection behind these gates will be loaded more heavily further from the barrier. This was shown to lead to higher conditional failure probabilities for the bottom protection in Figure 9.15, and higher conditional failure probabilities for the barrier in Figure 9.24.

Due to this behaviour, of jet formation allowing high flow velocities to reach the second layer of bottom protection, the conservative flow scenario leads to a significantly higher failure probability of the barrier of 2.45E-4 per closure request. This failure probability is mainly caused by the deeper sills in the barrier, R10-R16, and found at a distance of approximately 50m from the barrier.

The failure probabilities computed in this chapter are based on several assumptions. Most notable, the distance from the barrier has been assumed to be distance towards the axis of the barrier. This assumption was made for simplicity, but it also brings inaccuracy. The barrier protrudes from the axis of the barrier, mostly at the piers, with parts of this protrusion (partially) buried. By using the axis of the barrier, the assessment failure probability might be optimistic, as the distance between a scour hole and the structure is smaller in reality. A more detailed assessment of the maximum allowed scour depths per location is therefor recommended.

10

Conclusions and recommendations

This chapter will finish up the report in two ways. Firstly, the assessment of the Eastern Scheldt barrier will be concluded. This will give an overview of the assessment of the barrier as described in this report. Secondly, the bigger picture of fragility-based assessment will be examined. This will assess the assessment methodology; whether the methodology offers advantages (or disadvantages) and whether the methodology can offer probabilistic custom assessment for complex forward barriers.

10.1. Eastern Scheldt barrier

Two failure mechanisms have been assessed in this report; the height of the Roompot lock and failure due to the failure to close a gate when requested. The results from these assessments will be briefly discussed below.

The height of the Roompot lock has been assessed to have a failure probability of 7.14E-6 per year. The failure of the lock, with regard to the failure mechanism 'height' has been determined to be mostly influenced by the doors of the lock, which become vulnerable when high outside water levels occur.

The failure of the Roompot section of the barrier, as a result of the failure of one of the gates failing to close has been determined to be 2.78E-11 per closure request in the optimistic flow scenario and 2.45E-4 per closure request in the conservative flow scenario. This high failure probability in the conservative scenario is mostly caused by the potential failure of the bottom protection at a distance of 50m from the barrier, behind the deeper sections of the Roompot gully. At these locations failure of the bottom protection leads to scour which can directly endanger the barrier.

These failure mechanisms have been assessed in order to answer the research questions, posed in Chapter 5.

How can a fragility-based reliability method be applied to offer a custom assessment of a unique flood defence, such as the Eastern Scheldt barrier?

The assessment of the height mechanism has shown how three sub-mechanisms can be combined into a single assessment; the stability of the stones on the coupure, the stability of the stones behind the lock and the stability of the lock doors. By combining these mechanisms conditionally, the dependency between them could be handled conditionally as well; the mechanisms were considered independent in strength, while fully dependent in load. As several loading parameters needed to be considered (water level and wave height), the fragility curve was extended into a surface, as seen in Figure 10.1.

Similarly, by applying a conditional approach, the failure of the barrier as a result of a gate failing to close was assessed. Over a grid of locations behind each gate, the conditional failure probabilities were computed, along with the conditional transfer probabilities. While transfer probabilities have been applied in the past, the conditional approach applied in a fragility-based assessment allowed for a conditional assessment of the transfer probabilities as well. As such, the assessment of the failure mechanism is no longer limited to the assessment of the bottom protection. For each load condition for which the bottom protection was assessed,

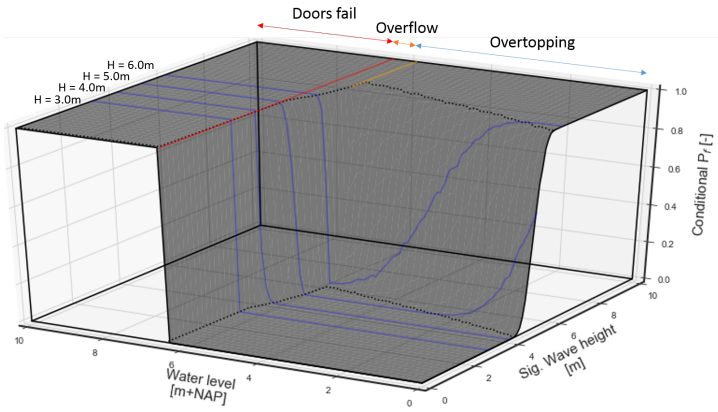

Figure 10.1: Insight into the influence of various mechanisms and loads can be gained through the fragility surface

the consequence of a failing bottom protection can now be assessed as well. This means the conditional formation of a scour hole, and thus the conditional transfer probability.

The application of these two custom assessments has shown that fragility-based assessment can offer a custom assessment of complex structures. The combining of mechanisms can be applied to full failure mechanisms (such as overtopping and overflow), or over different physical elements of the barrier (such as stones on a coupure and stones behind the barrier). As many of these mechanisms and elements are dependent on the same hydraulic loading variables, dependency can be taken into account by assuming dependence in loading only (and as such reducing the amount of conservatism introduced by an assumption of full independence in this series system of different mechanisms and elements). Additionally, the transfer probabilities in the unique mechanism 'failure due to failing closure' were made conditional and in loading fully dependent with the failure of the bottom protection while in strength fully independent, showing how a fragility-based assessment can be applied to provide a custom assessment of a complex and unique mechanism.

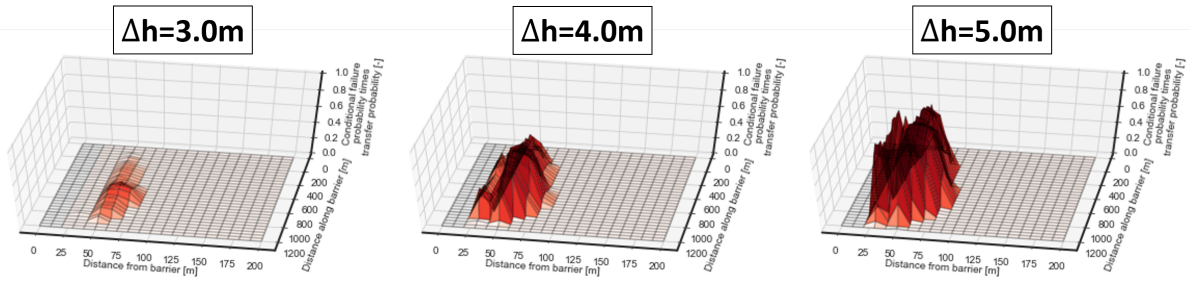

Figure 10.2: By assessing the conditional failure probability as well as the conditional transfer probability, vulnerabilities in the bottom protection can be shown

Can a fragility-based assessment offer increased insight into the processes that influence the failure probability?

The fragility-based assessment of the barrier has clearly increased the insight into the process influencing the failure probability. The fragility surface computed for the mechanism 'height' offers increased insight into how which mechanism influenced the failure probability. Most notable, the effects of the water level given different wave heights and vice versa can clearly be seen in the fragility surface. By applying a conditional approach to the mechanism 'failure due to failing closure' insight was gained into the vulnerabilities of the bottom protection, on different locations, under different loading conditions. For the different scenarios (optimistic and conservative) very different behaviour was modelled, leading to different failure probabilities and different transfer probabilities. In the optimistic scenario, the top layer of the bottom protection was only vulnerable to erosion, very near to the barrier, while in the conservative scenario the regions further from the barrier were shown to be vulnerable. The jet-like behaviour in the conservative scenario has been shown to be able to reach the second layer of bottom protection when certain gates are open, while a water level difference is present. At these locations the conditional transfer probability was also found to be high. As

such, it can now be seen which part of the bottom protection is vulnerable, behind which gate, under which conditions, and in which flow scenario. With this increase in insight, future decisions regarding the barrier and potential reinforcements will be better informed. Additionally, the behaviour of the system when the loading changes (for example through sea level rise) can be seen from the fragility surfaces.

Fragility-based assessment increases the insight gained in a safety assessment. By applying a fragility-based approach to the assessment of height, increased insight into the influence of various mechanisms on the failure probability was gained. Additionally, the influence of the various elements of the bottom protection, as well as the mechanisms of failure and transfer, have greatly increased the insight into the unique mechanism 'failure due to failing closure'.

10.2. Fragility-based assessment

The fragility-based assessment was applied to offer an assessment of the Eastern Scheldt barrier, a unique and complex forward barrier. Within this report two aspects of the methodology were analyzed; the probabilistic assessment and the dependence between various mechanisms, in order to answer two sub-questions regarding the methodology.

Can a fragility-based custom assessment be shown to be less conservative than a detailed assessment?

As explained in Chapter 1, safety assessment in the Netherlands is moving from a semi-probabilistic approach towards a probabilistic approach. The differences between the two have been explored in Chapter 7, and the fragility-based methodology was shown to be able to offer an alternative probabilistic assessment. This assessment, like a traditional probabilistic assessment, offers a failure probability as output, as opposed by a semi-probabilistic assessment, which offers a verdict (which requires a calibration relationship to estimate a failure probability). As the semi-probabilistic assessment is inherently an approximation, the methodology is also inherently conservative (considering that the calibration relation is set up to be conservative). The probabilistic fragility-based assessment has been shown to lead to a failure probability which is less conservative, as seen in Table 10.1.

The fragility-based assessment can be shown to be less conservative than the semi-probabilistic assessment for piping. This is due to the inherent conservatism brought by the approximation that the semi-probabilistic detailed assessment ultimately is. The fragility-based assessment does not introduce this conservatism, and is thus inherently less conservative.

Norm	$P_{f,\text{Semi-probabilistic}}$	$P_{f,\text{Fragility}}$	$P_{f,\max}$	Verdict semi-probabilistic	Verdict probabilistic
1/10	2.97E-3	6.29E-4	2.40E-2	Pass	Pass
1/30	4.59E-3	6.29E-4	8.00E-3	Pass	Pass
1/100	6.52E-3	6.29E-4	2.40E-3	Fail	Pass
1/300	8.34E-3	6.29E-4	8.00E-4	Fail	Pass
1/1.000	9.82E-3	6.29E-4	2.40E-4	Fail	Fail
1/3.000	8.11E-3	6.29E-4	8.00E-5	Fail	Fail
1/10.000	6.50E-3	6.29E-4	2.40E-5	Fail	Fail
1/30.000	5.27E-3	6.29E-4	8.00E-6	Fail	Fail
1/100.000	4.14E-3	6.29E-4	2.40E-6	Fail	Fail

Table 10.1: Through a comparison of the two, the fragility-based assessment was shown to be less conservative than the semi-probabilistic methodology

How can statistical dependency be taken into account in a fragility-based assessment?

The differences in statistic dependency have been shown to be potentially substantial in Chapter 6. While a semi-probabilistic methodology requires a failure probability budget and a length effect factor (which both bring conservatism, by definition), a fully probabilistic methodology can apply statistical dependency in more accurate manners. Additionally, by applying a fragility-based methodology, which assesses strength and load separately, the dependency of these components can assessed separately as well. This has been shown to be of potentially large importance as, even though traditional probabilistic assessments can discount for dependency, for example, through correlation coefficients, in practice they often rely on assumptions of full

dependence or full independence. The fragility-based assessment has been shown to offer a third possible assumption; of full independence in strength, yet full dependence in loading.

This assumption (when considered applicable/justified) can be of great importance when assessing a complex structure. As the structure needs to be divided into elements, each requiring a different type of assessment, for different failure mechanisms, and different strength component, an assumption of independent strength parameters might be justified. An assumption of full independence in load can almost never be justified however, as these blocks all undergo the same type of loading: hydraulic. An assumption of independence in loading or in strength and loading (as these components cannot be assessed separately in a traditional probabilistic assessment) would therefor lead to either a very conservative or a very unsafe design, depending on the system assessed (series or parallel).

A careful consideration of strength and loading should be made however! In this report it is frequently reported that the differences between R and S are arbitrary, which normally holds, as only the limit state (or Z) matters. When the fragility-based methodology is applied to describe situations of varying dependence between strength and load parameters however, it should not be forgotten which parameters have been discounted in R and which in S. An example can be seen in the Pilarczyk formula, applied in Chapter 8 and Chapter 9. While it can be justified to assume independence between certain strength parameters, the Pilarczyk formula applies certain parameters which might be better described as loading parameters, such as the turbulence factor and the depth parameter. By blurring this line between strength and load, it becomes more difficult to make assumptions (for example an assumption of dependent load, with independent strength, as applied several times in this report).

By applying a fragility-based assessment, additional assumptions regarding statistical dependency can be done when compared to traditional probabilistic or semi-probabilistic methods. Most notably, since strength and load are assessed in separate steps, the dependency of the strength and load can be set in separate steps as well. When this assumption is justified, it can greatly reduce conservatism in both series and parallel systems. It should be assessed carefully however whether this assumption is justified. As the distinction between strength and load is sometimes arbitrary, mistakes in assuming an independent strength can easily be made. An example is the critical flow velocity in the Pilarczyk formula, which applied a factor for turbulence. This introduces dependency from the loading into the strength parameters.

How can a fragility-based reliability method be developed and applied in a custom and probabilistic safety assessment of the Eastern Scheldt storm surge barrier and other complex flood defences?

This report has produced a partial fragility-based assessment of the Eastern Scheldt storm surge barrier. By developing the conditional failure probabilities, under various loading conditions and scenarios, it has been shown how fragility-based assessment looks and how it offers advantages over currently applied methodologies. The methodology was shown to apply the same probabilistic input, in the form of stochastic variables, but also in the form of the same theoretical formulas. Additionally, the mythology was shown to potentially reduce conservatism and thus lead to more accurate and economically beneficent designs and assessments. The methodology was shown to offer increased insight into the processes which govern the Eastern Scheldt barrier. As such, if increased insight into a complex structure is required, the fragility-based assessment can offer this.

Disadvantages have also been identified however. By computing the conditional failure probability over a vector of loading conditions, the computational effort required is vastly increased. As the curve is extended into a surface this computational effort grows exponentially, as more conditional failure probabilities need to be computed. This puts a constraint on the workability of the methodology, especially when failure mechanisms are assessed which already have a high computational cost (such as, for example, geotechnical failure mechanisms).

Additionally, due to the increased complexity of the methodology, as well as the unfamiliarity of hydraulic engineers with the methodology, the methodology can be experienced as difficult. This increase in both computational cost and complexity, requires a careful consideration when the methodology is to be applied. When a unique and complex forward barrier is to be assessed, this increase in costs might be considered justified, while the assessment of a simple dike might better be done with less expansive and more familiar tools. This can be determined by the user however.

Nonetheless, when a complex flood defence, such as the Eastern Scheldt barrier, is to be assessed, the fragility-

based assessment can offer a powerful tool. Both the possibility to assess complex mechanisms and elements probabilistically, as well as the reduction of conservatism by taking dependency between these mechanisms and elements into account make a fragility-based assessment ideal in the probabilistic assessment of complex structures.

10.3. Recommendations

This report looked at fragility-based assessment as a tools and assessed this methodology. The next step into this field of research is found along two paths; broadening the methodology and extending the methodology. Additionally, some recommendations on the assessment of the Eastern Scheldt barrier are offered.

Broadening the methodology
This report looked at failure mechanisms that can be described with limit state functions. Broadening the methodology requires a full fragility-based assessment for all types of failure mechanisms. In this way, the dependency, one of the major advantages offered by the methodology, can be applied over all failure mechanisms. In this way conservatism due to assumptions of (in)dependence or through failure probability budgets can be avoided. Other failure mechanisms might require other types of fragility based assessment however, other failure mechanisms might rely on other assessments types. These failure mechanisms might require numerical methods (often applied for geotechnical failure mechanisms) or miner-sums (often applied for asphalt revetments). How can fragility-based assessment be applied for failure mechanisms that do not necessarily or only partially rely on limit state functions? Can the increase in computational effort still be justified for these (sometimes already costly) assessment types? Additionally, the models applied in this report were very simple. Can the fragility-based assessment be applied with more complex flow models for the failure probabilities or with more complex geo-technical models for the transfer probabilities?

Extending the methodology
Extending the methodology requires a more general assessment of the methodology itself, specifically in a quantitative manner. This report looked at the fragility-based assessment in a very qualitative manner, often applying simplifications and assumptions. As a result, especially in the comparisons between current assessments and previous assessments, it was difficult to make quantitative comparisons. Additionally, a direct quantitative comparison with previous assessments was already difficult due to changes in flood risk assessment rules. This report recommends more quantitative research into the exact effects that a fragility-based assessment has on the conservatism of an assessment. This could be done by more thoroughly assessing a less complex structure. Does the assessment of less complex assessments also benefit from fragility-based assessment? Can a quantitative comparison be drawn between the two? This would require a full traditional assessment and a full fragility-based assessment of all failure mechanisms to compare.

Assessment of the Eastern Scheld barrier
Within this report the assessment of the Eastern Scheldt barrier has been limited due to constraints in time and resources (computational power). As such, there are several recommendations which can be done to further the custom assessment of the Eastern Scheldt barrier.

To assess the failure probabilities computed in this report a full probabilistic assessment of the barrier, for all failure mechanisms, is required. The failure probabilities of the mechanisms can then be combined into a failure probability of the barrier, which can be compared to the norm. This is one of the main advantages of a probabilistic assessment; that no failure probability budget is required and failure probabilities per mechanism can be added into a probability per section or structure.

The custom assessment now performed for the mechanism 'failure due to failing closure' can be extended. This report has not investigated the dependency between outside water level, and probability of occurrence of each scenario (optimistic and conservative). The next step into this research can be found here; if the occurrence of the optimistic or the conservative scenario can be tied to certain loading parameters the conditional model can be completed. The potential occurrence of jet-like behaviour might be tied to the flow velocities through the gate. As such, the flow characteristics can be made dependent on the water level difference. Even if these dependency on the water level difference cannot be found (or does not exist), a probability of occurrence for the optimistic and conservative scenario would be very insightful. After all, this would allow a definitive failure probability to be computed for the mechanism, as opposed to the probabilities per scenario computed in this report (which differ very much).

A

Variables applied

Within this appendix an overview is presented of the variables applied in Chapter 8. These variables can be seen in Table A.1. The variables that have not been sourced have been assumed.

Symbol	Variable	Distribution	Parameter I	Parameter II
g	Gravitational constant	Det.	9.81	-
Δ	Relative density	Normal	μ=1.65	σ=0.05
D_{coupure}	Thickness of stones	Lognormal	μ=0.18 [85]	cov=0.1
D_{behind}	Thickness of stones	Lognormal	μ=0.38 [85]	cov=0.375
$\Psi_{\text{cr,coupure}}$	Shear stress parameter	Det.	0.07 [16]	-
$\Psi_{\text{cr,behind}}$	Shear stress parameter	Det.	0.05 [16]	-
k_{sl}	Slope parameter	Det.	1.0 [16]	-
$\varphi_{\text{sc,coupure}}$	Stability parameter	Det.	0.5 [16]	-
$\varphi_{\text{sc,behind}}$	Stability parameter	Det.	1.5 [16]	-
k_t^2	Turbulence parameter	Det.	2.0 [16]	-
T	Wave period	Normal	μ=20.0	σ=2.0
d_{NS}	Bottom height on North Sea side	Det.	-6.20 [84]	-
h_{str}	Height of the structure	Det.	5.80 [85]	-
h_{OS}	Water depth on the Eastern Scheldt	Normal	μ=1.0 [12]	σ=0.1

Table A.1: Variables applied in Chapter 8

B

Discharge formulae

The discharge formulae applied in the schematization of the Eastern Scheldt barrier as a broad-crested weir are described below. The schematization of the weir, with the positions of the different depths (H_0,H_1 and H_2) can be seen in Figure B.1.

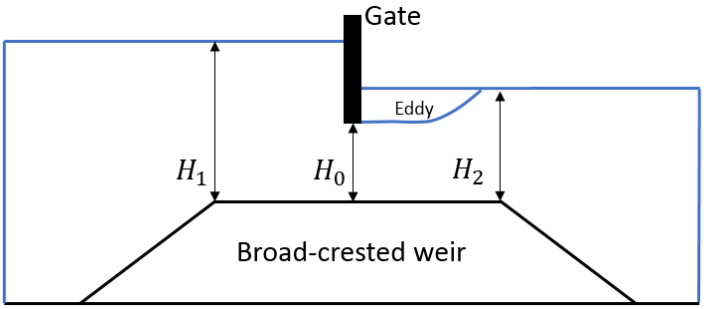

Figure B.1: Parameters influencing the type of discharge

The first 3 discharge equations, (Equation B.1, Equation B.3 and Equation B.5, describe supercritical flow. In supercritical flow, no information can travel upstream, and as such, the discharge is only determined by the upstream water level.

Underflow, supercritical flow

$$Q = \mu_0 A \sqrt{2g(H_1 - H_0)} \quad \text{and} \quad A = B H_0 \tag{B.1}$$

$$\text{for:} \quad \frac{H_1}{H_0} > 1.5 \cap \frac{H_2}{H_0} =< 1 \tag{B.2}$$

Between underflow and free surface flow, supercritical flow

$$Q = \mu_t A \sqrt{\frac{2}{3} g H_1} \quad \text{and} \quad A = B \frac{2}{3} H_1 \tag{B.3}$$

$$\text{for:} \quad 1 \leq \frac{H_1}{H_0} \leq 1.5 \cap H_2 \leq \frac{2}{3} H_1 \tag{B.4}$$

Free surface flow, supercritical flow

$$Q = \mu_v A \sqrt{\frac{2}{3} g H_1} \quad \text{and} \quad A = B \frac{2}{3} H_1 \tag{B.5}$$

$$\text{for:} \qquad \frac{H_1}{H_0} \leq 1.0 \cap H_2 \leq \frac{2}{3} H_1 \tag{B.6}$$

The last 4 discharge equations, (Equation B.7, Equation B.9, Equation B.11 and Equation B.13, describe subcritical flow. In subcritical flow, information can travel upstream, and as such, the discharge is determined by both the upstream- and the downstream water level. For the scenario of underflow, three types of underflow are considered, depending on the up- and downstream water levels. The main difference between these three types is the contraction coefficient.

Free surface flow, subcritical flow

$$Q = \mu_v A \sqrt{2g(H_1 - H_2)} \quad \text{and} \quad A = B H_2 \tag{B.7}$$

$$\text{for:} \qquad \frac{H_1}{H_0} \leq 1.0 \cap H_2 \geq \frac{2}{3} H_1 \tag{B.8}$$

Underflow, subcritical flow, type 1

$$Q = \mu_t A \sqrt{2g(H_1 - H_2)} \quad \text{and} \quad A = B H_2 \tag{B.9}$$

$$\text{for:} \qquad 1 < \frac{H_1}{H_0} \leq 1.5 \cap H_2 > \frac{2}{3} H_1 \cap \frac{H_2}{H_0} \leq 1 \tag{B.10}$$

Underflow, subcritical flow, type 2

$$Q = \mu_t A \sqrt{2g(H_1 - H_2)} \quad \text{and} \quad A = B H_0 \tag{B.11}$$

$$\text{for:} \qquad 1 < \frac{H_1}{H_0} \leq 1.5 \cap H_2 > \frac{2}{3} H_1 \cap \frac{H_2}{H_0} > 1 \tag{B.12}$$

Underflow, subcritical flow, type 3

$$Q = \mu_0 A \sqrt{2g(H_1 - H_2)} \quad \text{and} \quad A = B H_0 \tag{B.13}$$

$$\text{for:} \qquad \frac{H_1}{H_0} > 1.5 \cap \frac{H_2}{H_0} > 1 \tag{B.14}$$

Where:

H_0	[m]	The flow depth under the door
H_1	[m]	The upstream water level above the weir
H_2	[m]	The downstream water level above the weir
g	[m/s^2]	The gravitational constant
B	[m]	The width of the weir
μ_i	[-]	Different types of contraction coefficients

C

Previous safety studies

As mentioned in Chapter 1, previous safety studies were consulted to identify important failure mechanisms for the Eastern Scheldt barrier, functioning as a boundary to the report scope. The three most recent safety studies will be explained in this appendix; the assessment of the barrier during the previous assessment round (which ended in 2011), an extra safety study ordered when damage to the barrier was found, and a buckling analysis[1] looking at future threats to the barrier.

C.1. ARCADIS, 2010

In 2010, during the previous assessment round (VTV2006), the Eastern Scheldt barrier has been assessed on safety by ARCADIS [68]. This safety study focused on the civil parts of the barrier (as opposed to the electo-technical and mechanical parts, which were not assessed). The study found that the civil parts of the barrier were not negligible when assessing the barrier. Failure of the Eastern Scheldt barrier was split into processes. The top event was defined as the flooding of parts of the Zeeland province. This event was reached when two events took place. The first event was starting failure of the barrier. The second event was continued failure of the barrier. These events were separated by a so called transfer probability. This transfer probability is defined as the probability that starting failure leads to continued failure. In the study this transfer probability was assumed to be 1.0, meaning that damage in any form to the barrier would lead to failure of protecting Zeeland. Starting failure of the barrier would thus be the top event of the tree (as it would be assumed that it always leads to flooding of Zeeland). As such, the fault tree was defined as shown in Figure C.1.

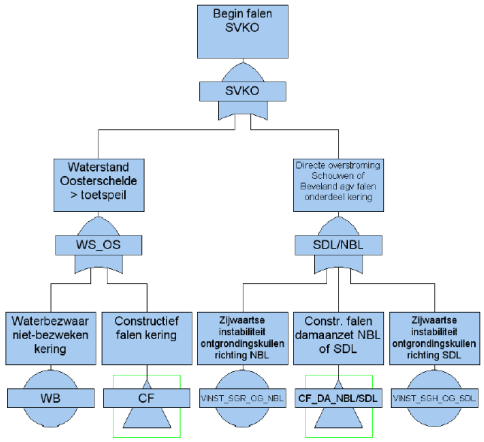

Figure C.1: Fault tree in the ARCADIS study[67]

[1] A buckling analysis increases the loading on a structure and assesses which parts of the structure would fail (buckle) first. In case of the Eastern Scheldt barrier, the study looked at sea level rise over the next century.

The study by ARCADIS was also the first to identify a new failure mode, sliding failure to the side on the sea side. Sliding failure of the slope towards the barrier was previously considered, however the sliding towards the dikes on the sides of the bottom protection was not identified as a failure mechanism previously. Nonetheless, this mechanism was only identified, but not taken into account (the probability was set to zero). It was assumed that with the current state of the scour holes in front of the barrier the mechanisms would not be relevant.

The study looked at the barrier in two states: closed and partially opened. When closed, the failure probabilities of the barrier were concluded to be negligible, both on the level of structural integrity and water storage (of the Eastern Scheldt basin). When partially opened however (such as a door failing to close when requested) instability of the bottom protection just passed the assessment. The study concluded that, although the barrier passed the assessment, the most vulnerable failure mechanism was a single door failing to close when the barrier should be closed, particularly the bottom protection behind this failing door.

Two important recommendations were done; first the behaviour of the bottom protection after the initiation of failure was to be investigated. Especially after a door failing to close, the bottom protection was deemed vulnerable and research into the transfer probability was recommended. Second, the dependency between failure mechanisms was to be investigated. This report assumed the failure mechanisms to be independent, which it admitted was a conservative approach.

C.2. Rijkswaterstaat, 2014

In 2014, a unique study into the safety of the Eastern Scheldt barrier was undertaken [13] as parties from (local) governments, research institutes and market companies worked together in an assessment of the bottom protection of the barrier. This study was started as damage to the bottom protection was found, which had compromised safety of a part of the dike along the Eastern Scheldt.

The study looked at the failure trees of the barrier and concluded that some important knowledge gaps exist, such as the difference between starting failure and continued failure.

One of these knowledge gaps involved the transfer probabilities of the bottom protection (which describe the probability of failure of the barrier given the failure of the bottom protection). The transfer probabilities that had previously been applied (both in the original design and in subsequent assessments) could not be traced back to any source. The study concluded that a more detailed model of the bottom protection and transfer probabilities was required.

C.3. Witteveen+Bos, 2016

In 2016, an integral safety study of flood safety in the next century was conduced by Witteveen+Bos [45]. In this study the entire Eastern Scheldt basin was assessed, which included the Eastern Scheldt barrier. Goal of the study was to identify vulnerable areas of the system, with rising sea levels in mind.

The most important buckling point of the barrier under rising sea level was the Roompotsluis, due to the low retaining height of the lock and the coupure in which it is situated. Additionally, due to the increased load on the dikes behind the barrier, the closure regime of the barrier (currently at 3.00m+NAP) might have to be revised. It was predicted that a 1.25m rise in sea level would require the barrier to close 100 times per year (as opposed to the current 1 time per year). The study could not accurately assess the bottom protection under the condition where a door failed to close, as it concluded that more research, into the bottom protection and the effects of failure of the bottom protection, was needed (especially when a quantitative assessment was required). Due to the conservative nature of previous assessment rounds (the ARCADIS study[68]) where starting failure of the bottom protection would lead to failure of the barrier, the bottom protection was deemed not an especially vulnerable area. It was however advised that more studies into the bottom protection were done, and that a probabilistic analysis was needed to accurately assess the safety (transfer probabilities were mentioned as one of the areas where more research was needed.

The study concluded that the Roompotsluis, due to a low retaining height, was the most vulnerable part of the barrier within the next 50 years. As such the study identified the bottom protection as the largest uncertainty and the lock as the largest buckling point.

D

Rock classes distributions

The different rock classes applied in the bottom protection behind the Eastern Scheldt barrier can be found described in Schiereck, 2016 [61]. The distributions applied to describe these different rock classes can be found in this appendix.

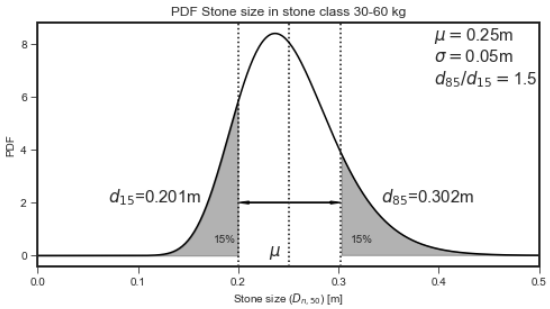

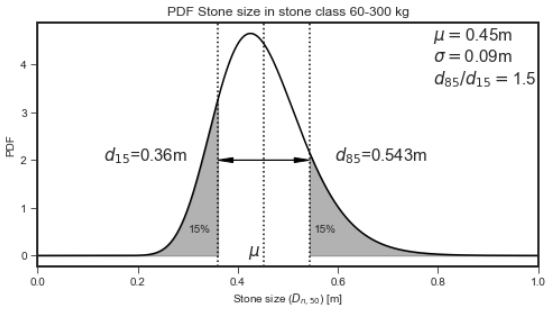

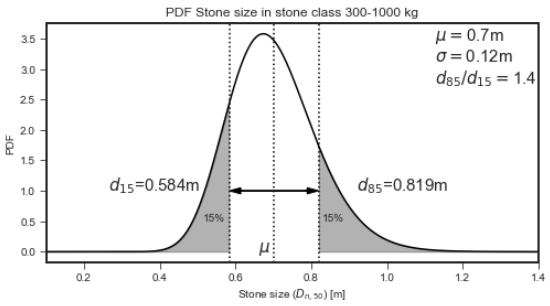

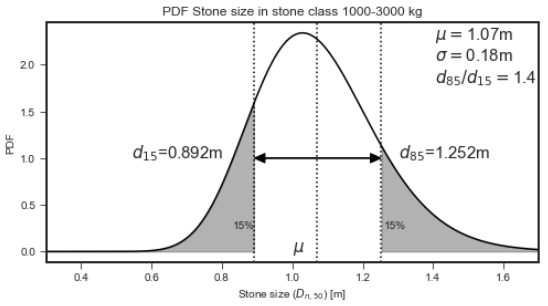

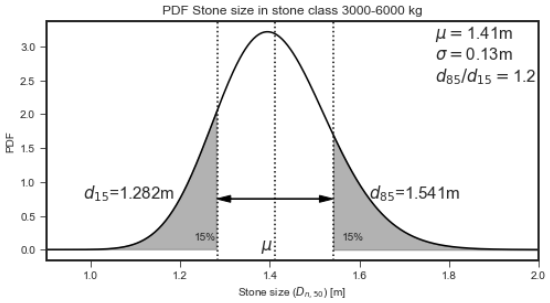

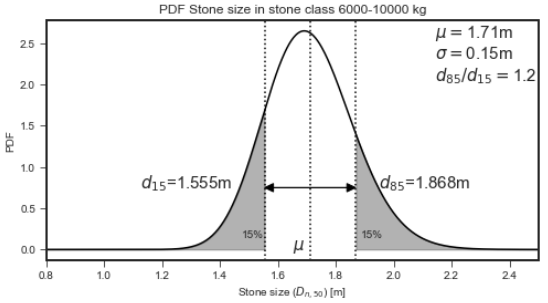

E

Hydraulic conditions

To assess the fragility curves a distribution for the hydraulic conditions is required. These hydraulic conditions are determined using the IMPLIC data base from the Hydro-MeteoCentrum Zeeland, Rijkswaterstaat [60][63]. This data base can be used to constructe the parameters that describe the hydraulic conditions in a probabilistic manner. The data is extracted with the PresPeil2017 model. Both models will be discussed in this chapter.

E.1. IMPLIC

The IMPLIC model is a 1d flow model that has been applied to calculate the hydraulic conditions on the Eastern Scheldt since the Eastern Scheldt barrier opened [63]. The Eastern Scheldt is modelled as a network of 1d flow channels connected by nodes. For each channel the flow carrying cross-section, the storage width and the hydraulic radius for various height levels have been defined. The schematization of the Eastern Scheldt can be seen in Figure E.1. IMPLIC discretizes in space and time to solve to differential equation: conservation of mass (Equation E.1) and conservation of impuls (Equation E.2).

$$\frac{\delta Q}{\delta x} + B\frac{\delta H}{\delta t} = 0 \tag{E.1}$$

$$\frac{\delta H}{\delta x} + \frac{1}{gA}\frac{\delta Q}{\delta t} + \frac{2Q}{gA^2}\frac{\delta Q}{\delta x} - \frac{Q^2}{gA^3}\frac{\delta A}{\delta x} + \frac{Q|Q|}{C^2A^2R} + \frac{H_w\delta\rho}{2\rho\delta x} - \frac{\gamma W^2\cos(\Theta-\phi)}{gH_w} = 0 \tag{E.2}$$

The schematization of the Eastern Scheldt in IMPLIC can be seen in Figure E.1.

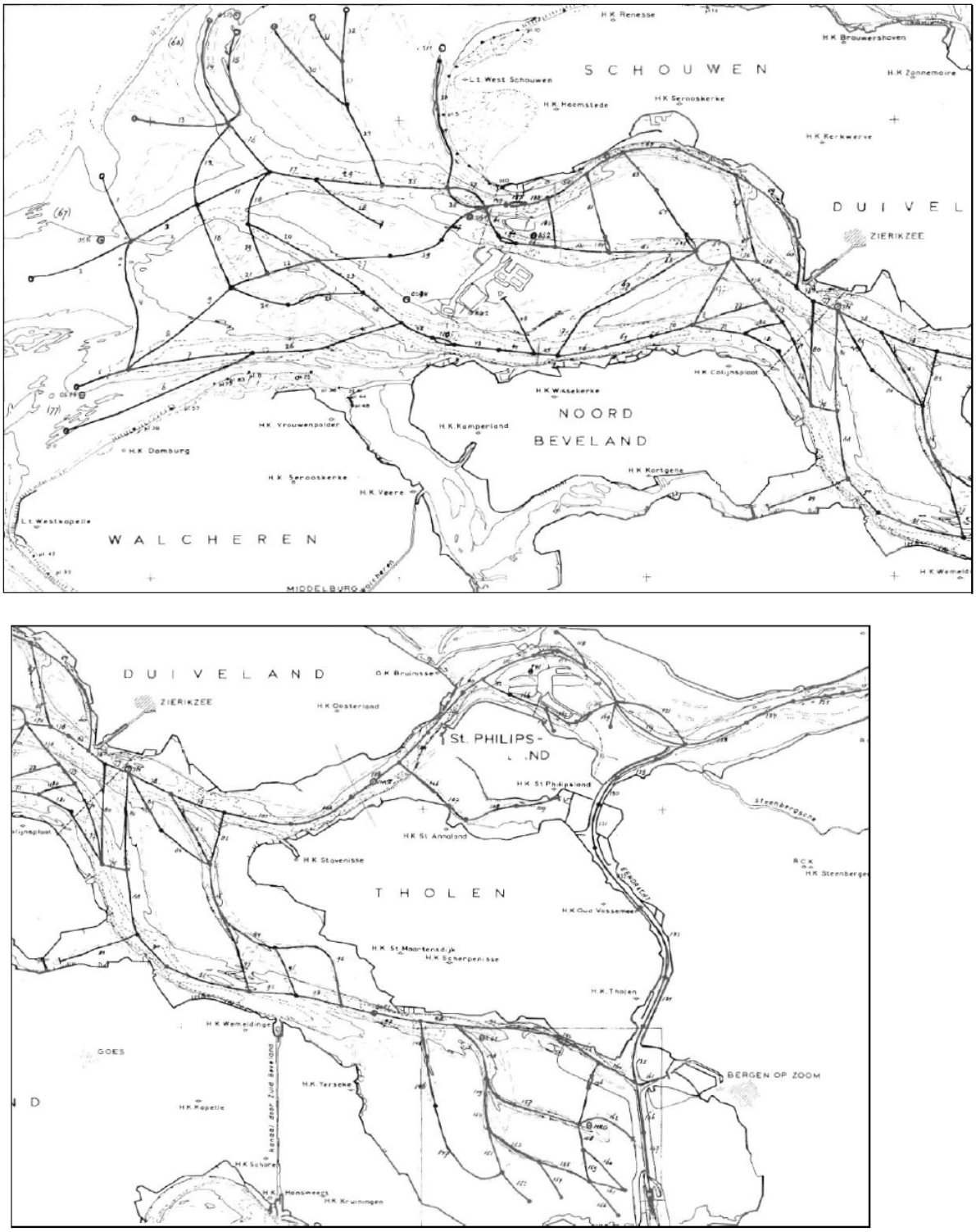

Figure E.1: Schematisation IMPLIC Eastern Scheldt[63]

E.1.1. Scenarios

The IMPLIC model has been used to calculate the conditions on the Eastern Scheldt for a large number of scenarios. Each scenario is determined by a number of input variables. Each input variable is discretized into bins, and each possible combination of input has been computed in IMPLIC.

Water level on the North Sea side of the barrier
The water levels on the North Sea side of the barrier have been categorized into 51 bins, from 1.50m+NAP to 6.50m+NAP with step size 0.1m.

Wind speed
The wind speed has been categorized into 21 bins, from 10 m/s to 50 m/s with step size 2 m/s. This wind speed is assumed to be uniform over the Eastern Scheldt basin.

Wind direction
The wind direction has been categorized into 12 bins, from 30° to 360° with step size 30°.

Storm duration
The storm duration is categorized into 5 bins, from 20 hours to 100 hours.

Phase difference
The phase difference between the peak of the high water tide and the peak of the storm set up is categorized into 7 bins. These bins are chosen in such a way that the peaks can occur on the same time (phase = 0) or that the peak of the storm can occur on the low water tide (phase = -/+320), with several options in between.

Water level OS11	Maximum wind speed	Wind direction	Storm duration	Phase
1.50 m+NAP	10 m/s	30°	20 hours	-320 minutes
1.60 m+NAP	12 m/s	60°	40 hours	-210 ""
...	...	...	...	-100 ""
...	...	...	...	0 ""
...	...	...	...	+100 ""
...	...	...	...	+210 ""
6.50 m+NAP	50 m/s	360°	100 hours	+320""

Table E.1: Bins for all variables

Closure strategies
When the Eastern Scheldt barrier is closed (manned or unmanned), failure to close can occur (partially). There are 9 different closure scenarios, for both the manned and unmanned situations. The different probabilities between manned and unmanned closure are mainly due to repair options in the manned scenarios [60]. The various closing scenarios can be seen in Table E.2

Scenario	Manned	Unmanned
0 (No doors fail)	9.86E-01	9.40E-01
1 (1 door fails)	1.18E-02	5.41E-02
2 (2 doors fail)	3.81E-04	1.83E-03
5 (3, 4 or 5 doors fail)	1.88E-04	2.00E-03
10 (6-10 doors fail)	5.88E-04	9.72E-04
16 (25% of doors fail)	3.77E-04	6.07E-04
31 (50% of doors fail)	1.70E-04	2.31E-04
47 (75% of doors fail)	7.12E-08	9.47E-08
62 (All doors fail)	2.05E-05	7.53E-04

Table E.2: Failure to close on request [12]

The total amount of scenarios run through IMPLIC is over 8 million (51 water levels * 21 wind speeds * 12 wind directions * 5 storm durations * 7 phase shifts * 18 closure scenarios = 8096760 scenarios). For all these scenarios the hydraulic conditions for all output locations along the Eastern Scheldt and the Eastern Scheldt barrier are calculated.

E.2. PresPeil2017

The database of scenarios computed with IMPLIC is loaded into PresPeil2017. With this model, which is run in MATLAB, probabilistic calculations can be done on the data from IMPLIC, to compute exceedance graphs for various stochastic variables at the Eastern Scheldt barrier. A screen shot of the PresPeil2017 model can be seen in Figure E.2, in which the different variables which PresPeil2017 can compute can be seen.

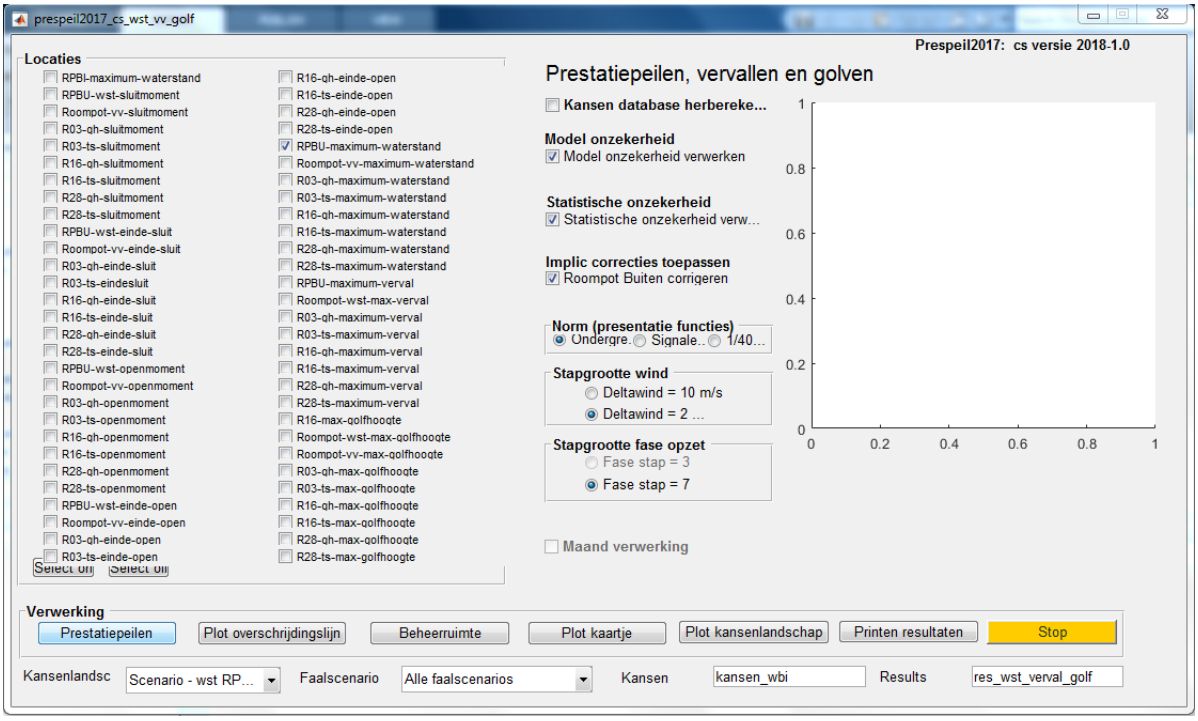

Figure E.2: Overview of the different possible parameters which can be computed

Prespeil2017 is applied in this report to compute the exceedance graphs of the water level as well as the wave heights at the Eastern Scheldt barrier. These exceedance graphs are then translated into probability density functions.

F

History on the usage of fragility curves for flood risk assessment in literature

Fragility curves have been applied to estimate or calculate the risk within various disciplines. In Schultz, 2010 [64], an overview has been established of papers in literature on estimating fragility curves. An overview of the literature will be presented in this chapter.

Schult, 2010 [64] has identified and catalogued examples of the usage of fragility curves in literature. Most literature in the field of fragility curves has been within the field of seismology. They also concluded that research into fragility curves has been on the rise, although this is from a 2010 perspective. In Figure F.1 and Figure F.2, an overview of the amount of literature into fragility curves over time, as well as an overview of the respective fields of that literature can be found [64]. An explanation of the rising in the number of examples could lie in the fact that the computational power required for developing accurate fragility curves has become more available over the past decades.

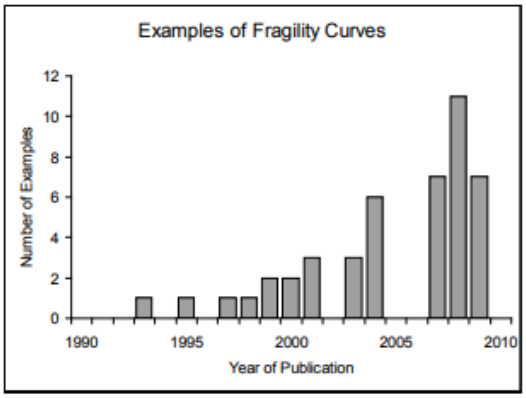

Figure F.1: Examples of fragility curves in literature over time until 2010 [64]

Method	Number
Judgmental	2
Empirical	5
Analytical	35
Hybrid	3
Total	**45**

Hazard Domain	Number
Flood	12
Seismic	30
Fire	1
Wind	2
Total	**45**

Structure Type	Number
Bridges	14
Buildings	15
Flood protection	12
Electrical	2
Other	2
Total	**45**

Figure F.2: Examples of fragility curves in literature by discipline until 2010 [64]

A small summary/timeline of several papers on fragility curves has been included below. Only papers that deal with fragility curves within the field of flood risk have been included here.

In 1995, Patev et al. attempted to assess the reliability of a reinforced concrete drainage structure. In this paper the authors estimated the reliability for several flood events, with different return periods. This was done by first building a deterministic model of the structure and then giving all the variables a distribution. Then a First-Order Second Moment method was applied, which was calculated with a Taylor Series Finite Difference method. This is a reliability method that uses a log-normal formulation for the reliability index. They also applied an Advanced Second Moment method. This technique can be use to find the minimum distance (reliability index) to a failure surface in a multivariable space. Finally a Monte Carlo simulation was run to compare both the FOSM methods. By comparing first order approximations with Monte Carlo simulations, the authors were able to demonstrate that first-order approximations were an accurate way to determine reliability. A full fragility curve was not developed however [46].

In 2002, Ellingwood and Tekie attempted to develop the fragility of concrete gravity dams to assess their performance against hydraulic and seismic hazards. It mainly focused on the performance to a dam under seismic loading. Interestingly, this appears to be the first usage of fully developed fragility curves in flood risk. In the study, they found that the modelling of hydraulic fragility is less computationally demanding than the modelling fragility of seismic activity. They were thus able to simulate 1000 Monte Carlo simulations (although they concluded that 100 would have been enough). It was found that the failure probability computed for the considered dam with fragility curves was much lower than the failure probabilities found in other literature [72].

In 2003, Hall et al. attempted to established fragility curves for different types of hydraulic failure mechanisms, specifically overtopping and breaching by overtopping. As analytical relations for overtopping were not yet fully established at the time, they used empirical data as well as expert judgement to draw the curves. The authors looked on a national scale and found that this involved the development of a large amount of fragility curve for a large amount of different hydraulic structures (61), when also considering different conditions). The paper concluded that fragility curves could offer a significant advance on the assessment of flood risk by being fully probabilistic and process-based [27]. In 2008, Gouldby et al. expanded on this work by looking on a regional scale. Similarly, the authors found that a large amount of fragility curves is required and, using a FORM approach, 600 generic fragility curves where developed. Again, different gradations of deterioration of structures lead to a large amount of fragility curves. The authors concluded that the regional model was already a more efficient and robust than the national model. A site/structure specific model could lead to even more significant improvements still [26].

In 2004, Apel et al. developed fragility curve for levees and incorporated these curves into a flood risk model along the Rhine river downstream of Cologne. They extended the fragility curves by introducing the usage of two loading variables, overtopping height and overtopping time. This way the fragility curves were extended into fragility surfaces. They intentionally kept the model relatively simple to be able to apply Monte Carlo simulations as the extension from curves to surfaces bought an increase in the number of computation points. To assess the flood risk of the river, which stretched from Cologne to Rees, a model chain was set up. This model can be seen in Figure F.3. The model first considered a random discharge along the river. From this discharge a flood wave was constructed, which was used to test the levees at several points. Several tributaries fed discharge to the river along the way, which were (statistically) dependent on the discharge in the river. In the end, this Monte Carlo simulation was used to transform the input discharge upstream to a distribution function of the damage downstream. The paper concluded that this type of approach is well suited to integrated flood risk assessment [3].

In 2008, Ebeling et al. considered uncertainty in strength, uplift parameters, silt-induced earth pressure and post-tensioned anchor forces when developing the fragility curves (the USACE uses the phase System Response Curve) for a concrete dam. First the authors set up equations of equilibrium (vertical, horizontal, moment) from a free body diagram. These equations could then be used to compute safety factors. To reduce computation time, Latin Hypercube sampling was applied, instead of a Monte Carlo simulation. Extra effect had to be put into the correct correlations in the multivariate case. Specialized software was used to set the correlations. With this sampling method system response curve was developed for sliding and overturning of the dam. The system response curve was then numerically differentiated to generate the probability density function (PDF) for sliding. In this PDF the probability of failure was plotted against a load. By splitting the PDF into sections, the authors then build an event tree from the PDF. The PDF and event tree build

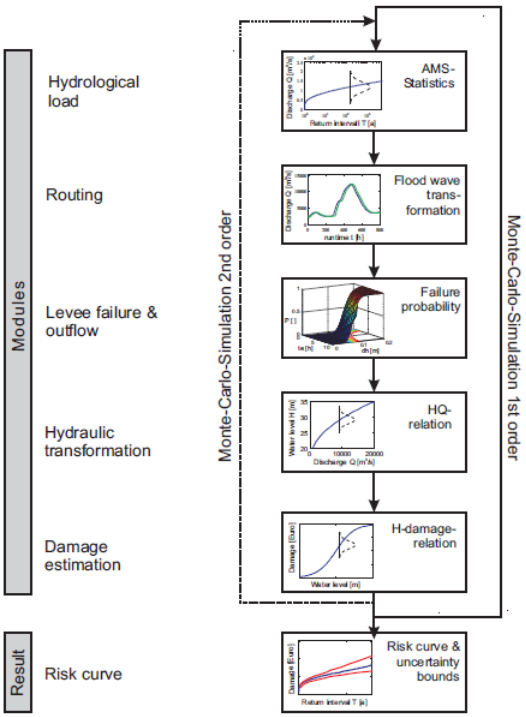

Figure F.3: Model used by Apel et al.[3]

from it can be seen in Figure F.4. The paper concluded on recommendations, which included the expansion of additional failure mechanisms into the limit states [21].

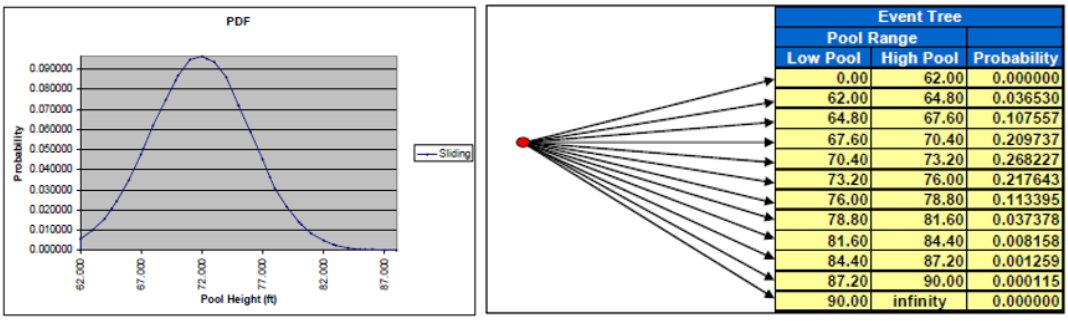

Event Tree		
Pool Range		
Low Pool	High Pool	Probability
0.00	62.00	0.000000
62.00	64.80	0.036530
64.80	67.60	0.107557
67.60	70.40	0.209737
70.40	73.20	0.268227
73.20	76.00	0.217643
76.00	78.80	0.113395
78.80	81.60	0.037378
81.60	84.40	0.008158
84.40	87.20	0.001259
87.20	90.00	0.000115
90.00	infinity	0.000000

Figure F.4: Model used by Ebeling et al.[21]

In 2009, the IPET (Interagency Performance Evaluation Task Force) used fragility curves to define the performance of stretches of- and structures within the New Orleans flood defences after hurricane Katrina. To incorporate different failure mechanisms in the curves, a hybrid approach was used. To construct fragility curves for nonovertopping water elevations, a first-order approximation was applied and to construct fragility curves for overtopping water elevations, empirical data was used. This empirical data was gathered using post-Katrina field data. An image of this hybrid curve can be seen in Figure F.5. The two combined fragility curves can be distinguished with an overlap around the top of the levee/wall (where overtopping starts). At lower water elevations the fragility curve represents the strength of the structure to resist the forces created by the water. As overtopping starts to occur, the possibility of erosion on the back side of the structure increases, as does the failure probability [31].

In 2009, Kinston et al. used an artificial neural network to fit a response surface. With this response surface method, a limit state function is approximated in a relatively small number of points, for example in the form of a polynomial [64]. The authors used an artificial neural network to fit a limit state function in situations where a limit state function in the form of an equation is not available, such as finite element models

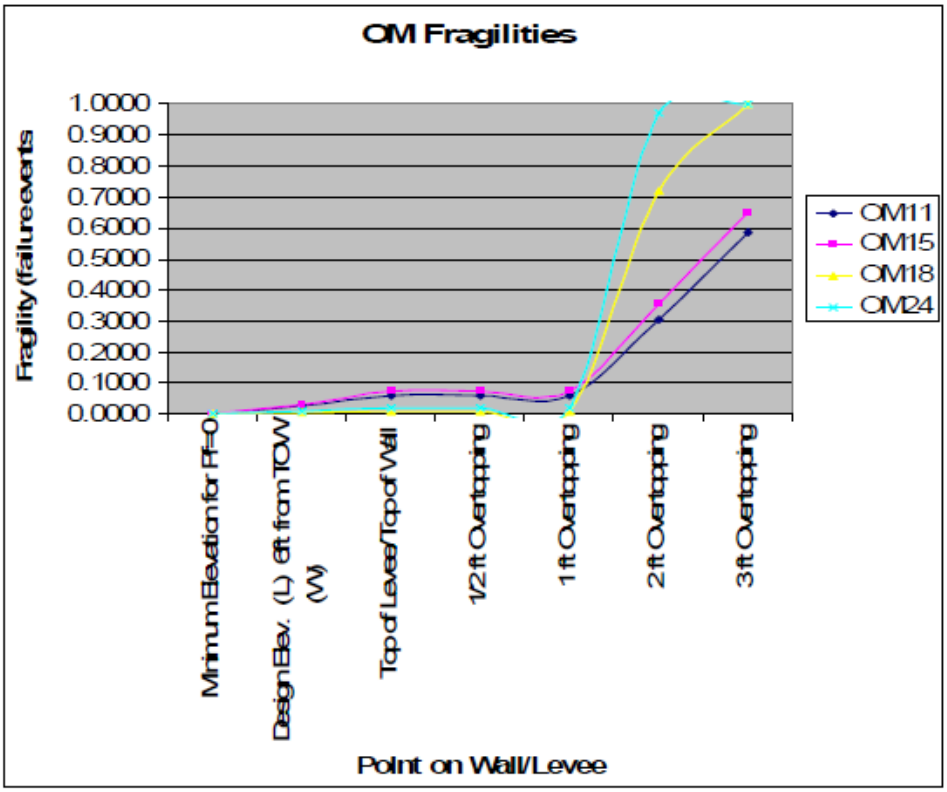

Figure F.5: Hybrid fragility curves set up by IPET[31]

in geotechnical failures for example. These failure mechanisms can only be evaluated implicitly, meaning analytic approaches such as FORM are impossible. Numerical approaches such as Monte Carlo are not practical as applying it to a finite element model would increase the computational time significantly [39]. These response surfaces can then be used to reduce the computational effort, but it should be remembered that they also introduce an added layer of approximation [64]. In the model used by the authors. an artificial neural network (ANN) was set up to emulate the complex finite element model within a Monte Carlo simulation. With this ANN they were able to build a so called response surface function. This is done with a so called genetic algorithm. This algorithm is used to train the ANN, and build an approximation of the limit state function. A case study was included in which a flood wall in New Orleans was modelled. The authors ended on the conclusion that the usage of the ANN was less computational efficient when compared to other response surface methods which rely on a quadratic representation of the limit state function. The ANN does rely on less crude assumptions and may thus offer additional robustness [39].

In 2009, Simm et al. applied hybrid fragility curves when assessing the flood defences along the Thames river, UK. Comparable to [27] and [26] a dataset of fragility curves for several structures in several states of degradation where developed (15 in this case). These fragility curves were site-specific so more accurate than the general curves developed before. All curves were still based on standardized defence heights however (1.5m in this case). The authors conclude that with the right knowledge, full site-specific fragility curves can be achieved, by combining key failure modes. This includes failure modes with a well-defined limit state function, as well as failure modes where more complex methods are required, such as finite element methods. Fragility curves also allow for an increased understanding of the effects of intervention works on asset reliability. A final recommendation includes the usage of local and historical knowledge to reduce uncertainty in the fragility curve [65].

In 2009, Vorogushyn et al. developed fragility curves for earthen fluvial dikes, considering two failure mechanisms: piping and slope stability failure caused by seepage. These two mechanisms were defined with physics-based relations and both dependent on duration of loading conditions. Fragility curves normally do not account for this duration of load. The authors took into account the gradual load change in the determination of the fragility curves developed [86].

In 2008, Van Der Meer, developed fragility curves by setting up the Z-functions for overtopping and piping. In this case-study, both a fragility curve for a high sea dike and a lake dike were developed. It concluded on the remark that fragility curves are a helpful tool in assessing reliability of dike sections, both for high river discharges as well as overtopping at sea dikes [77]. In 2009 another paper by Van Der Meer et al. reiterated this point by again developing fragility curves for overtopping and piping. This time a new approach was used, where the failure probabilities were directly plotted against return periods (as opposed to a load and a separate probability density function of that load [76].

In 2008, Bachmann et al. developed a fragility curve by running a Monte Carlo simulation. This paper describes how fragility curves can be set up by using Z-functions and Level III and Level II methods to calculate the curve. It also included a list of methods to reduce the computational effect required for a Monte Carlo approach. 'Automatic run-length control' can automatically stop the Monte Carlo run when the failure probability has converged to within a defined limit. 'Dynamic step size adaption' can reduce the number of calculations done around the straight parts of the curve. This is done by calculating the gradient of the curve and increasing or decreasing the step size when below or above a set value. Finally, 'dynamic fault tree adaption' can be used to 'shut off' certain branches of a fault tree when they do not contribute to a total failure probability [7].

In 2015, Wojchiechowska et al. looked at the applicability of fragility curves in flood risk assessment. In the paper the authors derived fragility curves for dikes for the failure mechanisms overtopping, piping and macro-stability and combinations of them. This was done by manually altering input files in the program PC-Ring, as this program is unable to draw the curves itself. PC-ring code was altered to facilitate the calculation of fragility curves for complicated water systems, such as the sea. The paper showed that fragility curves can have added value when it comes to reliability assessments within flood risk. Recommendations included the development of visual tools to aid in the understanding of the fragility curves [89].

In 2016, Schoemaker, applied fragility curves for the mechanisms overtopping and macrostability in a master thesis that looked into the effects of risk reducing strategies. These fragility curves were constructed in very simple manners. For macrostability, the curves were based on a proven strenght analysis, combined with the safety factors from assessment reports. This can be seen in Figure F.6.

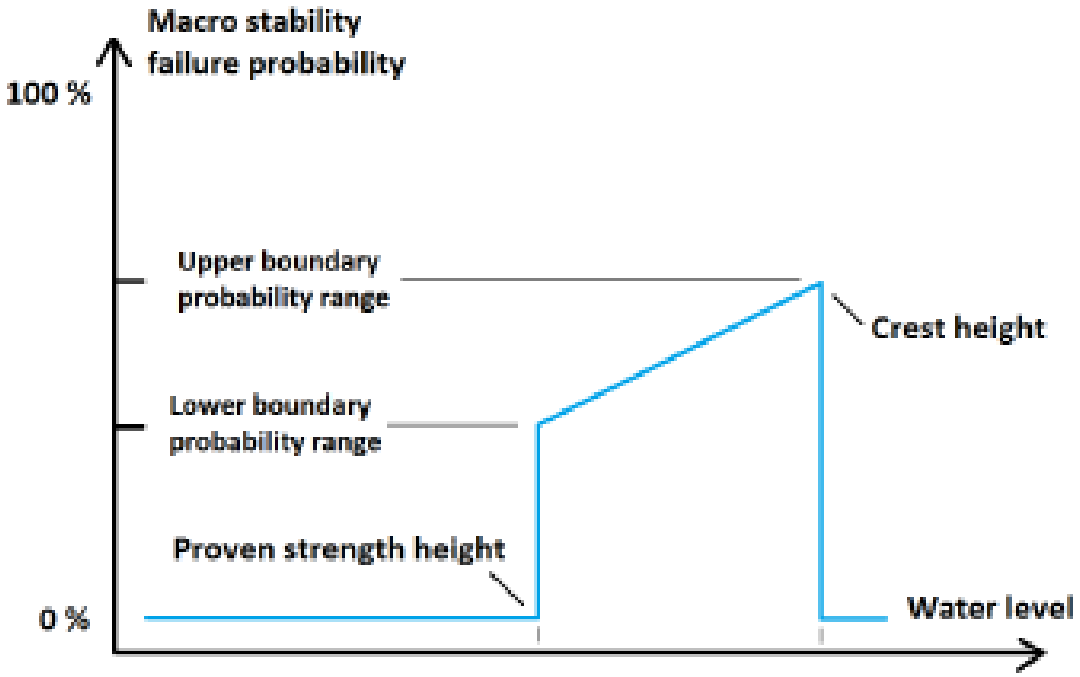

Figure F.6: Set-up of fragility curves for macrostability by [62]

The author cut off the fragility curve at crest height, as it was argued that overtopping/overflow would become dominant. The paper shows how fragility curves can be constructed in a very simple and flexible manner [62].

In 2016, Bischiniotis et al. developed a cost-optimization method for river dikes that applied fragility curves in the assessment of cross-sections of dikes. When comparing a fully probabilistic fragility curve based method to a semi-probabilistic safety standard based method, the authors found a cost reduction of 15% for the fragility curve method. This was attributed to the increased flexibility the fragility curves offered. This allowed the authors to find a more optimal dike geometry [11].

F.1. Conclusion

As has been shown in the paragraphs above, although fragility curve usage in flood risk is not unheard of, there are only limited examples of it available. Additionally, these fragility curves were often generalized curves, applicable to various structures for example the large number of curves used by Hall, 2003 [27] and Gouldby, 2008 [26].

These generalized structures have not been combined into single section flood risk assessments. They have been combined into risk assessments for stretches of dike, however the combination of various curves, with for example varying states of dependency with each other, for flood risk assessment of a single complex structure cannot be found in literature.

The application of fragility curve on single failure mechanisms has been shown in many papers, most notable Wojchiechowska, 2015 [89] and Van Der Meer, 2008 [77] and 2009 [76].

The complexity in the approach of constructing fragility curves varies a lot. Very complex method, such as artificial neural networks have been applied, such as Kingston, 2009 [39]. Much more simple methods have also been shown to be applicable as well however, like Schoemaker, 2016 [62].

G

Sensitivity analysis

To assess the behaviour of the reducing due to application of the conditional transfer probabilities, a sensitivity analysis has been performed. Three different parameters have been considered in this analysis; the critical shear parameter, the maximum gradient between the scour depth and the barrier and the turbulence. These three parameters (which were all rough estimates in this assessment) influence different parts of the assessment. The critical shear stress influences the conditional failure probability of the bottom protection, while not influencing the conditional transfer probabilities. The maximum allowed gradient influences the conditional transfer probability per location while not influencing the conditional failure probability of the bottom protection. The turbulence influences both; the conditional failure probability of the bottom protection is influenced through the turbulence factor while the scour depth (and thus the conditional transfer probability) is influenced through the alpha-factor. As such, these three parameters should give insight into not only the effects they have themselves, but also the effects of the conditional failure probability of the bottom protection and the conditional transfer probability.

For all three sensitivity analyses, two interesting values will be researched. Firstly, the sensitivity of the failure probability of the Eastern Scheldt barrier to changing a variable. As such, this part of the sensitivity analysis assesses the Eastern Scheldt barrier. Secondly however, the sensitivity of the influence of the conditional failure probabilities is considered interesting. It can offer insight into whether a conditional approach towards transfer probabilities offers an advantages and whether this advantages is sensitive to the variables applied. As such, this part of the sensitivity analysis assesses the assessment of the Eastern Scheldt barrier.

G.1. Varying the conditional failure probability of the bottom protection

The failure of the bottom protection is defined with the critical shear stress parameter. Due to the rarity of a gate failing to close, a high value for the parameter was selected, which was dependent on the amount of stones that are allowed to be removed from the bottom protection during the time that the protection is loaded. If the parameter is changed, for example through changing the amount of stones that are allowed to be removed before the protection is considered to have failed, the conditional failure probability of the bottom protection can be controlled. This allows for assessing the influence of the conditional failure probability of the bottom protection on the final failure probability of the barrier as well as on the effects of applying conditional transfer probability.

The effects of altering the critical shear parameter[1] can be seen in Table G.1. Decreasing the amount of transport that is allowed out of the bottom protection before failure is assumed, increases the failure probabilities, both when applying the conditional transfer probabilities as well as when not applying the conditional transfer probabilities. This is seen in both the optimistic and the conservative flow scenarios. The reduction due to

[1] It should be noted that increasing the amount of stones allowed to be removed increases the resulting shear stress parameter applied to above 0.1 for some stones sizes. Equation 9.2 is only applicable for values of Ψ_{cr}<0.1, so the resulting transport is not physically correct anymore. Nonetheless, the analysis can still give insight into the relative influence of this parameter on the conditional transfer probabilities.

the application of the transfer probabilities also slightly increases, even though the critical shear parameter does not influence the transfer probabilities per location. This can be explained due to the fact that relative weight given to the conditional transfer probabilities per location is influenced by the conditional failure probabilities. If the transfer probabilities per location remain constant, while the conditional failure probabilities of the bottom protection change, the influence of the application of conditional transfer probabilities on the final integrated failure probability can still change. Nonetheless, although the failure probability of the barrier varies quite a lot with the critical shear parameter, the influence of the conditional transfer probabilities appears relatively constant.

	Optimistic	Conservative
N_{faal} = 8 stones per running meter		
With transfer probabilities	8.75E-12	1.57E-4
Without transfer probabilities	1.36E-11	1.63E-4
Reduction	35.4%	3.49%
N_{faal} = 5 stones per running meter (default)		
With transfer probabilities	2.78E-11	2.45E-4
Without transfer probabilities	4.50E-11	2.54E-4
Reduction	38.4%	3.74%
N_{faal} = 2 stones per running meter		
With transfer probabilities	2.27E-10	5.06E-4
Without transfer probabilities	3.98E-10	5.27E-4
Reduction	42.9%	3.9%

Table G.1: Failure probabilities and influence of conditional transfer probability under varying failure definitions of the bottom protection

G.2. Varying the conditional transfer probabilities

The conditional transfer probabilities are defined with the maximum allowed gradient between the bottom of a scour hole and the barrier. This maximum allowed gradient thus only influences the conditional transfer probabilities, not the conditional failure probabilities of the bottom protection. As a result, the values in the rows 'without transfer probabilities' are constant and equal to the default scenario. The effects of varying the conditional transfer probabilities can be seen in Table G.2.

	Optimistic	Conservative
$N_{s,max}$=1:3		
With transfer probabilities	1.02E-12	1.37E-4
Without transfer probabilities	4.50E-11	2.54E-4
Reduction	97.7%	46.3%
$N_{s,max}$=1:6 (default)		
With transfer probabilities	2.78E-11	2.45E-4
Without transfer probabilities	4.50E-11	2.54E-4
Reduction	38.4%	3.74%
$N_{s,max}$=1:12		
With transfer probabilities	4.22E-11	2.54E-4
Without transfer probabilities	4.50E-11	2.54E-4
Reduction	6.67%	0.3%

Table G.2: Failure probabilities and influence of conditional transfer probability under varying maximum scour depths

The effect of varying the conditional transfer probabilities can be seen in Table G.2. It can be seen that decreasing the maximum allowed gradient decreases the influence of the conditional transfer probability and increases the failure probability. As the maximum allowed gradient is increased, the influence of the transfer probabilities grows rapidly, as the maximum allowed conditional scour depth grows rapidly as well. As a result, the failure probability decreases (remember that a large influence of the conditional transfer probabilities means a low failure probability, as not taking the conditional transfer probabilities into account means

$P_{transfer}$)=1.0). The influence of the conditional transfer probabilities is tied to the maximum allowed gradient in a much stronger way, when compared to the critical shear stress. The failure probability is tied to the maximum allowed gradient much less strong however.

G.3. Varying both the conditional failure probability of the bottom protection and the conditional transfer probability

Unlike the shear stress parameter and the maximum allowed gradient between the scour hole and the barrier, both of which only alter either the conditional failure probability of the bottom protection or the conditional transfer probability, the turbulence influences both. Increasing the amount of turbulence will both increase the probability that a stone is moved from the bottom protection as well as the probability that a scour hole grows large enough to endanger the barrier. The turbulence decreases with distance from the barrier, with the water depth determining how fast. The amount of turbulence will be changed by changing the value of k_t near the barrier.

	Optimistic	Conservative
$k_{t,barrier}$=3.0		
With transfer probabilities	7.79E-7	1.88E-3
Without transfer probabilities	8.97E-7	1.89E-3
Reduction	13.2%	0.9%
$k_{t,barrier}$=2.0 (default)		
With transfer probabilities	2.78E-11	2.45E-4
Without transfer probabilities	4.50E-11	2.54E-4
Reduction	38.4%	3.74%
$k_{t,barrier}$=1.0		
With transfer probabilities	2.19E-13	2.91E-6
Without transfer probabilities	1.09E-12	3.65E-6
Reduction	79.9%	20.2%

Table G.3: Failure probabilities and influence of conditional transfer probability under varying turbulence

It can be seen that an increase in turbulence leads to an increase in failure probabilities, but a decrease in the influence of the conditional transfer probabilities. As the turbulence near the barrier is lowered, the conditional failure probabilities near the barrier decrease. At these location near the barrier, the conditional transfer probabilities do not influence the barrier, as they approach a value of 1.0. They approach a value of 1.0 as the maximum allowed scour depth at these locations is low, such that failure of the bottom protection implies failure of the barrier. As the turbulence is lowered the influence of locations further away from the barrier in increased. At these locations the maximum allowed scour depth is large, such that failure of the bottom protection never implies failure of the barrier. This leads to the situation that is seen in Table G.3, where an increase in turbulence increases the failure probability of the barrier through an increase in conditional failure probability of the bottom protection as well as through an increase in the transfer probability (seen through the decrease in reduction).

Bibliography

[1] Agema, J. (1982). 30 years of development of the design criteria for flood protection and water-control works. *Proceedings of the Delta Barrier Symposium, Rotterdam, 13-15 October 1982, pp. 6-14.*

[2] Allsop, N., Pullen, T., Van der Meer, J., Bruce, T., Schuttrumpf, H., and Kortenhaus, A. (2008). *Improvements in wave overtopping analysis: the EurOtop overtopping manual and calculation tool.* COPEDEC VII, Dubai, United Arab Emirates.

[3] Apel, H., Thieken, A., Merz, B., and Blöschl, G. (2004). Flood risk assessment and associated uncertainty. *Natural Hazards and Earth System Sciences*, 4(2):295–308.

[4] Au, S. (2005). Reliability-based design sensitivity by efficient simulation. *Computers & Structures*, 83(14):1048–1061.

[5] Au, S. and Beck, J. (2001). Estimation of small failure probabilities in high dimensions by subset simulation. *Probabilistic Engineering Mechanics*, 16(4):263–277.

[6] Au, S., Ching, J., and Beck, J. (2006). Application of subset simulation methods to reliability benchmark problems. *Structural Safety*, 29(3):183–193.

[7] Bachmann, D., Huber, N., and Schüttrumpf, H. (2008). Fragility curve calculation for technical flood protection measures by the monte carlo analysis. *Flood risk management: research and practice; proceedings of the European Conference on Flood Risk Management Research into Practice (FLOODRISK 2008), Oxford, UK, 30 September - 2 October 2008, pp. 120-120.*

[8] Battjes, J. (2002). *Vloeistofmechanica, Lecture notes CT2100.* Delft University of Technology, Delft, The Netherlands.

[9] Baudin, M., Dutfoy, A., Iooss, B., and Popelin, A. (2015). Openturns: An industrial software for uncertainty quantification in simulation. *Handbook of Uncertainty Quantification, pp. 2001-2038.*

[10] Bezuyen, K., Stive, M., Vaes, G., Vrijling, J., and Zitman, T. (2007). *Inleiding waterbouwkunde, Lecture notes CT2320.* Delft University of Technology, Delft, The Netherlands.

[11] Bischiniotis, K., Kanning, W., Jonkman, S., and Kok, M. (2016). Cost-optimal design of river dikes using probabilistic methods. *Journal of flood risk management*, 11(2):1002–1014.

[12] Bouw, R., Van Der Meer, A., De Niet, A., and Versluis, M. (2017). *Verkenning beoordeling Oosterscheldekering.* Witteveen+Bos Raadgevende ingenieurs B.V. |Deventer, Rotterdam, The Netherlands.

[13] Bouw, R. et al. (2014). *Herbeschouwing bodembescherming en herijking faalkans Oosterscheldekering.* Rijkswaterstaat Water, Verkeer en Leefomgeving.

[14] Cator, E. (2006). *Kansrekening en statistiek, Lecture notes WI2605.* Delft University of Technology, Delft, The Netherlands.

[15] Chrisman, L. (2014). *Latin Hypercube vs. Monte Carlo Sampling.* `http://www.lumina.com/blog/latin-hypercube-vs.-monte-carlo-sampling` (accessed July 21st, 2018).

[16] CIRIA, CUR, and CETMEF (2012). *The Rock Manual. The use of rock in hydraulic engineering (2nd edition).* C683, CIRIA.

[17] De Boer, G. (1998). *Transport van stenen van een granulaire bodemverdediging.* TU Delft master student thesis, Delft.

[18] De Lange, S. (1989). *Inleiding Kansrekenening en Statistiek.* VSSD, Delft, The Netherlands.

[19] Den Bieman, J. and Groeneweg, J. (2017). *Hydraulische Belastingen Oosterschelde - Wettelijk Beoordelingsinstrumentarium 2017*. Deltares, Delft, The Netherlands.

[20] Diermanse, F. (2016). *WBI - Onzekerheden, Overzicht van belasting- en sterkteonzekerheden in het wettelijk beoordelingsinstrumentarium*. Deltares, Delft, The Netherlands.

[21] Ebeling, R., Fong, M., and Arredondo, E. (2008). *Fragility Analysis of a concrete Gravity Dam and Its System Response Curve computed by the Analytical Program GDLAD_Sloping_Base*. U.S. Army Corps of Engineers, Pittsburgh, USA.

[22] Fenton, J. and McKee, W. (1990). On calculating the lengths of water waves. *Coastal Engineering*, 14(6):499–513.

[23] Fiolet, D. (2018). Notulen overleg ir j.w. topshuis, 28 mei 2018.

[24] Fiolet, D. and Saman, K. (2018a). *Personal contact Eastern Scheldt barrier administation, 19-07-2018*.

[25] Fiolet, D. and Saman, K. (2018b). *Personal contact Eastern Scheldt barrier administation, 28-05-2018*.

[26] Gouldby, B., Sayers, P., Mulet-Marti, J., Hassan, M., and Benwell, D. (2008). A methodology for regional-scale flood risk assessment. *Proceedings of the Institution of Civil Engineers - Water Management*, 161(3):169–182.

[27] Hall, J., Dawson, R., Sayers, P., Rosu, C., Chatterton, J., and Deakin, R. (2003). A methodology for national-scale flood risk assessment. *Proceedings of the Institution of Civil Engineers - Water and Maritime Engineering*, 156(3):235–247.

[28] Holthuijsen (2007). *Waves in Oceanic and Coastal Waters*. Cambridge University Press, Cambridge, United Kingdom.

[29] Huis in 't Veld, J., Stuip, J., Walther, A., and Van Westen, J. (1987). *The closure of tidal basins, closing of estuaries, tidal inlets and dike breaches*. Delft University Press, Delft, The Netherlands.

[30] Informatiehuis Water (2018). *Waterveiligheidsportaal*. `https://waterveiligheidsportaal.nl/#/nss/nss/norm` (accessed October 16th, 2018).

[31] IPET (2009). *Performance Evaluation of the New Orleans and Southeast Louisiana Hurricane Protection System Final Report of the Interagency Performance Evaluation Task Force Volume VIII – Engineering and Operational Risk and Reliability Analysis*. U.S. Army Corps of Engineers, Louisiana, USA.

[32] Jongejan, R. (2013a). *Kalibratie van semi-probabilistische toetsvoorschriften*. Deltares, Delft, The Netherlands.

[33] Jongejan, R. (2013b). *Vaststellen uitgangspunten definitieve kalibratie*. Deltares, Delft, The Netherlands.

[34] Jongejan, R. (2017). *WBI2017 Code Calibration*. Rijkswaterstaat Water, Verkeer en Leefomgeving, Utrecht, The Netherlands.

[35] Jongejan, R., Stefess, H., Roode, N., Ter Horst, W., and Maaskant, B. (2011). *The VNK2 project: a detailed, large-scale quantitative flood risk analysis for the Netherlands*. Rijkswaterstaat VNK Project Office, Utrecht, The Netherlands.

[36] Jonkman, S., Jongejan, R., and Maaskant, B. (2011). The use of individual and societal risk criteria within the dutch flood safety policy—nationwide estimates of societal risk and policy applications. *Risk Analysis*, 31(2):282–300.

[37] Jonkman, S., Steenbergen, R., Morales-Nápoles, O., Vrouwenvelder, A., and Vrijling, J. (2017). *Probabilistic design: Risk and Reliability Analysis in Civil Engineering, Lecture notes CIE4130*. Delft University of Technology, Delft, The Netherlands.

[38] Jorissen, R., De Looff, H., and Labrujere, A. (2013). *Beheer Oosterscheldekering nader bekeken*. Rijkswaterstaat.

[39] Kingston, G., Rajabalinejad, M., Gouldby, B., and Van Gelder, P. (2009). Computational intelligence methods for the efficient reliability analysis of complex flood defence structures. *Structural Safety*, 33(1):64–73.

[40] Lievense, P. (2007). *Implic berekeningen prestatiepeilen Oosterschelde*. Rijkswaterstaat Zeeland, Middelburg, The Netherlands.

[41] Mooij (2018). *Kaart Nederland*. `https://mooji.nl/wp-content/uploads/2015/01/kaart-nederland.jpg` (accessed October 16th, 2018).

[42] Mooyaart, L. and Jonkman, S. (2017). Overview and design considerations of storm surge barriers. *Journal of Waterway, Port, Coastal, and Ocean Engineering*, 143(2):34–45.

[43] Mulder, T. and Vrijling, J. (1980). *Hydraulic aspects of coastal structures, part 1: developments in hydraulic engineering related to the design of the Oosterschelde Storm Surge Barrier in the Netherlands, Probabilistic load determination*. Delft University Press, Delft, The Netherlands.

[44] Navionics, a Garmin Ltd. company (2018). *Sonar depth charts*. `https://webapp.navionics.com/?lang=en#boating@10&key=qbczHg~tU` (accessed July 31st, 2018).

[45] Nieuwkamer, R. and Helder, A. (2017). *Integrale veiligheid Oosterschelde, MIRT onderzoek - knikpunten, oplossingsrichtingen en effecten*. Rijkswaterstaat Zee en Delta, Middelburg, The Netherlands.

[46] Patev, R. and Leggett, M. (1995). Reliability analysis of a reinforced concrete drainage structure. *Proceedings of 3rd International Symposium on Uncertainty Modeling and Analysis and Annual Conference of the North American Fuzzy Information Processing Society, pp. 466-471*.

[47] Pilarczyk, K. (1995). Simplification of stability formulae for revetments under current and wave attack. *Preprints of the international riprap workshop: theory, policy and practive of erosion control using riprap, armour stone and rubble, Fort Collins, Colorado, United States, 12-16 july 1993*.

[48] Rajaratnam, J. (1976). *Turbulent Jets, Volume 5, 1st Edition*. Elsevier Science, Amsterdam, The Netherlands.

[49] Rijkswaterstaat (2016). *The storm surge barrier in the Eastern Scheldt*. Rijkswaterstaat, Middelburg, The Netherlands.

[50] Rijkswaterstaat, Afdeling Multimedia (1999). *Beeldbank Rijkswaterstaat*. `https://beeldbank.rws.nl`, (accessed November 22nd, 2018).

[51] Rijkswaterstaat Dienst Weg- en Waterbouw (2007). *Voorschrift Toetsen op Veiligheid Primaire Waterkeringen*. Ministerie van Verkeer en Waterstaat, The Hague, The Netherlands.

[52] Rijkswaterstaat, Water Verkeer en Leefomgeving (2016a). *Regeling veiligheid primaire waterkeringen 2017*. Ministerie van Infrastructuur en Milieu, The Hague, The Netherlands.

[53] Rijkswaterstaat, Water Verkeer en Leefomgeving (2016b). *Regeling veiligheid primaire waterkeringen 2017, Bijlage I: Procedure*. Ministerie van Infrastructuur en Milieu, The Hague, The Netherlands.

[54] Rijkswaterstaat, Water Verkeer en Leefomgeving (2016c). *Regeling veiligheid primaire waterkeringen 2017, Bijlage II: Voorschriften bepaling hydraulische belasting primaire waterkeringen*. Ministerie van Infrastructuur en Milieu, The Hague, The Netherlands.

[55] Rijkswaterstaat, Water Verkeer en Leefomgeving (2016d). *Regeling veiligheid primaire waterkeringen 2017, Bijlage III: Sterkte en veiligheid*. Ministerie van Infrastructuur en Milieu, The Hague, The Netherlands.

[56] Rijkswaterstaat, Water Verkeer en Leefomgeving (2016e). *Schematiseringshandleiding Betrouwbaarheid sluiten Kunstwerk*. Ministerie van Infrastructuur en Milieu, The Hague, The Netherlands.

[57] Rijkswaterstaat, Water Verkeer en Leefomgeving (2016f). *Schematiseringshandleiding Hoogte*. Ministerie van Infrastructuur en Milieu, The Hague, The Netherlands.

[58] Rijkswaterstaat, Water Verkeer en Leefomgeving (2016g). *Schematiseringshandleiding Hoogte Kunstwerk*. Ministerie van Infrastructuur en Milieu, The Hague, The Netherlands.

[59] Rijkswaterstaat, Water Verkeer en Leefomgeving (2016h). *Schematiseringshandleiding Piping*. Ministerie van Infrastructuur en Milieu, The Hague, The Netherlands.

[60] Saman, K. (2017). *Prestatiepeilenmodel Oosterscheldekering 2017*. Rijkswaterstaat Zee en Delta District Noord Oosterscheldekering.

[61] Schiereck, G. (1993). *Introduction to bed, bank, shore protection*. Delft Academic Press / VSSD, Delft, The Netherlands.

[62] Schoemaker, M. (2016). *Master thesis: Flood Risk Assessment & Investment Framework, A framework for flood risk reduction strategies in the Hollandsche IJssel*. TU Delft master student thesis, Delft.

[63] Schrijver, M., Saman, K., and Lievense, P. (2010). *Het gebruik van het model Implic bij het bepalen van de prestatiepeilen Oosterschelde - Aanpassing en verificatie van het model - Papport PO-2010-004*. Rijkswaterstaat Zeeland, Middelburg, The Netherlands.

[64] Schultz, M., Gouldby, B., Simm, J., and Wibowo, J. (2010). *Beyond the Factor of Safety: Developing Fragility Curves to Characterize System Reliability*. U.S. Army Corps of Engineers, Washington DC, USA.

[65] Simm, J., Gouldby, B., Sayers, P., J.J., F., Wersching, S., and Bramley, M. (2009). Representing fragility of flood and coastal defences: getting into the detail. *Flood Risk Management: Research and Practice*, 1(1):621–631.

[66] Slootjes, N. and Van der Most, H. (2016). *Achtergronden bij de normering van de primaire waterkeringen in Nederland, Hoofdrapport*. Ministerie van Infrastructuur en Milieu, DG Ruimte en Water, Directie Algemeen Waterbeleid en Veiligheid, The Hague, The Netherlands.

[67] Steenepoorte, K. and Zegers, N. (2010a). *Faalkansanalyse Civiele delen Stormvloedkering Oosterschelde Coverrapportage*. Rijkswaterstaat Zeeland, Middelburg, The Netherlands.

[68] Steenepoorte, K. and Zegers, N. (2010b). *VTV Toetsrapportage Stormvloedkering Osoterschelde*. Rijkswaterstaat Zeeland, Middelburg, The Netherlands.

[69] 't Hart, R., De Bruijn, H., and De Vries, G. (2016). *Fenomenologische beschrijving, faalmechanismen WTI*. Deltares, Delft, The Netherlands.

[70] Technische Adviescommissie voor de Waterkeringen (1999). *Technisch Rapport: Zandmeevoerende Wellen*. Rijkswaterstaat Dienst Weg- en Waterbouw, Delft, The Netherlands.

[71] Technische Adviescommissie voor de Waterkeringen (2003). *Leidraad Kunstwerken*. Rijkswaterstaat, Dienst Weg- en Waterbouw, Delft, The Netherlands.

[72] Tekie, P. and Ellingwood, B. (2002). Fragility analysis of concrete gravity dams. *Journal of Infrastructure Systems*, 7(2).

[73] Van Bree, B. (2015a). *WTI2017 Kunstwerken Achtergrondrapport toetsspoor Hoogte I - Modellering optredend overslag-/overloopdebiet*. Deltares, Delft, The Netherlands.

[74] Van Bree, B. (2015b). *WTI2017 Kunstwerken Achtergrondrapport toetsspoor Hoogte II - Bepaling kritiek overslag-/overloopdebiet*. Deltares, Delft, The Netherlands.

[75] Van Bree, B. (2015c). *WTI2017 Kunstwerken Toetsspoorrapport Hoogte*. Deltares, Delft, The Netherlands.

[76] Van Der Meer, J. (2009). *Coastal flooding: A view from a practical Dutchman on present and future strategies*. Flood Risk Management: Research and Practice – Samuels et al. (eds) 2009 Taylor & Francis Group, London.

[77] Van Der Meer, J., Ter Horst, W., and Van Velzen, E. (2009). *Calculation of fragility curves for flood defence assets*. Flood Risk Management: Research and Practice – Samuels et al. (eds) 2009 Taylor & Francis Group, London.

[78] Van Dixhoorn, J. (1982). Introduction eastern scheldt storm surge barrier. *Proceedings of the Delta Barrier Symposium Rotterdam, 13-15 October 1982*.

[79] Van Manen, S. (2007). *Prestatiepeilen Oosterschelde*. Rijkswaterstaat Zeeland, Middelburg, The Netherlands.

[80] Van Steeg, P. (2015). *Stabiliteit van bekledingen onder overstortbelasting en plonsbelasting*. Deltares, Delft, The Netherlands.

[81] Venn, J. (1880). On the diagrammatic and mechanical representation of propositions and reasonings. *Philosophical Magazine Series 5*, 10(59):1–18.

[82] Verhagen, H., d'Angremond, K., and Van Roode, F. (2012). *Breakwaters and closure dams, 2nd edition*. VSSD, Delft, The Netherlands.

[83] Visser, T. (1986a). *Ontwerpnota Stormvloedkering Oosterschelde, Deel 1: Totaalontwerp en ontwerpfilosofie*. Rijkswaterstaat, Deltadienst.

[84] Visser, T. (1986b). *Ontwerpnota Stormvloedkering Oosterschelde, Deel 2: De Waterbouwkundige Werken*. Rijkswaterstaat, Deltadienst.

[85] Visser, T. (1986c). *Ontwerpnota Stormvloedkering Oosterschelde, Deel 3: De Betonwerken*. Rijkswaterstaat, Deltadienst.

[86] Vorogushyn, S., Merz, B., and Apel, H. (2009). Development of dike fragility curves for piping and micro-instability breach mechanisms. *Natural hazards and earth system sciences*, 9(4):1383–1401.

[87] Vrijling, J. and Van Gelder, P. (2006). *Probabilistic Design in Hydraulic Engineering, Lecture notes CIE5310*. Delft University of Technology, Delft, The Netherlands.

[88] Vásconez, P. (2013). *Performance of reliability methods in geomechanical applications*. TU Delft master student thesis, Delft.

[89] Wojciechowska, K., Pleijter, G., Zethof, M., Havinga, F.J. Van Haaren, D., and Ter Horst, W. (2015). *Application of Fragility Curves in Operational Flood Risk Assessment*. Geotechnical Safety and Risk V, T. Schweckendiek et al. (Eds.).

[90] Zuidwestelijke Delta (2018). *Pilot getijdenenergy Oosterscheldekering*. `https://www.zwdelta.nl/projecten/pilot-getijdenenergie-oosterscheldekering` (accessed October 16th, 2018).